INTERFEROMETRY DEPTH SOUNDING ON THE ATHABASCA GLACIER

DEVELOPMENT OF THE INTERFEROMETRY TECHNIQUE FOR LUNAR EXPLORATION

by

JAMES R. ROSSITER

DEPARTMENT OF PHYSICS
UNIVERSITY OF TORONTO
TORONTO 181, ONTARIO
CANADA

MARCH 1971

INTERFEROMETRY DEPTH SOUNDING ON THE ATHABASCA GLACIER

DEVELOPMENT OF THE INTERFEROMETRY TECHNIQUE FOR LUNAR EXPLORATION

by

James R. Rossiter

Department of Physics

University of Toronto

Toronto 181, Ontario

CANADA

March 1971

This thesis is submitted in conformity
with the requirements for the
Degree of Master of Science
in the
University of Toronto.

The Lunar Science Institute Contribution No. 31

ABSTRACT

There is increasing interest in very resistive geological environments, such as ice sheets and the lunar surface. In these, radio waves penetrate with little attenuation and any reflected waves interfere with direct waves. Theoretical and scale-model studies have indicated that the resulting interference pattern is indicative of both the electrical parameters and depth of the surface layer. The first successful field tests are described here.

This technique is planned for use as the Surface Electrical Properties Experiment on Apollo 17. Therefore, the published results of dielectric-property measurements of lunar samples are summarized. The dielectric constant near 1 MHz is about 3 for fines, and about 10 for solid samples. The loss tangent is between .03 and .10. These are somewhat higher than expected, and evidence is presented here that all the samples measured so far have been slightly water-contaminated.

Experiments were made in March, 1970, on the Athabasca Glacier, Canada, which has been extensively mapped and drilled, as reported by various authors. Frequencies between 2 and 24 MHz were used. A careful comparison has been made between the results, many suites of theoretical solutions, and the known parameters of the Athabasca Glacier. General agreement is found; most of discrepancies are attributed to the simple geometry of the theoretical model, i.e., infinite horizontal layers.

Development of an interpretational technique has been started. Effects of random scattering are present (especially in the higher frequencies), and the data were enhanced by a simple filter. The effects are not severe in these data. The rate of decay of analytical solutions appears characteristic of the dielectric losses of the medium. Ice has a frequency-dependent loss tangent, and this is clearly shown in the field results. The field strengths decay as $r^{-(2.2)}$ for the higher losses, to $r^{-(0.6)}$ for low losses.

Further development of interpretational techniques for more complex geometries is necessary. However, it is concluded that radio-frequency interferometry can usefully sound low-loss geological environments, both on the earth and the moon.

ACKNOWLEDGMENTS

I thank Dr. David W. Strangway, my thesis supervisor, for suggesting this project, for his considerable helpful advice, and for his constant enthusiasm during the work. His unflagging optimism is one of his greatest assets.

The Surface Electrical Properties Experiment is a team effort, of which this work is a small part. Mr. Peter Annan laid the essential groundwork for this thesis. Mr. Ray Watts and Mr. Larry Bannister contributed many helpful suggestions. The field equipment was built and organized by Mr. Everett Johnston and Mr. Gerry LaTorraca, and came from the Center for Space Research and from Dr. Gene Simmons, M.I.T., Cambridge, Massachusetts.

I thank the National and Historic Parks Branch of the Canadian Department of Indian Affairs and Northern Development for permission to work on the Athabasca Glacier. The National Parks Service, the Administration of Jasper National Park, and Brewster Transport Company all offered useful logistic advice and support.

The project was financed by NASA Grant No. NGL 22-009-257 (Principal Investigator, G. Simmons). Support was also received through a Graduate Fellowship from the Province of Ontario. This thesis was prepared at The Lunar Science Institute, Houston, Texas, under the joint support of the Universities Space

Research Association and the National Aeronautics and Space Administration Manned Spacecraft Center under Contract No. NSR 09-051-001.

TABLE OF CONTENTS

CHAPTER ONE: INTRODUCTION AND PURPOSE

1.1 Background

One of the most interesting aspects of the Apollo manned landings on the surface of the moon is the opportunity to learn something about the lunar surface and subsurface. Not only is this of interest *per se*, but it will doubtless yield important clues to the nature and history of the earth and the rest of the solar system. Since drilling through the subsurface has proved impossible below a few tens of centimeters (at the time of writing), it has been necessary to develop more subtle means of probing through the surface material.

One technique, using the interference behavior of radio waves, is being developed as the Surface Electrical Properties (S.E.P.) Experiment planned for *Apollo 17*. It is hoped that it will measure the depth to electrical interfaces, and *in situ* electrical properties of surface material. This method of depth-sounding depends on the transparency of the sounded medium to radio waves. Although it is being primarily developed for the moon, it is hoped that it will also be useful over ice, and perhaps over certain highly resistive salt-layers or desert regions. These areas are of increasing geophysical importance, especially to the oil industry.

Although the idea of radio-frequency interferometry is not new, it has not received much study. Most terrestrial

environments contain too much moisture to make them amenable to this type of depth-sounding. It was, however, suggested by Stern as early as 1927 (reported by Evans, 1963) as a glacier-sounding technique, and El-Said (1956) proposed the method to determine the depth to the water-table in the Sahara. He even ran a number of field surveys, but his interpretation appears to be faulty. In order to develop the technique for a lunar experiment, a comprehensive study was undertaken by Annan (1970).

His work consisted of theoretical studies (including calculated field-strength patterns), an analogue scale-model, and field work on the Gorner Glacier, Switzerland. Although his theoretical and scale-model studies gave good agreement, the glacier was too deep to obtain reflections, and the results remained inconclusive. Therefore, the primary purpose of this thesis was to show that under realistic field conditions the technique could be used to depth-sound. A subsidiary purpose was to develop the optimum means of carrying out the experiment for the design of flight hardware. This work is still continuing (see Appendix 1 for a brief description of the S.E.P Experiment).

1.2 Radio-frequency Interferometry

The technique, radio-frequency interferometry, can be simply described as follows. A transmitting antenna is set up on the surface to be probed, and a receiver is set up some

distance from it (Figure 1-1(a)). There are then several waves which reach the receiver. In general, these waves travel different distances, at different velocities, and will therefore interfere with each other.

An interference pattern can be generated in one of two different ways. Either the separation between the transmitter and receiver can be varied, keeping frequency of transmission constant (Figure 1-1(b)), or the frequency of the transmitted signal can be continuously varied, keeping the separation constant (Figure 1-1(c)). Because it is not at present practically feasible to build a sweep-frequency antenna that gives interpretable results (K. G. Balmain, private communication), we are concerned only with the former technique. Interpretation of the pattern obtained should give information on the depth to the reflector.

Two criteria must be met for this technique of sounding to be effective. The medium probed must not be too lossy or the amplitude of the reflected waves will be too low to interfere well with the direct wave—i.e., the medium probed must be transparent at the frequency used. Secondly, there must exist a strong electrical contrast below the surface in order to reflect energy. It is these electrical boundaries that the technique is designed to locate.

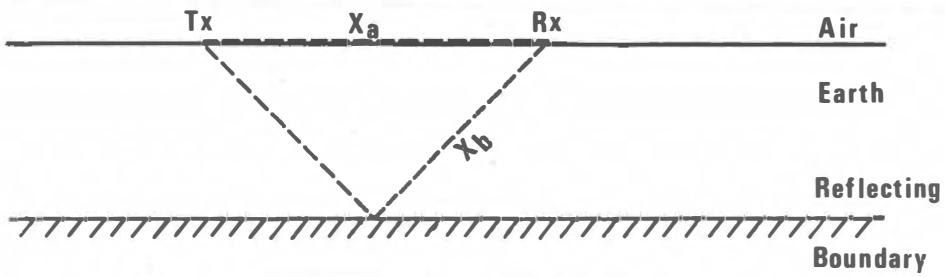

(a) Transmitter Tx and Receiver Rx on earth's surface (schematic)

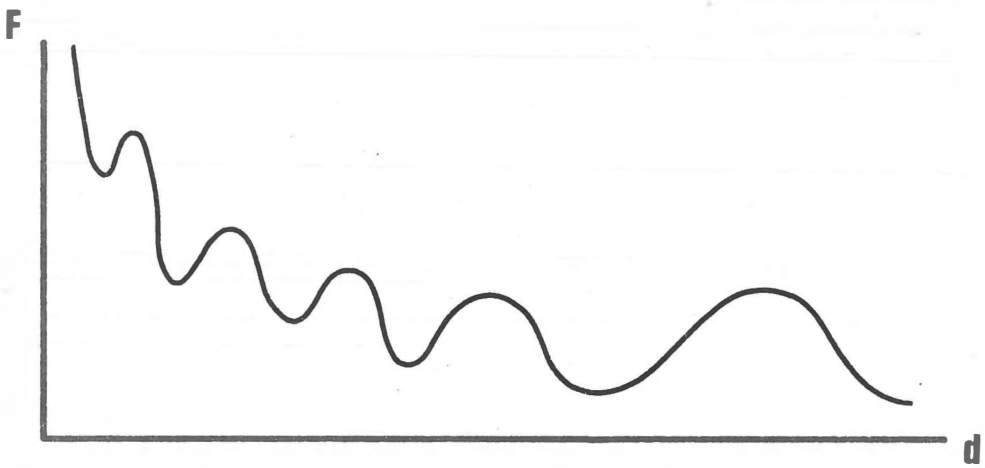

(b) Field strength F versus Tx - Rx seperation d (schematic)

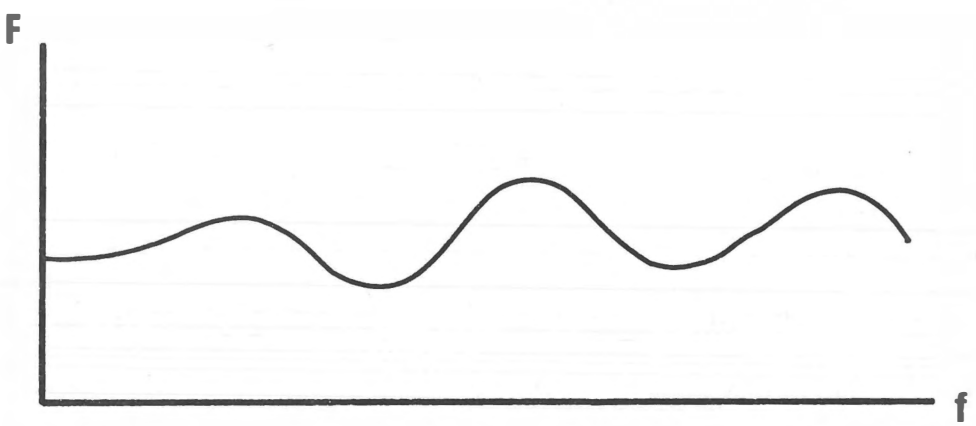

(c) Field strength F versus frequency f, with d fixed (schematic)
(after Annan, '70)

FIGURE I-1

1.3 The Lunar Environment

There is increasing evidence that the moon satisfies these two conditions. Both earth-based and bistatic radar have indicated for some time that the moon's surface had a very low loss tangent (Tyler, 1968; Weaver, 1965). This is supported by extensive testing of dry, powdered terrestrial rocks, which have similar properties (Saint-Amant and Strangway, 1970; Strangway, 1969; Campbell and Ulrichs, 1969).

There is now direct evidence from examination of samples returned on Apollo 11 and Apollo 12, summarized in Figure 1-2. The attenuation distance $\frac{1}{\alpha}$ (the distance through which the field strength falls to $\frac{1}{e} = 0.368$ of its original value), for a non-magnetic material, when $\tan \delta << 1$, is given by (von Hippel, 1954a):

$$\frac{1}{\alpha} = \frac{3 \times 10^8}{\pi f \sqrt{K'} \tan \delta} \text{ meters} \qquad (1\text{-}1)$$

where f is the frequency in Hz,

K' is the relative dielectric constant,

and $\tan \delta$ is the loss tangent.

Figure 1-2 shows that for frequencies around 1 MHz the attenuation distance is in the order of a kilometer for the majority of the lunar samples tested so far. The graph also shows that $(\sqrt{K'} \cdot \tan \delta)$ appears to be approximately constant over a

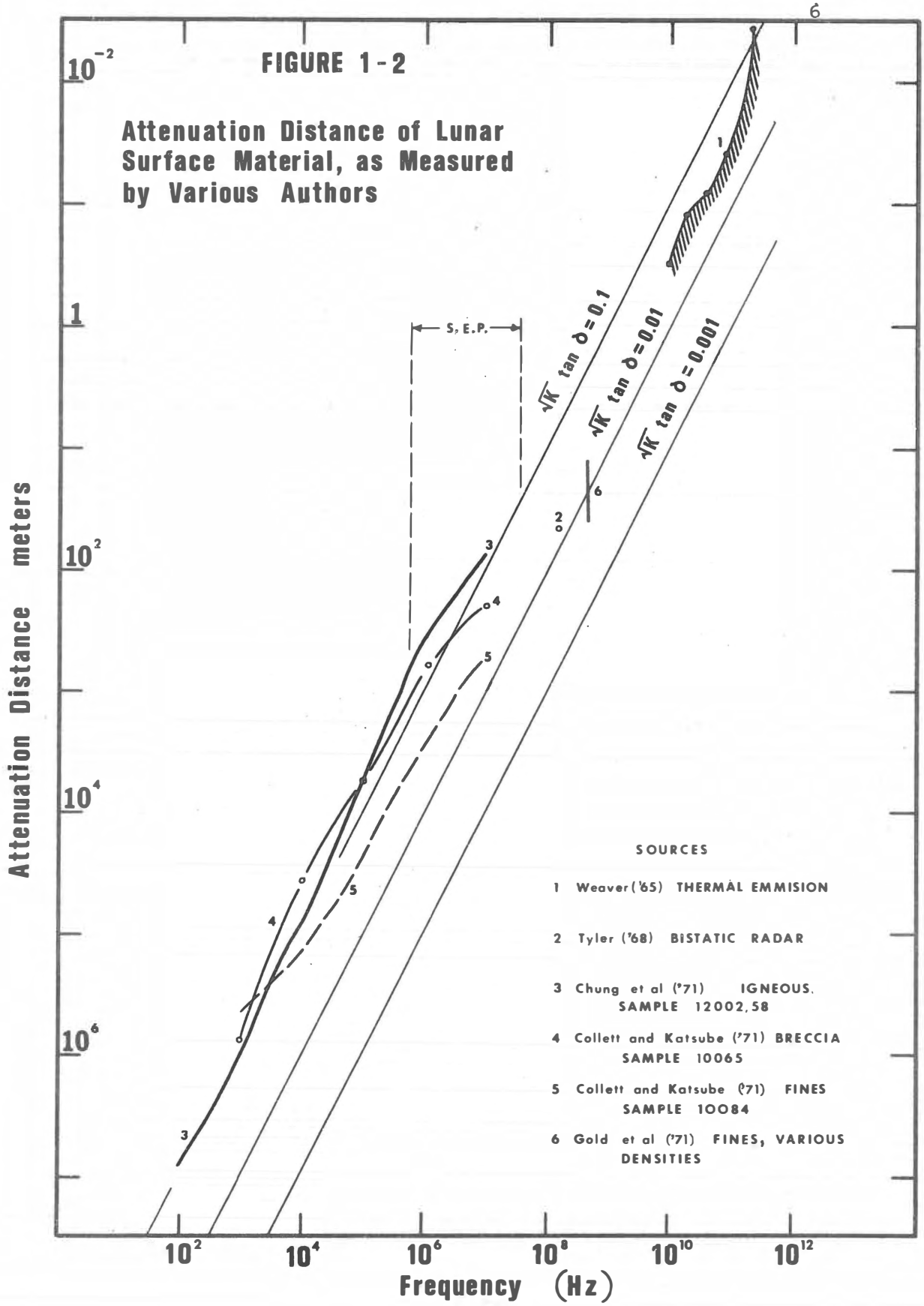
FIGURE 1-2
Attenuation Distance of Lunar Surface Material, as Measured by Various Authors
Attenuation Distance meters
Frequency (Hz)
S, E.P.
√K tan δ = 0.1
√K tan δ = 0.01
√K tan δ = 0.001
SOURCES
1 Weaver ('65) THERMAL EMMISION
2 Tyler ('68) BISTATIC RADAR
3 Chung et al ('71) IGNEOUS. SAMPLE 12002,58
4 Collett and Katsube ('71) BRECCIA SAMPLE 10065
5 Collett and Katsube ('71) FINES SAMPLE 10084
6 Gold et al ('71) FINES, VARIOUS DENSITIES

large frequency range. The dielectric properties of terrestrial and lunar rocks are discussed in more detail in Chapter 2.

The major factor allowing very low lunar loss tangents is very low water content: few hydrous minerals were found in lunar samples. However, this still leaves unanswered the question of whether or not there is water in the subsurface. Many of the surface features have been attributed to past erosion by water or ice (e.g., Schubert et. al., 1970; Gold, 1962). Moreover, igneous processes, as we know them on earth, depend on the presence of water to reduce the melting points of silicates. Therefore, the absence of water in the moon would demonstrate that igneous processes do not operate on the moon in analogous fashion to those on the earth. This would imply greatly different thermal models for the two bodies; however, there is now independent evidence that they may not be dissimilar. Magnetic measurements on lunar samples have indicated the possibility of a magnetic field on the moon during at least some of its history (e.g., Strangway, et. al., 1970a, 1970b).

Therefore, there is considerable reason for postulating a moist or a frozen-water layer in the subsurface. Moreover, it is very likely that there is a boundary between the lunar surface dust, and the bedrock beneath it. It is likely that the regolith has been formed by the continuous impact of meteoric bodies through geologic time (Shoemaker et. al., 1970a).

Recent estimates of its depth are from 3 to 6 m. at Tranquillity Base (Shoemaker et. al., 1970b), and 5 to 15 m. in Oceanus Procellarum (Oberbeck and Quaide, 1967), but no measurement of it has been made. (A Russian drilling experiment encountered rock at about 30 cm., in Mare Fecunditatis, but it is not clear that this was bedrock, and initial results from the Apollo 14 active seismic experiment indicate a regolith depth of about 8 m. at Fra Mauro). Therefore, a measurement of the depth to bedrock is important in determining lunar history.

A further possibility remains. If the depth to the water-ice interface could be determined, it would represent the zero-degree isotherm. This depth, together with the knowledge of thermal conductivity estimated from lunar samples, could give an independent estimate of the lunar thermal flux. (A heat flow experiment is planned for Apollo 15). This, in turn, would provide important clues to the nature of the moon's core.

Thus there is good reason to believe that the following conditions for EM interferometry will be met on the moon:

(a) that the surface layers will be transparent to radio-frequency waves,

(b) that there will be sufficient layering to provide good reflections from the subsurface, and

(c) that the layering information obtained is scientifically significant.

1.4 Interference Patterns

The bulk of Annan's work (1970) is a theoretical description of the fields surrounding a vertical magnetic dipole and surrounding a horizontal electric dipole above a two-layer earth. This theory is very mathematical, and the results are, of necessity, only approximate. However, a few basic ideas about the behavior of the fields around a dipole on the surface of a dielectric can be deduced. These are important in understanding the complex nature of the interference patterns.

The basic concept of the interferometry method was stated in Section 1.2: a transmitting antenna is set up on the surface that is to be probed, and a receiver is moved over the surface at some distance from the transmitter (see Figure 1-3). At least two waves reach the receiver: a direct wave along the surface (X_a), and a reflected wave from the subsurface (X_b).

In general, these two waves travel different distances at different velocities, and therefore interfere with each other. In some cases the interference is destructive, in others, constructive. The result is a series of peaks and nulls in the received field strength as the separation between the receiver and the transmitter is changed. It is this interference pattern of peaks and nulls which is indicative of the electrical properties of the medium and of the depth to the reflector.

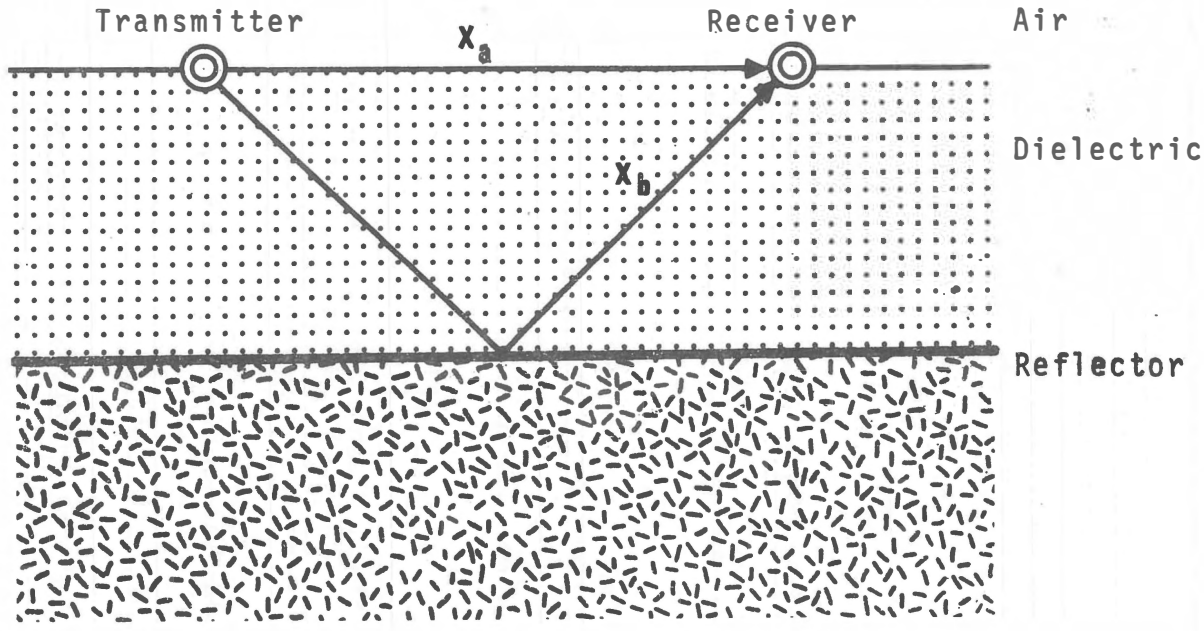

FIGURE 1-3: BASIC INTERFEROMETRY CONCEPT

In practice the situation is not quite so simple. There are, in fact, a number of different waves generated. As shown by Figure 1-4, there are two spherical waves, A and C, traveling directly between the transmitter and the receiver. Wave C travels in the upper medium (air or vacuum), and wave A, in the earth. Since these two waves have different velocities, they will interfere with each other. It is this interference which gives a measure of the dielectric constant of the lower medium, since the greater the difference in the velocities of these two waves, the greater will be their rate of interference.

Another wave of some importance is the flank, head, or lateral wave, B. This wave is responsible for the directionality of the antenna pattern below the surface. It develops in order to satisfy the boundary conditions of wave C at the interface, since the phase velocity of some wave in the earth must be the same as the phase velocity of wave C, in the upper medium. This condition is satisfied if plane wave B propagates downward at some tilt angle. This angle is shown as β, the angle of total internal reflection between the two media.

Hence,

$$\sin \beta = \sqrt{\frac{K_o}{K_1}} \qquad (1\text{-}2)$$

where β is the angle between the z-axis and the direction of the wave,

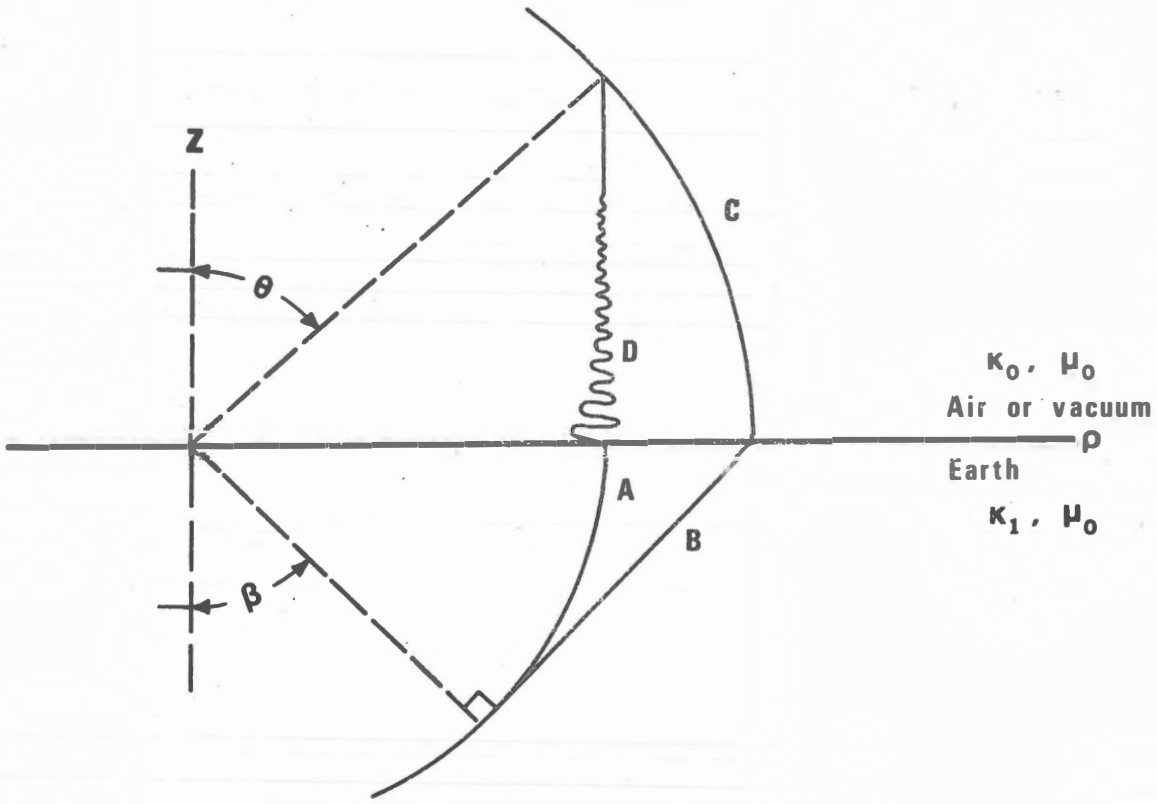

A – spherical wave in earth

B – flank or head wave in earth

C – spherical wave in air or vacuum

D – inhomogeneous wave in air or vacuum

FIGURE 1-4

SKETCH OF WAVEFRONTS AT THE AIR-EARTH INTERFACE

(After Annan 70)

and

$\frac{K_o}{K_1}$ is the ratio of dielectric constants

across the boundary (assuming non-magnetic media). The importance of this wave is that it effectively gives the antenna radiation pattern a lobe at angle β.

The spherical wave A, traveling in the lower medium, also matches the boundary conditions, but in a different way. An inhomogeneous wave, D, is produced at the surface; this wave propogates radially with the velocity of A, but decays exponentially with height above the surface. This wave is significant near the boundary, and its effect depends on the distance of the receiver from the surface.

The geometry used by Annan for calculating the fields around a horizontal electric dipole is shown in Figure 1-5. He went on to derive the waves produced for $h = 0$, and to compute the interference pattern of the vertical magnetic component at the air-earth interface (H_z), for a traverse perpendicular to the dipole. Samples of these are shown in Figures 1-6 to 1-10. In these figures each curve is calculated for a given set of parameters, and is scaled so that the largest peak is full-scale. This theoretical work has been confirmed by Sinha (1971), and he has compiled suites of curves for H_z, for the radial magnetic field H_ρ, and for the tangential

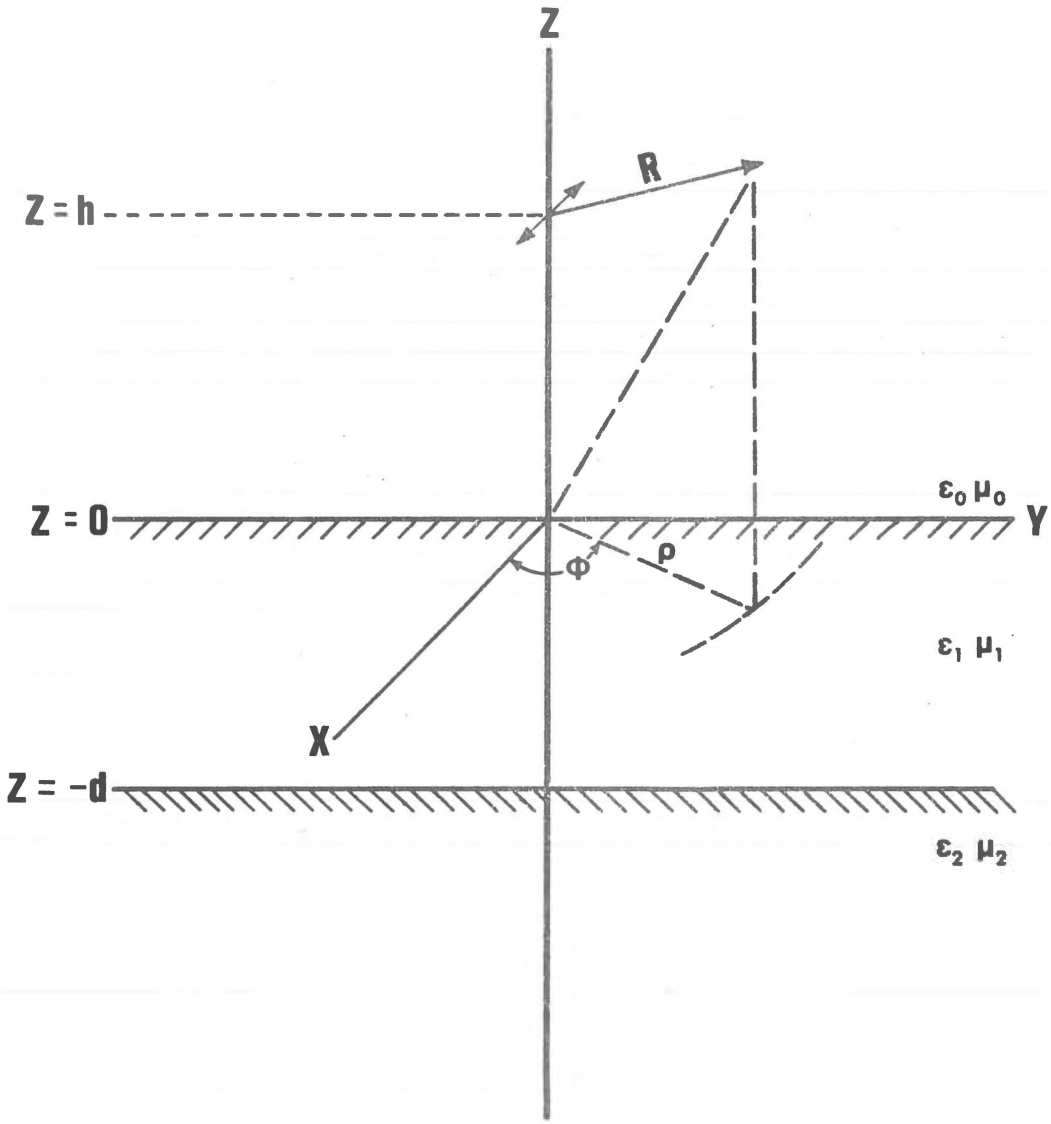

Horizontal electric dipole over a 2 layer earth.

(after Annan, '70)

FIGURE 1-5

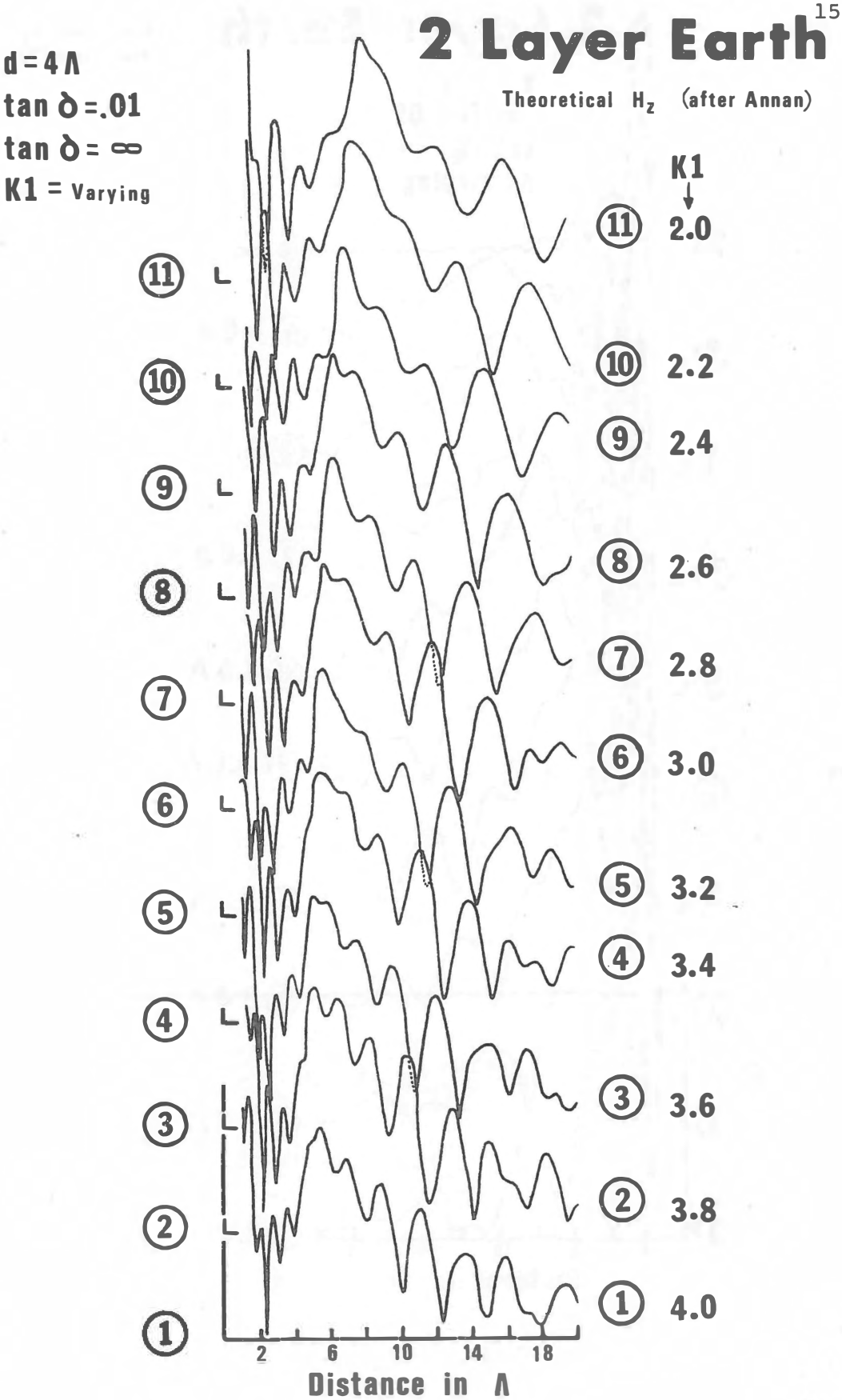
2 Layer Earth
Theoretical H_z (after Annan)
d = 4 Λ
tan δ = .01
tan δ = ∞
K1 = Varying
K1
11 2.0
10 2.2
9 2.4
8 2.6
7 2.8
6 3.0
5 3.2
4 3.4
3 3.6
2 3.8
1 4.0
2
6
10
14
18
Distance in Λ

FIGURE I-6

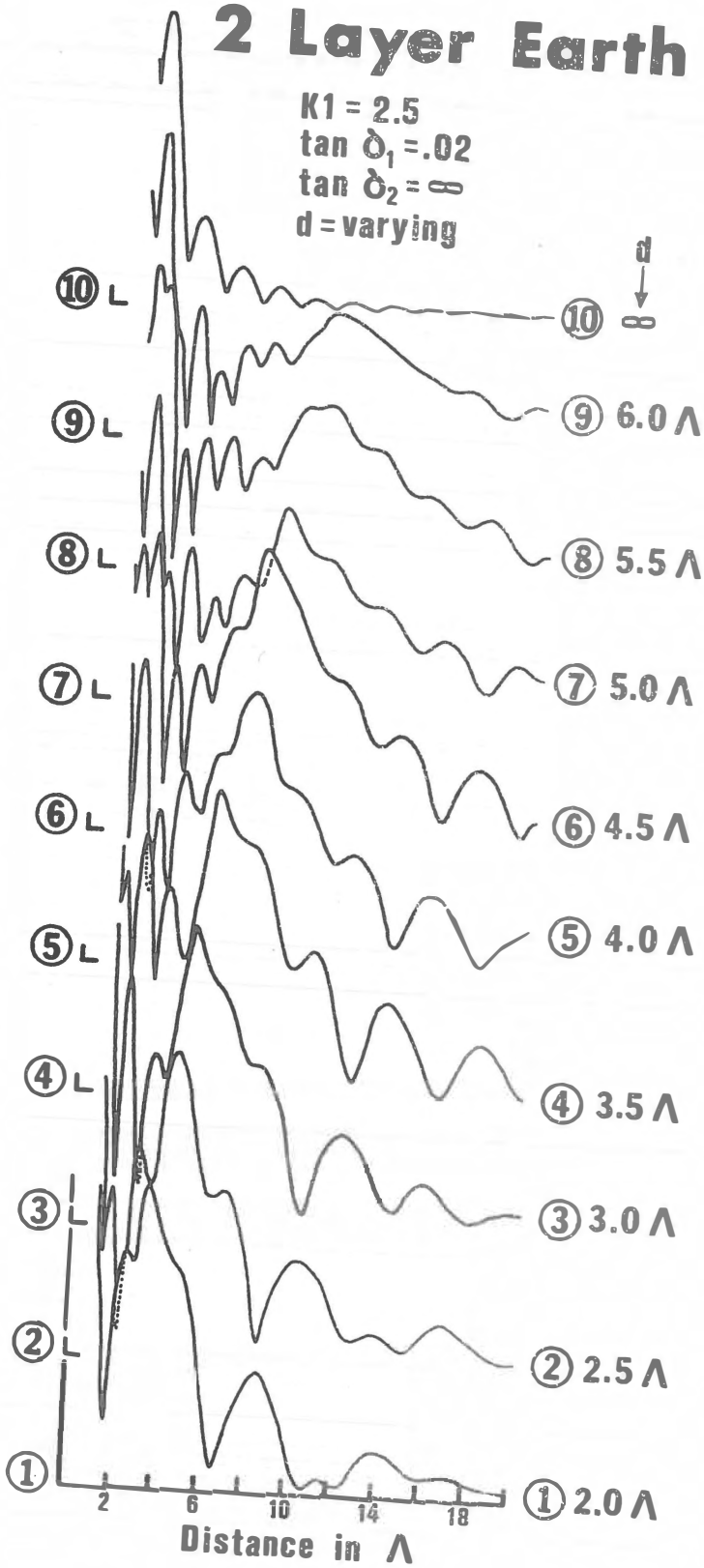
2 Layer Earth
K1 = 2.5
tan δ1 = .02
tan δ2 = ∞
d = varying
Theoretical Hz
(after Annan, '70)
d
⑩ L
⑨ L
⑧ L
⑦ L
⑥ L
⑤ L
④ L
③ L
② L
①
⑩ ∞
⑨ 6.0 Λ
⑧ 5.5 Λ
⑦ 5.0 Λ
⑥ 4.5 Λ
⑤ 4.0 Λ
④ 3.5 Λ
③ 3.0 Λ
② 2.5 Λ
① 2.0 Λ
2
6
10
14
18
Distance in Λ

FIGURE I-7

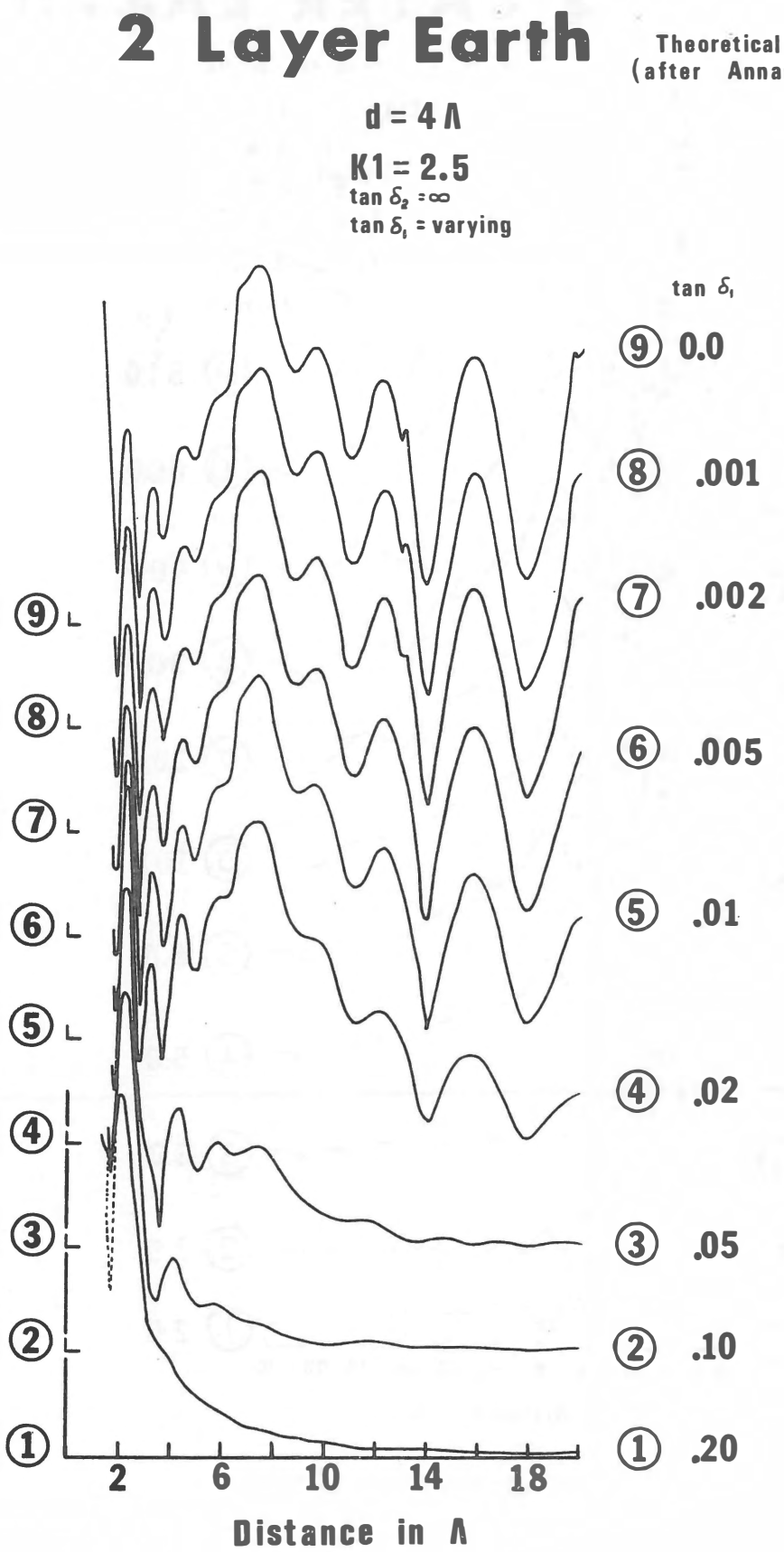
2 Layer Earth
Theoretical H_z
(after Annan 70)
d = 4 Λ
K1 = 2.5
tan δ_2 = ∞
tan δ_1 = varying
tan δ_1
⑨ 0.0
⑧ .001
⑦ .002
⑥ .005
⑤ .01
④ .02
③ .05
② .10
① .20
2
6
10
14
18
Distance in Λ

FIGURE 1-8

2 LAYER EARTH

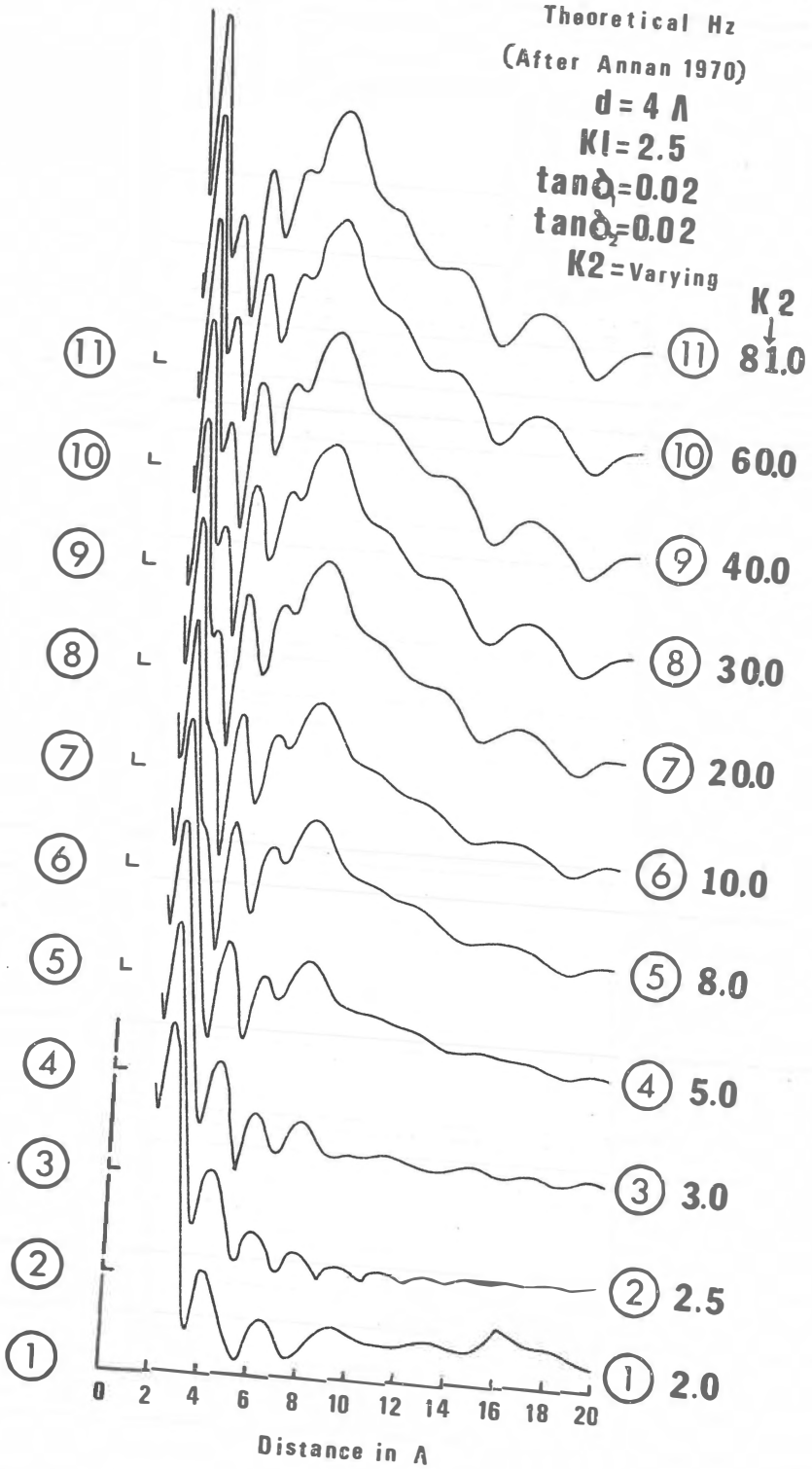

FIGURE 1-9

2 Layer Earth

Theoretical Hz
(after Annan, '70)

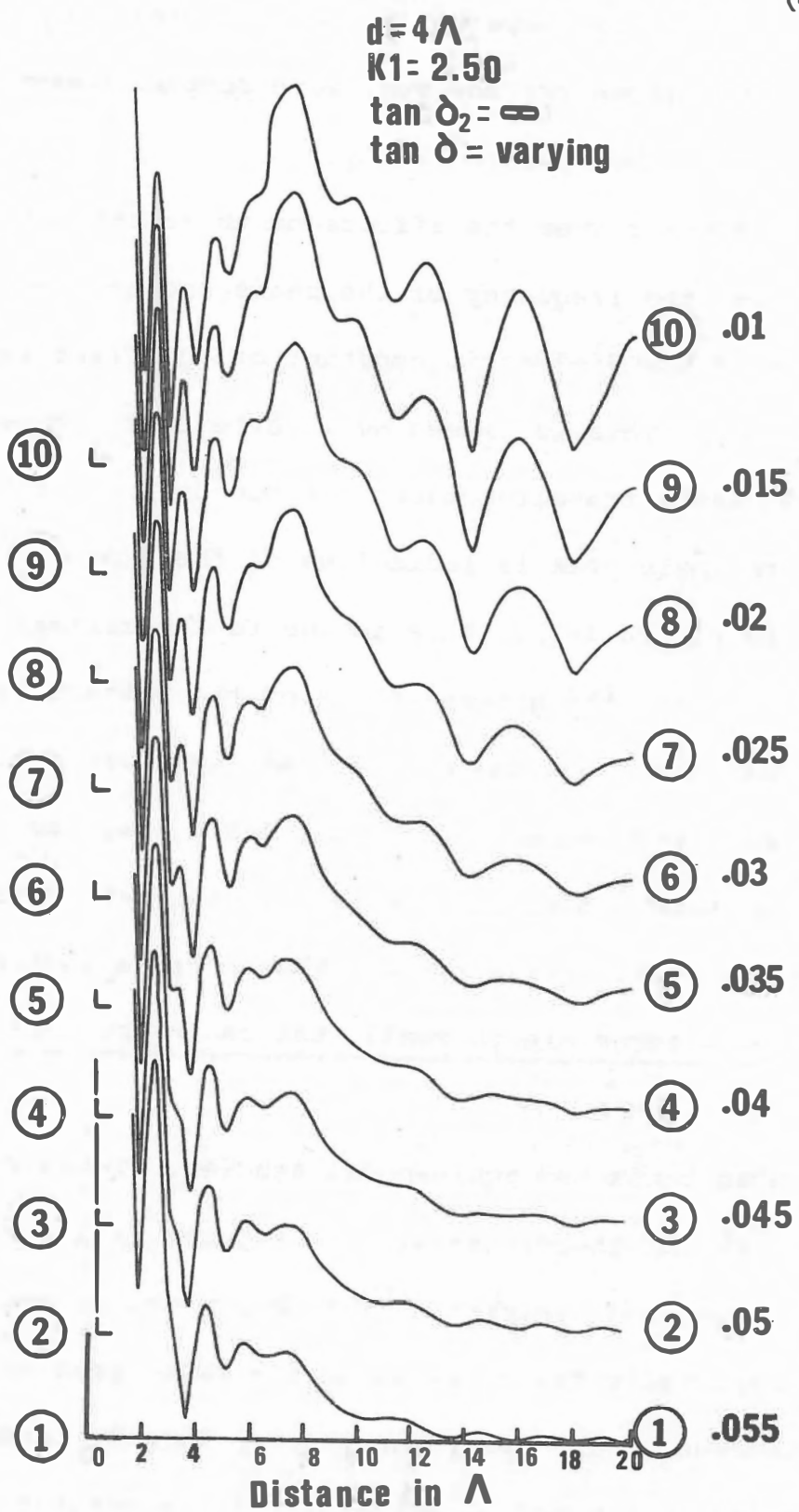

FIGURE 1-10

electric field, E_ϕ. The tangential magnetic field, H_ϕ, does not exist in this geometry; however, more complex geometries are virtually insoluble theoretically.

From the given curves the effects of three parameters can be seen. First, the frequency of the peaks and troughs is a rough measure of the dielectric constant of the first layer (see Figure 1-6). This is caused by interference between the two spherical waves traveling along the boundary. Second, the position of the main peak is indicative of the depth to the reflector (see Figure 1-7). This is due to the arrival of the head wave. Thirdly, the general shape of the pattern is indicative of signal losses to the medium, and therefore of the loss tangent of the upper medium (see Figure 1-8). Figures 1-9 and 1-10 show that both a dielectric or a loss tangent contrast should give reasonable reflections. These curves indicate how sensitive the patterns are to small changes in the various parameters.

Annan also conducted scale-model studies. These compared reasonably with the theory, as seen in Figures 1-11 to 1-13. Certainly the general features of the theory are present in the model, especially the move-out of the major peak as the depth is increased. The discrepancies can largely be explained by deficiencies in the model, especially since several of the model parameters were not known with much accuracy.

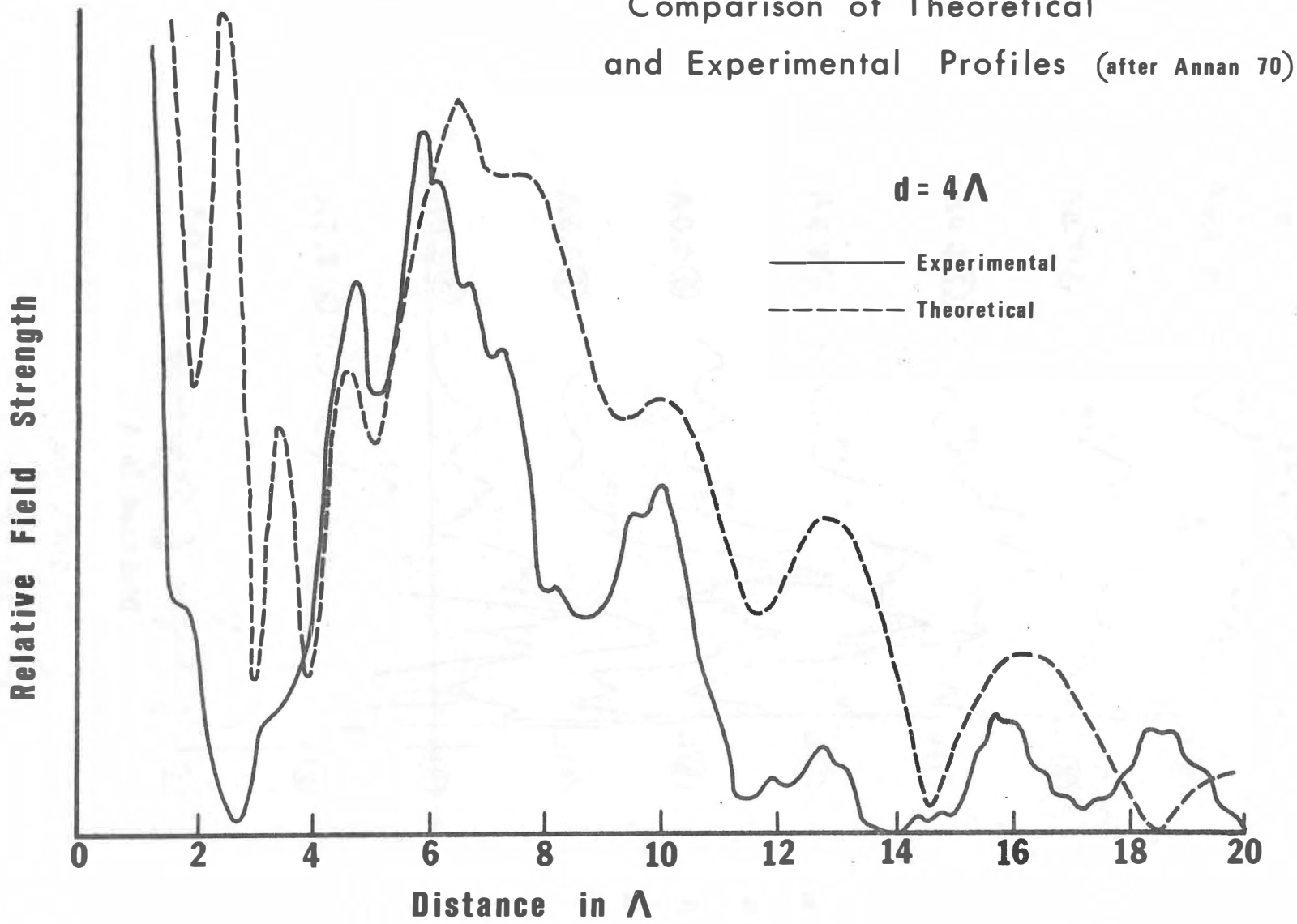
Comparison of Theoretical
and Experimental Profiles (after Annan 70)
d = 4Λ
Experimental
Theoretical
Relative Field Strength
0
2
4
6
8
10
12
14
16
18
20
Distance in Λ

FIGURE I-11

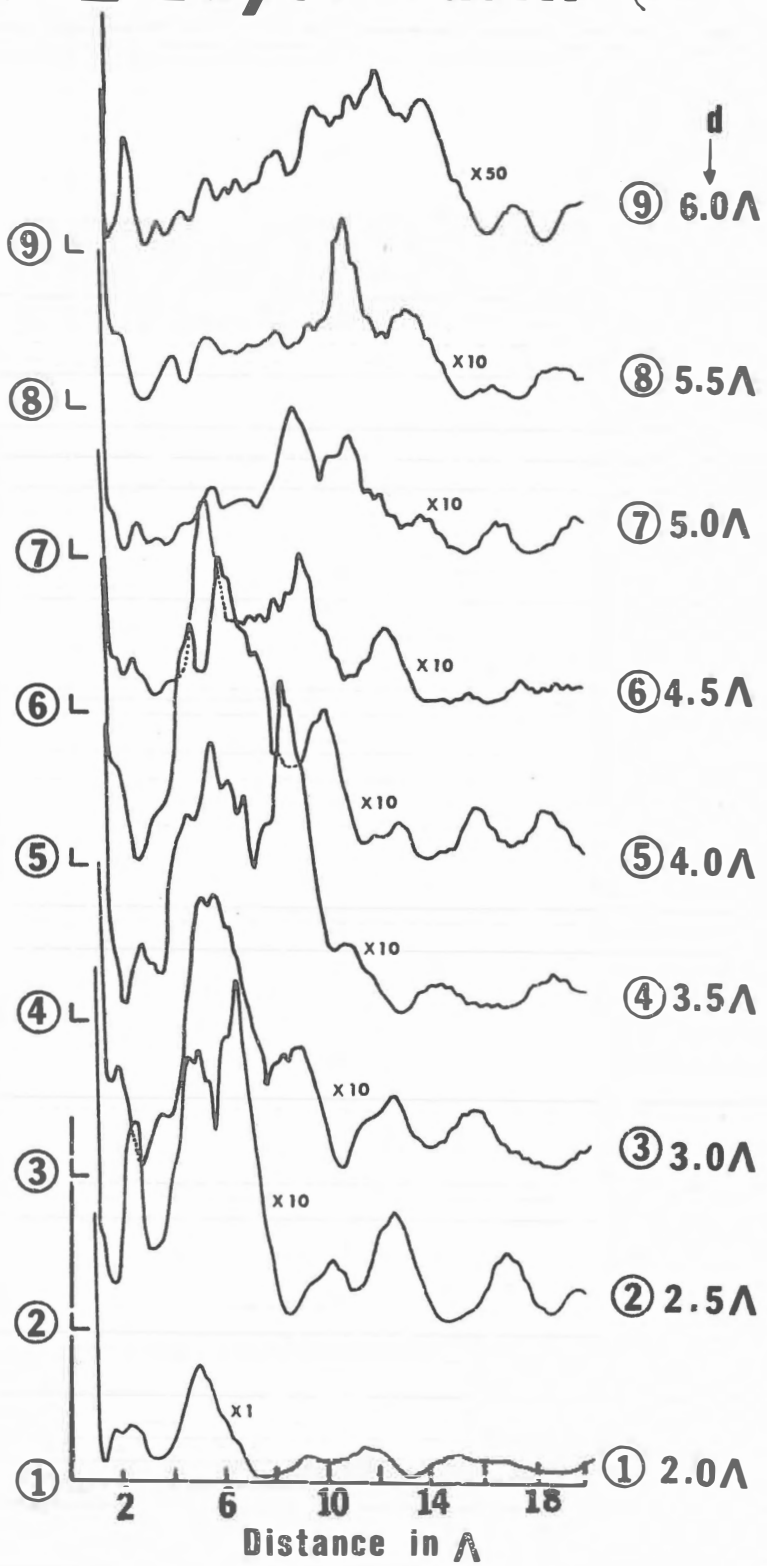
Scale Model 2 Layer Earth (after Annan '70)
d
⑨ 6.0Λ
⑧ 5.5Λ
⑦ 5.0Λ
⑥ 4.5Λ
⑤ 4.0Λ
④ 3.5Λ
③ 3.0Λ
② 2.5Λ
① 2.0Λ
X50
X10
X10
X10
X10
X10
X10
X1
⑨ L
⑧ L
⑦ L
⑥ L
⑤ L
④ L
③ L
② L
① L
2
6
10
14
18
Distance in Λ

FIGURE 1-12

Theoretical H_Z 2 Layer Earth

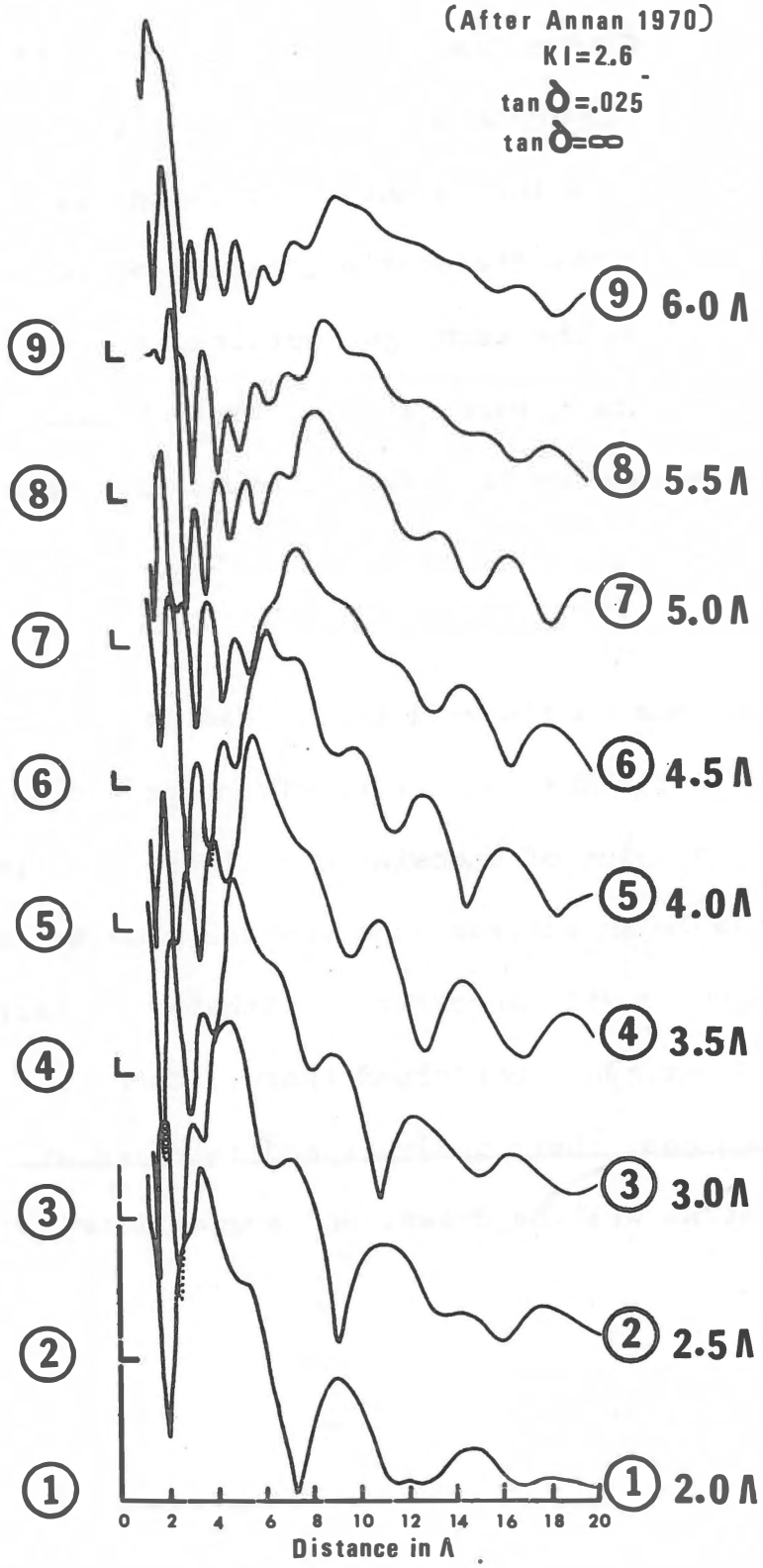

FIGURE 1-13

The results of the Gorner Glacier field work were also encouraging. They gave very good agreement with the theoretical half-space curves (which had the advantage of being exact solutions), and the value for the dielectric constant of ice was obtainable from them using the technique outlined above (see Figure 1-14). However, the larger question still remained — could the technique be used successfully to find the depth to a subsurface reflector?

1.5 Thesis Outline

The remainder of the thesis will be divided into four main parts. Chapter 2 will discuss the dielectric properties of lunar materials, the problem of choosing a full-scale terrestrial analogue to the lunar surface, and why ice provides a good analogue. Chapter 3 will describe the Athabasca Glacier test site, and the experiments performed there. Chapter 4 will present the data obtained, their analysis and interpretation. In Chapter 5 conclusions will be drawn, and suggestions for further work made.

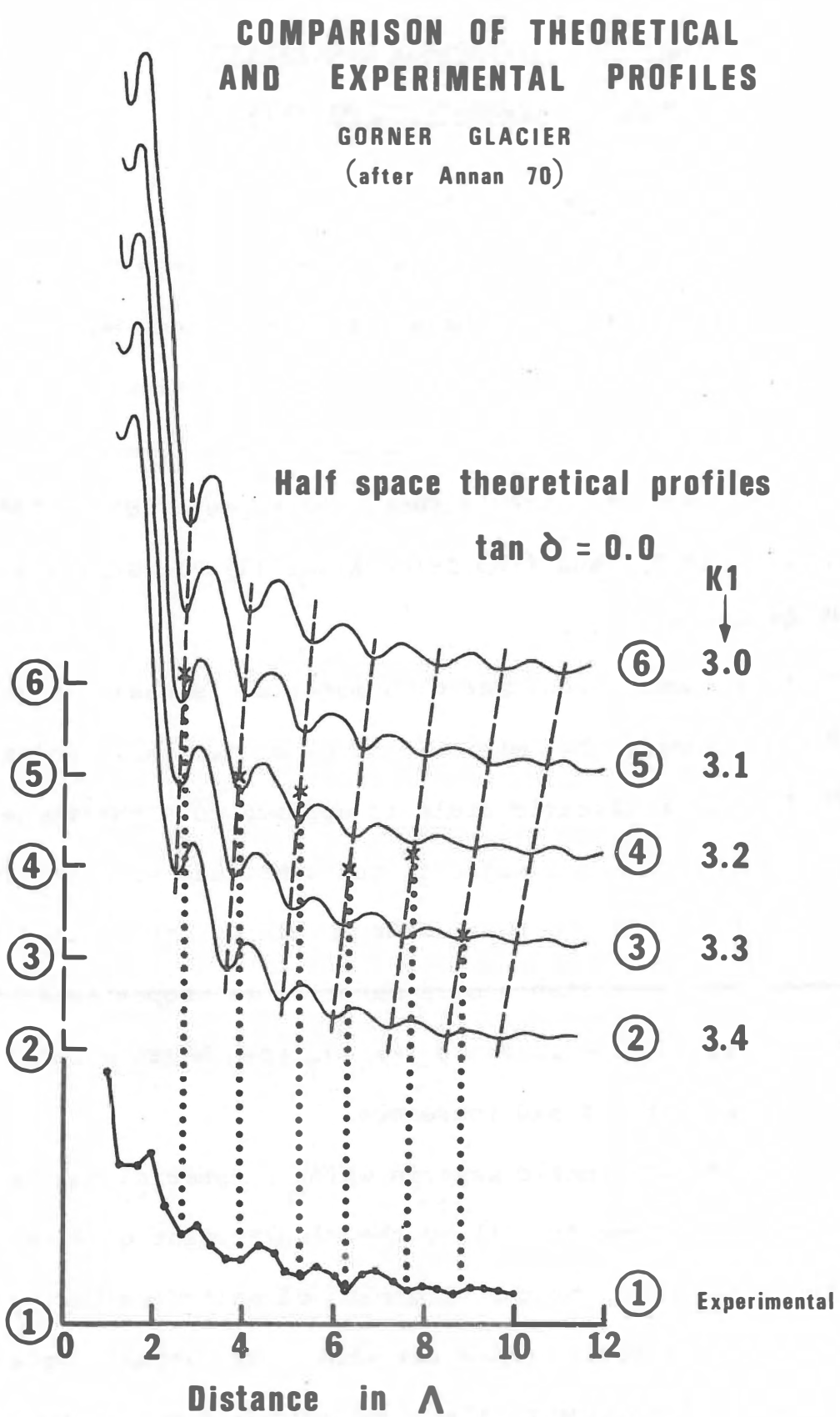
COMPARISON OF THEORETICAL
AND EXPERIMENTAL PROFILES
GORNER GLACIER
(after Annan 70)
Half space theoretical profiles
tan δ = 0.0
K1
6
3.0
5
3.1
4
3.2
3
3.3
2
3.4
1
Experimental
0
2
4
6
8
10
12
Distance in Λ

FIGURE 1-14

CHAPTER TWO: DIELECTRIC PROPERTIES OF LUNAR AND TERRESTRIAL MATERIALS

2.1 The Dielectric Mechanism

An understanding of the dielectric and loss mechanisms in solids is essential to the S.E.P. Experiment, and of course to any analogue of it. Therefore, a brief review of these mechanisms will follow. It is taken largely from standard references, such as Kittel (1968), von Hippel (1954a; 1954b), and Dekker (1957), and from Saint-Amant (1968), Strangway (1968), and Parkhomenko (1967).

The dielectric constant of a material is basically a measure of how easily the material can be electrically polarized. Obviously, if an electric field is applied to a substance, the positive and negative charges in the substance will try to separate in a direction that tends to cancel the applied field. Therefore, the capacitance of a material is proportional to the dielectric constant, since its surface charge accumulation in a given electric field increases.

There are four basic ways in which a material can become electrically polarized: (i) by the displacement of free charges to interfaces; (ii) by the alignment of molecules having a permanent dipole moment which are otherwise randomly oriented; (iii) by the alteration of the relative positions of ions; and (iv) by the changing of the electron density within an atom

(see Figure 2-1). If an alternating field is now applied, these mechanisms will react in different ways because they all require physical dispacements of some kind, on either a (i) granular, (ii) molecular, (iii) ionic, or (iv) atomic size scale, respectively. Therefore each process will have at least one resonant frequency associated with it, along with a damping mechanism and a restoring force.

Because the size scale of these mechanisms is different, they are in general also related to different frequency bands: (i) DC to audio, (ii) audio to radio frequencies, (iii) the infrared, and (iv) the ultra-violet, respectively (see Figure 2-2). Therefore, we are interested primarily in the first two processes. These are generally associated with small restoring forces (usually thermal agitation) and large damping forces, especially in solids. In fact, the damping is generally over-critical, and relaxation dispersion is seen rather than true resonance.

Various different hypotheses result in the Debye relaxation formula involving a single frequency for the complex dielectric constant of a material. For an applied field of the form $e^{i\omega t}$ ($i = \sqrt{-1}$), the complex dielectric constant has the form:

$$K^* = K' - iK'' \qquad (2\text{-}1)$$

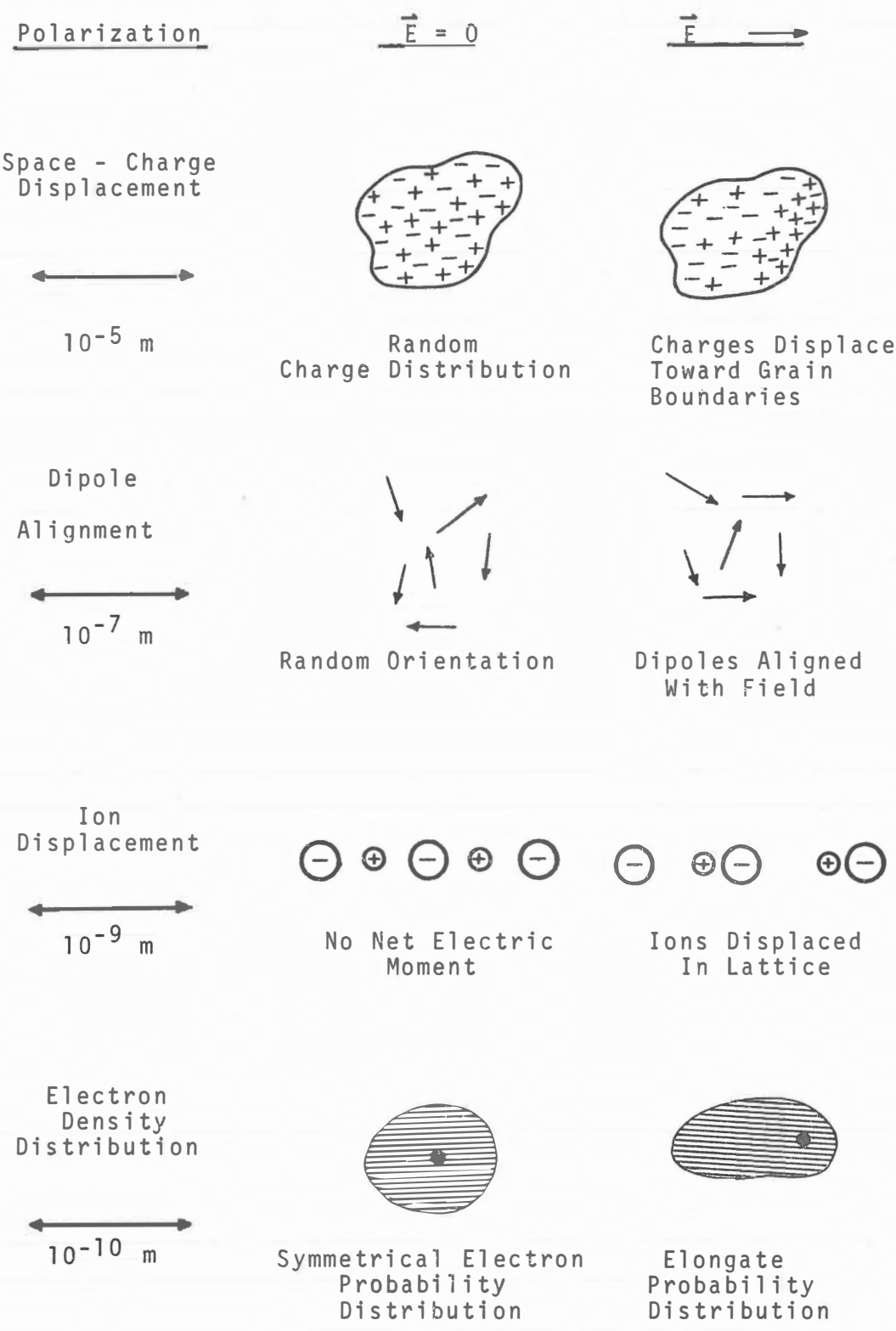

FIGURE 2-1: SCHEMATIC VIEW OF DIFFERENT WAYS A MATERIAL CAN BECOME ELECTRICALLY POLARIZED; ROUGH SIZE SCALE SHOWN.

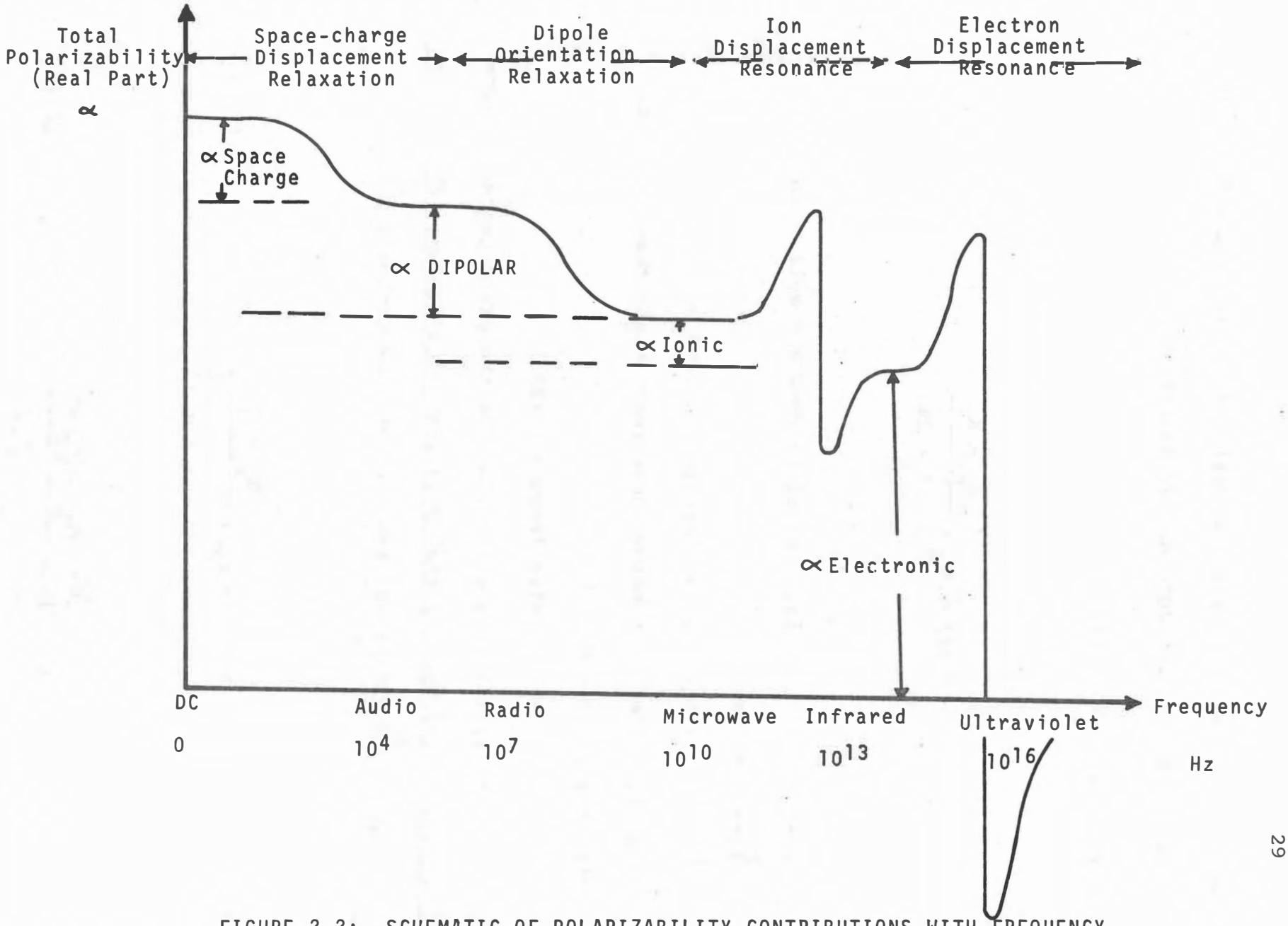

FIGURE 2-2: SCHEMATIC OF POLARIZABILITY CONTRIBUTIONS WITH FREQUENCY

where K' and K'' are the real and imaginary parts of the relative dielectric constant respectively.

The Debye formula is:

$$K^*(\omega) = K_\infty + \frac{K_s - K_\infty}{1 + i\omega\tau} \qquad (2\text{-}2)$$

where K_s is the real dielectric constant well below the relaxation time τ;

K_∞ is the real dielectric constant well above the relaxation time (but below other resonances; therefore, not strictly at $\omega = \infty$),

ω is the angular frequency ($2\pi f$),

and τ is the relaxation time for the given process. From equations 2-1 and 2-2 the $K'(\omega)$, and the losses, $K''(\omega)$, can be separated (although they are not independent):

$$K'(\omega) = K_\infty + \frac{K_s - K_\infty}{1 + \omega^2\tau^2} \qquad (2\text{-}3)$$

$$K''(\omega) = \frac{(K_s - K_\infty)\omega\tau}{1 + \omega^2\tau^2} \qquad (2\text{-}4)$$

These functions are shown in Figure 2-3(a) and (b). A useful measure of the losses in low-loss materials is the loss tangent, given by:

$$\tan \delta = \frac{K''}{K'} \qquad (2\text{-}5)$$

Combining 2-3, 2-4, and 2-5:

$$\tan \delta = \frac{(K_s - K_\infty)\omega\tau}{K_s + K_\infty \omega^2\tau^2} \qquad (2\text{-}6)$$

(see Figure 2-3(c)).

Most relaxation process are, as noted above, thermally activated, and therefore temperature dependent. Often the relaxation time can be described by:

$$\tau(T) = \tau_o e^{E/kT} \qquad (2\text{-}7)$$

where

τ_o is the relaxation time at $^1/T \rightarrow o$,

E is the activation energy,

k is Boltzmann's constant,

and T is absolute temperature.

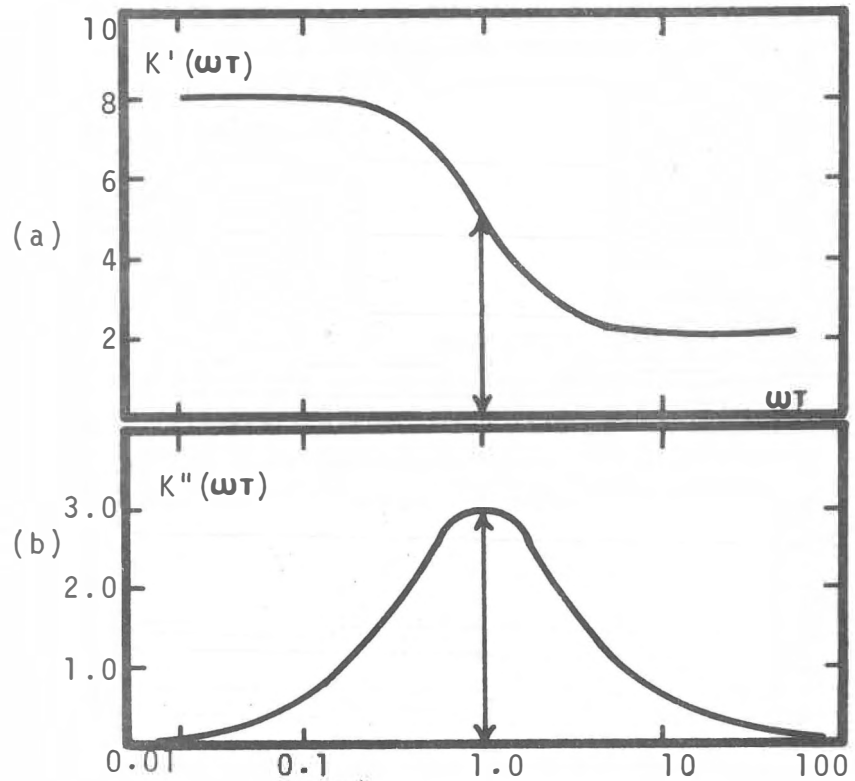

(a) The real part of K^* as a function of log $\omega\tau$ according to the Debye equations (2-3) for a dielectric with $K_\infty = 8$, $K_S = 2$;
(b) the imaginary part of K^* for the same dielectric.

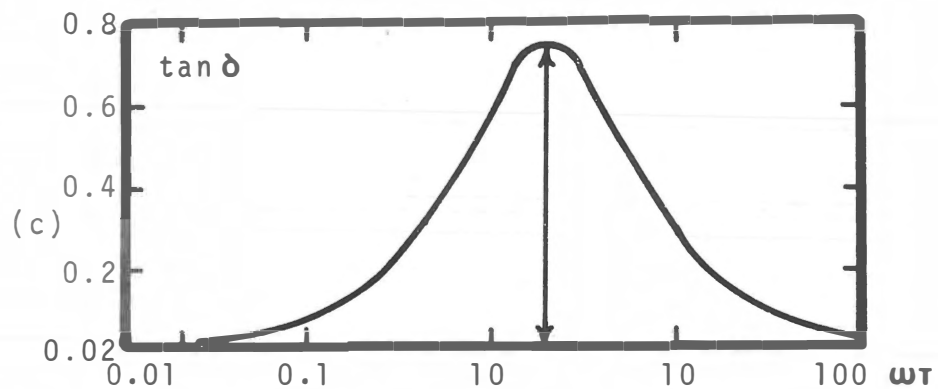

(c) The loss tangent for the dielectric illustrated above.

FIGURE 2-3: THE DEBYE EQUATIONS (AFTER ST. AMANT, 1968)

Both τ_o and E can vary with frequency. This gives a smearing of relaxation times with temperature (also, there is often a distribution of relaxation times at any one temperature).

A useful representation of Debye relaxations is a Cole-Cole plot. This is a plot of K' vs. K'' at various frequencies, and it can be shown from equations 2-3 and 2-4 that a true Debye relaxation will give a semi-circle with its centre on the K' axis. A distribution of relaxation times may also give a circular pattern, but with its centre off the K' axis.

2.2 Electromagnetic Losses

Various processes give rise to the loss observed at any given frequency (see Strangway, 1968). These may not just be electrical losses; magnetic losses will also contribute to the observed loss tangent at any given frequency. In fact, any energy-absorbing process will produce a loss. Table 2.1 lists the major EM losses in materials — it is interesting to note the rough parallels between dielectric (b) and magnetic (c) losses.

Usually the most important losses are associated with the conductivity of a material. These are due to heating by the current passing through the medium. The losses are given by:

$$K'' = \sigma_s/\omega\epsilon_o \qquad (2\text{-}8)$$

Table 2-1: Electromagnetic Loss Mechanisms

(a) Conductivity (electric currents)

  (i) bulk conductivity (conduction currents)

  (ii) particle conduction (eddy currents)

(b) Dielectric losses (charge displacement)

  (i) space-charge displacement loss

  (ii) molecular alignment loss

  (iii) ionic resonance

  (iv) electronic resonance

(c) Magnetic losses (magnetic moment displacement)

  (i) viscous loss

  (ii) hysteresis loss

  (iii) ferromagnetic resonance

  (iv) nuclear magnetic and electron spin resonance

where

σ_s is the D.C. conductivity, and

ϵ_o is the permittivity of free space.

Equation 2-8 is often turned around (causing considerable confusion in the literature) so that the losses, K'', are given as a frequency-dependent dielectric conductivity σ_f:

$$\sigma_f(\omega) = \omega\epsilon_o K''(\omega). \qquad (2\text{-}9)$$

Since K'' includes losses from various mechanisms, as discussed below, σ_f has no relation to the D.C. conductivity σ_s, except that $K''(\omega)$ may include a conductivity loss given by equation 2-8. This notation has also allowed equation 2-7 to be re-written as:

$$\sigma_f = \sigma_o e^{-E/KT} \qquad (2\text{-}10)$$

where

σ_o is the frequency-dependent conductivity as $\frac{1}{T} \rightarrow 0$.

There may also be losses due to eddy currents within conductive grains or between interfacial boundaries. These depend on the induction number of the conductive particles $(\sigma\mu\omega R^2)^{\frac{1}{2}}$ where σ is the conductivity of the particles, μ is their permeability, R is their radius, and ω is the applied

frequency. Of course the shape of, and the amount of interaction between, the various particles is also important.

There are losses associated with the displacement currents between boundaries of differing dielectric properties (the Maxwell-Wagner effect). Energy is absorbed moving charge carriers from one boundary to another. If the boundaries are parallel to the applied field, it can be shown that the relaxation produced is indistinguishable from that of a single dielectric. However, this is not true for other orientations, as the process is dependent on the shape and orientation of the boundaries concerned in a rather complex way (von Hippel, 1954a).

There is a loss associated with the relaxation phenomenon discussed earlier (equation 2-4). This is due to the energy absorbed in rotating molecules.

Losses due to ionic and electronic resonance are important only at high frequency, and will not be discussed here. They are caused by energy absorption as the ions or electrons are displaced from equilibrium.

Although a great deal is known about magnetic effects, the losses associated with them have not been considered greatly in geophysical electromagnetic methods. The most important is probably viscous loss, caused by the movement of magnetic domain walls. It is known to have a logarithmic time dependence, and some studies have indicated that it is important over a wide frequency range (Olhoeft, 1970).

Hysteresis losses, due to the orientation of magnetic moments, are probably not of interest because the fields generated will be too small. This is true for the magnetic resonances as well, which are due to precession of various magnetic moments around an internal field while absorbing energy from an applied alternating field. They are also high-frequency effects.

Therefore, the major loss mechanisms are the bulk conductivity and dielectric relaxation losses, with possible additions from space-charge displacements, eddy currents, and magnetic viscosity. The first two, given by equations 2-4 and 2-8 are:

$$K'' = \frac{(K_s - K_\infty)\omega\tau}{1 + \omega^2\tau^2} + \frac{\sigma_s}{\omega\varepsilon_o}, \qquad (2\text{-}11)$$

and are shown schematically in Figure 2-4.

2.3 Dielectric Properties of the Lunar Surface

For a number of years the lunar surface has been under intensive study, using various techniques, and frequencies from optical to radio. These are reported in Kopal and Mikhailov (1962), Aarons (1965), Hess et. al., (1966), and more recently interpreted by England et. al., (1968), Ward (1969), and Strangway (1969). These results have now been confirmed to a large extent by studies on lunar samples returned by Apollo 11 and Apollo 12. Since the S.E.P. experiment is based on the

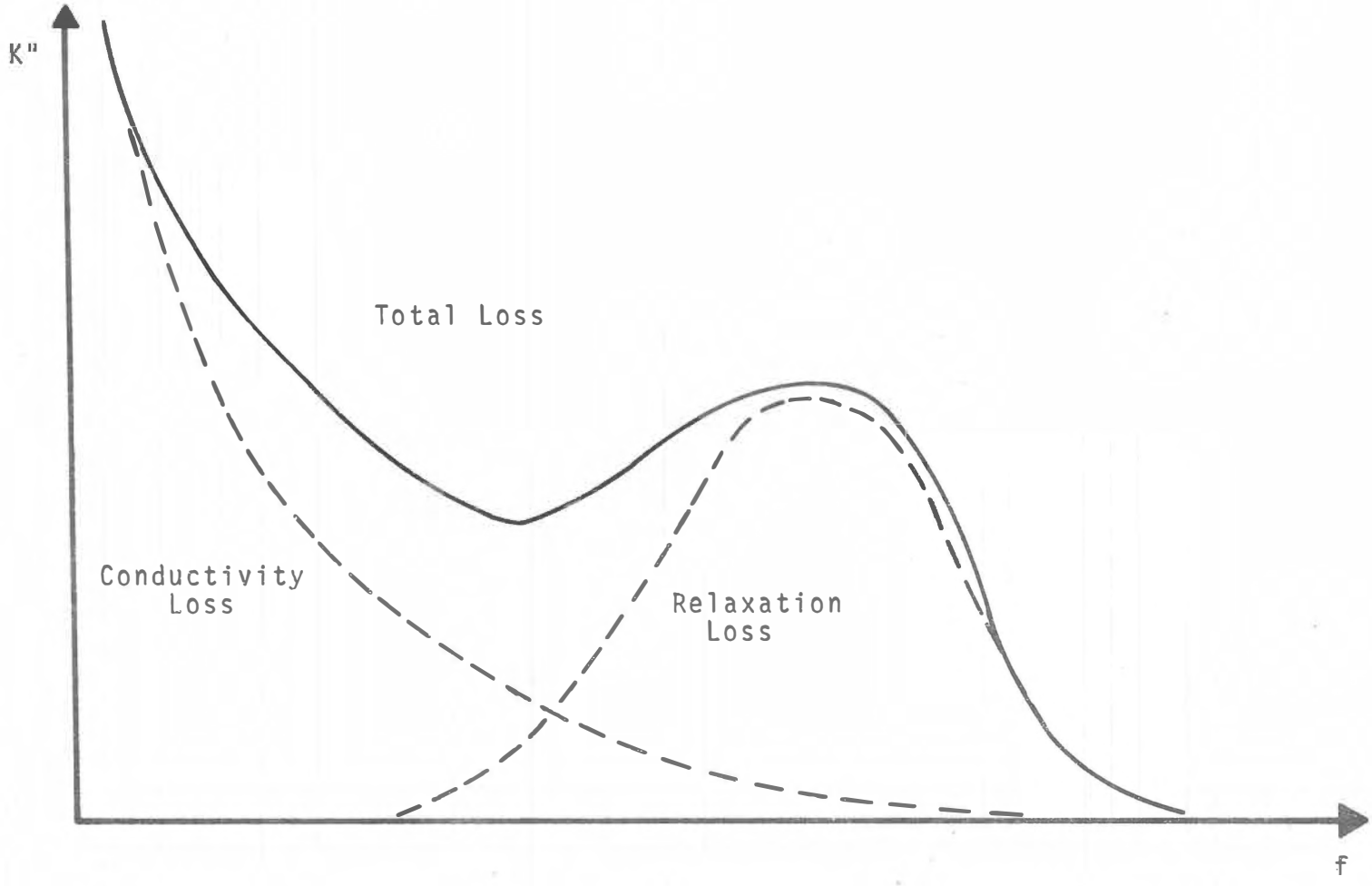

FIGURE 2-4: SCHEMATIC DIAGRAM OF THE TWO MAJOR DIELECTRIC LOSS MECHANISMS (AFTER VON HIPPEL, 195a)

electrical properties of the lunar surface, these results are reviewed here.

The earlier techniques were two fold: radio and radar reflection from earth-based stations, and microwave and infrared lunar thermal emission measurements. The former, using frequencies from 15 MHz to 37 GHz, gave virtually uniform radar cross sections over the lunar surface of 0.07. This can be easily converted to a dielectric constant of 2.5 to 3.0 using reflection laws (see Petengill, 1965; Hagfors, 1966). The technique does not give an independent estimate of the losses of the surface material—although they were assumed to be very low because of the low lunar reflectivity and because of its constancy over a wide frequency range. The low dielectric constant indicated a very porous top layer covering the moon's surface, with the possibility of a more compact layer some meters deep. This model was encouraged by slightly greater reflections at the longer wavelengths. Moreover, an estimate of the roughness of the lunar surface was made—indicating a roughness in the order of millimeters.

The values for dielectric constant obtained by measuring thermal emissivity at several frequencies or several angles of incidence were slightly lower — around 2. This was possibly due to a lower penetration depth of the higher frequencies used (Weaver, 1965), although there is a great deal of scatter in the results. However, measurement of thermal emission offered

the possibility of estimating the attenuation distance of the lunar surface, giving loss tangents of 0.02 or less.

An independent confirmation was made by Tyler (1968) using the telemetry carrier frequency of 136 MHz on Explorer 35. By measuring the Brewster angle as the orbiter swung around the moon, he obtained a dielectric constant of 3.0 ± 0.2. By substituting this value into a two-layer model of the surface, he obtained a loss tangent on the order of 0.01.

Several workers also published measurements of the dielectric properties of well dried terrestrial materials (Parkhomenko, 1967; Campbell and Ulrichs, 1969; Saint-Amant and Strangway, 1970). The salients points of these studies are shown in Figures 2-5 to 2-8. Both the dielectric constant and the loss tangent increase with decreasing frequency and with increasing temperature. The solids have a very high dispersion at low frequencies (probably related to grain boundaries), which seems to mask other effects. The powders show Debye-type relaxations that appear to be associated specifically with hydrous minerals. However, at high frequencies the dielectric constant and loss tangent approach a constant of about 3 and 0.01 respectively, and depend more on density than composition.

Three groups of workers have now published dielectric measurements on returned lunar samples: Chung et. al., (1970, 1971), Collett and Katsube (1971), and Gold et. al., (1970, 1971).

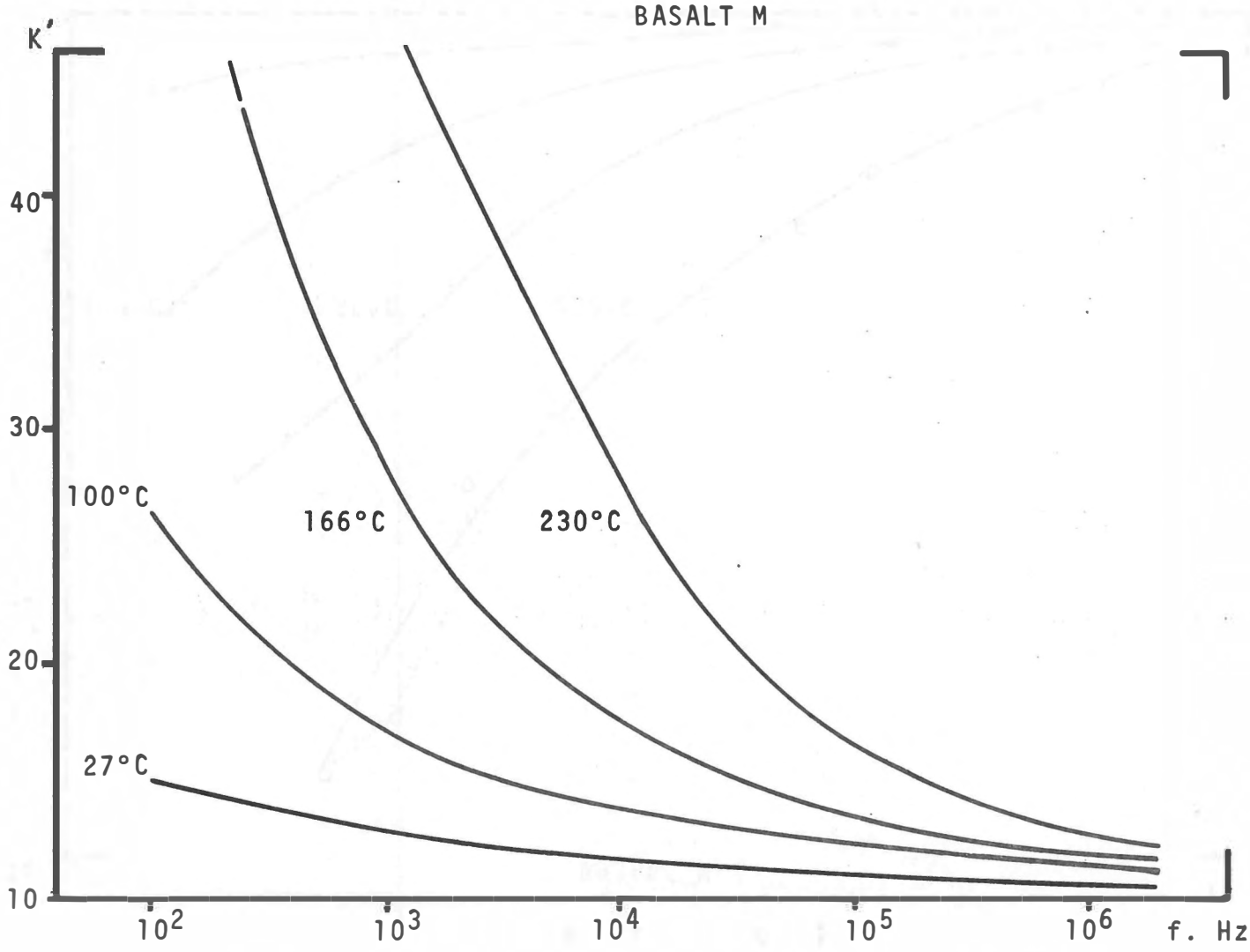

FIGURE 2-5: DIELECTRIC CONSTANT OF SOLID BASALT (AFTER ST. AMANT, 1968)

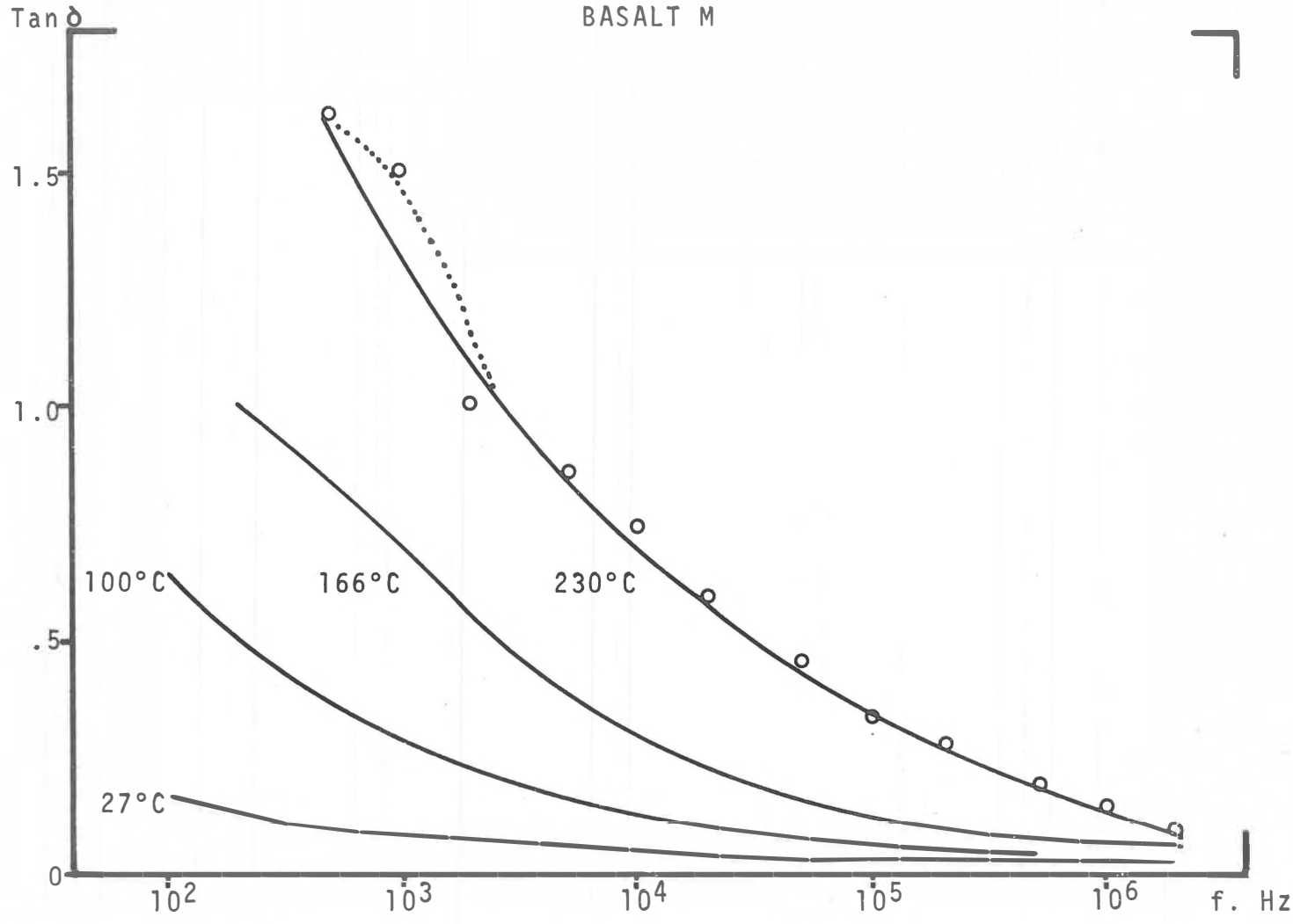

FIGURE 2-6: LOSS TANGENT OF SOLID BASALT (AFTER ST. AMANT, 1968)

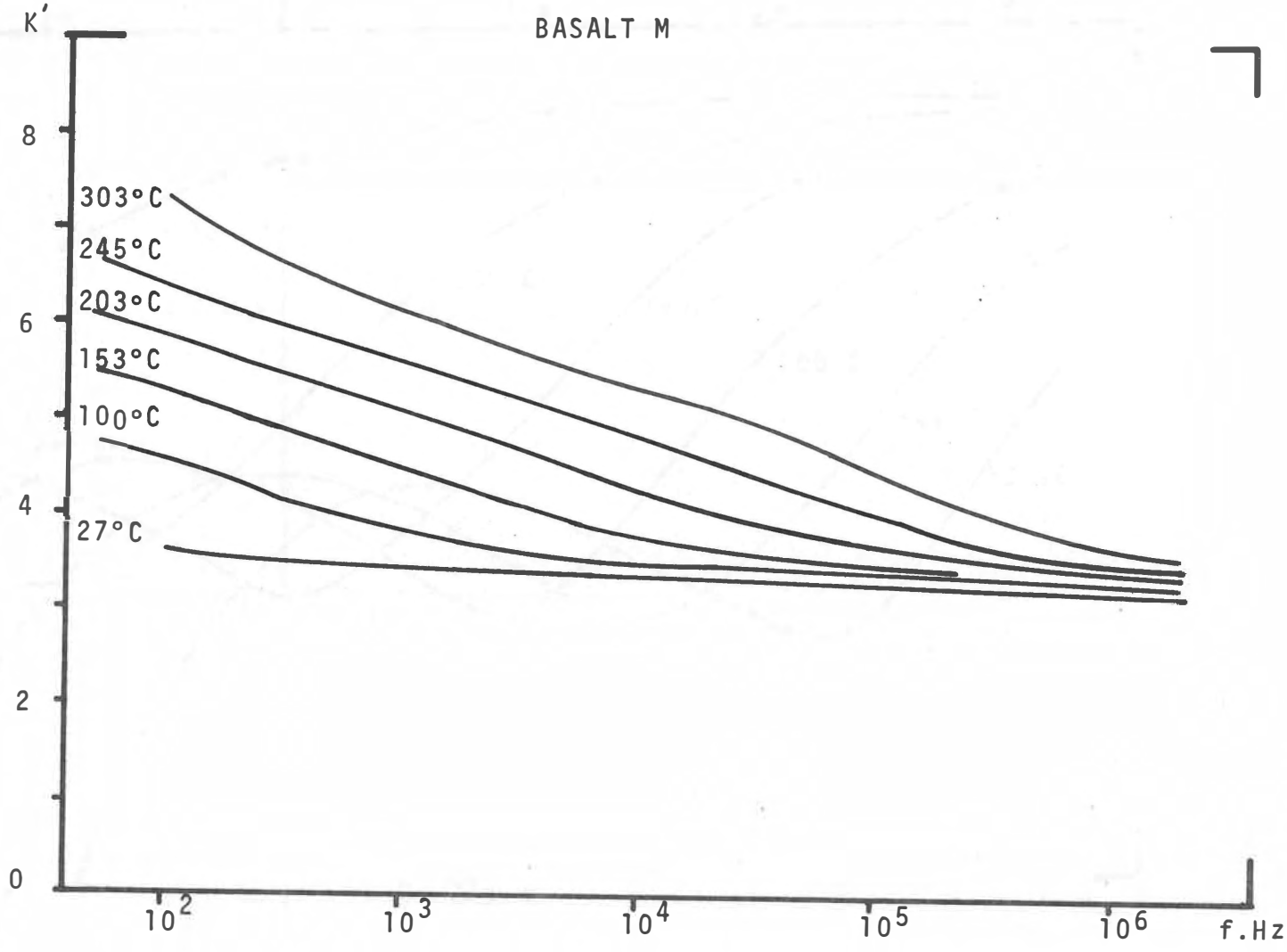

FIGURE 2-7: DIELECTRIC CONSTANT OF POWDERED BASALT (AFTER ST. AMANT, 1968).

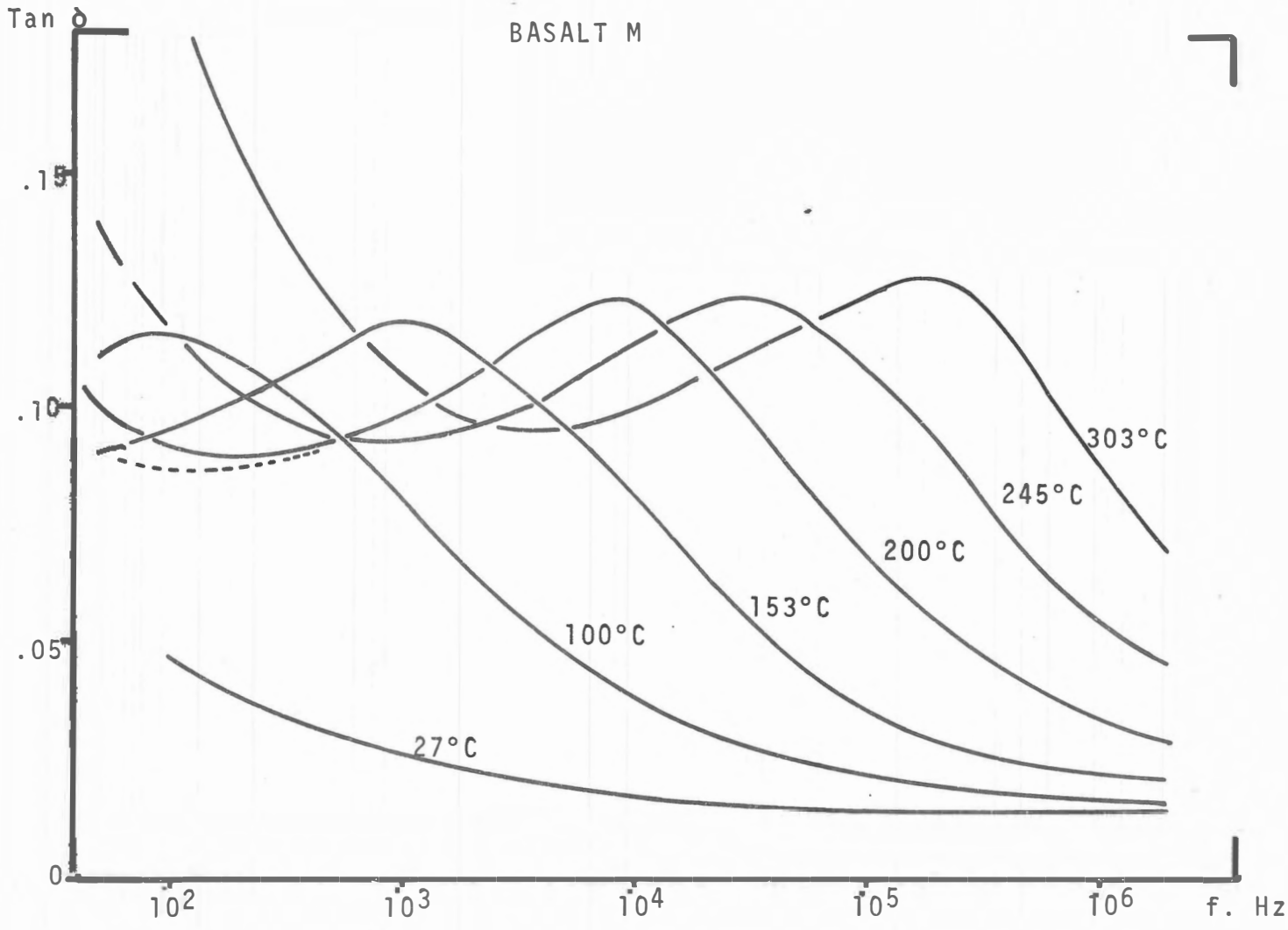

FIGURE 2-8: LOSS TANGENT OF POWDERED BASALT (AFTER ST. AMANT, 1968)

A summary of their results is given in Table 2-2. The measurements are of two major types: (a) the samples have been exposed to the earth's atmosphere for long periods (i.e. during transportation and storage); and (b) the samples have been maintained in "dry" nitrogen except for short periods (on the order of hours). These two sets of data are summarized in Figures 2-9 and 2-10, called "wet" and "dry" respectively. Temperature-dependent data measured by Chung et. al., is shown in Figures 2-11 to 2-14.

The composition of the lunar samples is similar to that of terrestrial vesicular basalts. The mineral content is roughly as follows:

Plagioclase	20 - 25%
Pyroxene	30 - 50%
Olivine	5 - 30%
Ilmenite	5 - 15%
Others	0 - 10%

Terrestrial basalts might have a composition similar to Cape Neddick basalt (Figures 2-5 to 2-8):

Plagioclase	55%
Pyroxene	25%
Olivine	20% (from Chung et. al., 1970).

The most significant difference is the ilmenite component.

The results obtained from the different authors agree fairly well, especially when they are separated by technique into "wets" and "drys". A good calibration point on the accuracy of these measurements can be made by comparing the results of

Workers	Samples (1)	Type	Frequency (Hz)	Temperature (^{o}K)	Density (g./cm^3)	K_∞	tan δ	Comments
Chung,	10020	Igneous	$10^2 - 10^7$	77 - 473	3.18	10 - 15	0.09 - 0.20	All samples except
Westphal,	10057	Igneous	$10^2 - 10^7$	77 - 473	2.88	9 - 13	0.09 - 0.20	12002 exposed to
and								atmosphere for
Simmons	10046	Breccia	$10^2 - 10^7$	77 - 473	2.21	6 - 9	0.05 - 0.09	long periods; some
(1970,	12002.58	Igneous	$10^2 - 10^7$	78 - 473	3.30	8 - 10	0.02 - 0.09	baking.
1971)	12022.60	Igneous	$10^2 - 10^7$	78 - 473	3.32	7 - 14	$.00^2$ - 0.20	12002 exposed for
	12022.95	Igneous	$10^2 - 10^7$	78 - 473	3.32	7 - 14	$.00^2$ - 0.20	short period.
Collett	10017	Igneous	$10^3 - 10^7$	298	3.10	9	0.20 - 0.90	Samples 12002 and
and	10065	Breccia	$10^3 - 10^7$	298	2.46	8	0.02 - 0.13	10065 exposed to
Katsube	10084	Fines	$10^3 - 10^7$	298	—	3	.009 - 0.10	atmosphere for
(1971)	12002.84	Igneous	$10^3 - 10^7$	298	3.10	8 - 9	.013 - 0.05	short periods.
	12002.85	Igneous	$10^3 - 10^7$	298	3.04	7 - 9	0.01 - 0.04	10017 measured
	12070	Fines	$10^3 - 10^7$	298	—	3	.005 - 0.12	differently; it also has high ilmenite content.
Gold,	10084	Fines	450×10^6	298	1.0 - 1.6	1.8 - 2.5	.006 - 0.01	All samples
Campbell,	10022	Igneous	450×10^6	298	3.1	5.2	0.06	assumed to have
and	10059	Breccia	450×10^6	298	2.2	5.9	0.05	been exposed to
O'Leary	12070	Fines	450×10^6	298 (2)	1.2 - 1.8	1.9 - 3.0	.004 - .008 (3)	atmosphere;
(1970,	12033	Fines	450×10^6	298	1.2 - 1.75	1.8 - 2.6	.005 - .006	no mention of
1971)	12063	Igneous	450×10^6	298	2.9	6.9	0.08	baking.
	12065	Igneous	450×10^6	298	2.9	7.3	0.08	

Notes: (1) 10000 series from Apollo 11; 12000 series, Apollo 12.
(2) Assumed temperature
(3) Calculated from formula in Campbell & Ulrichs (1969), p. 5873.

Table 2 - 2: Summary of Lunar Sample Dielectric Measurements

FIGURE 2-9: SUMMARY OF DIELECTRIC MEASUREMENTS ("WET")

LUNAR SAMPLES

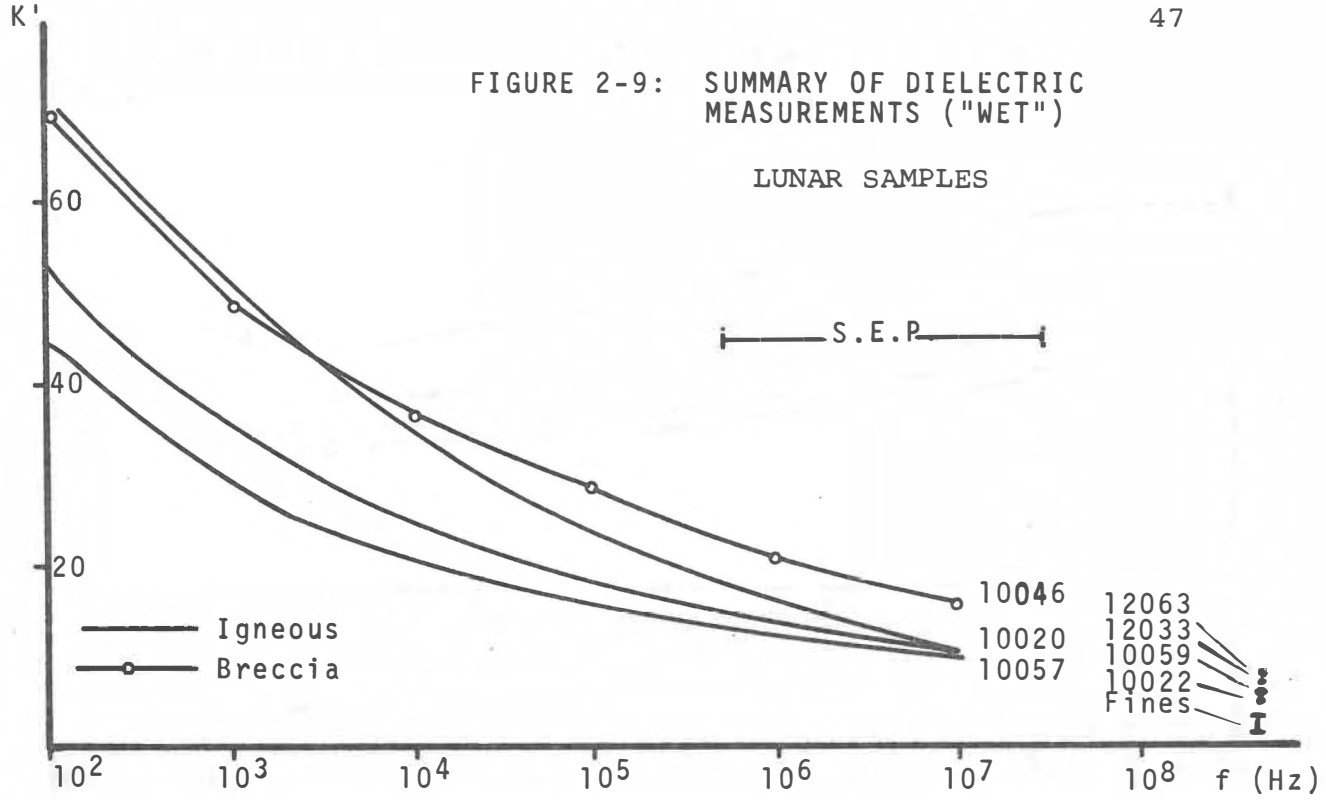

Dielectric Constant vs. Frequency at 298°K

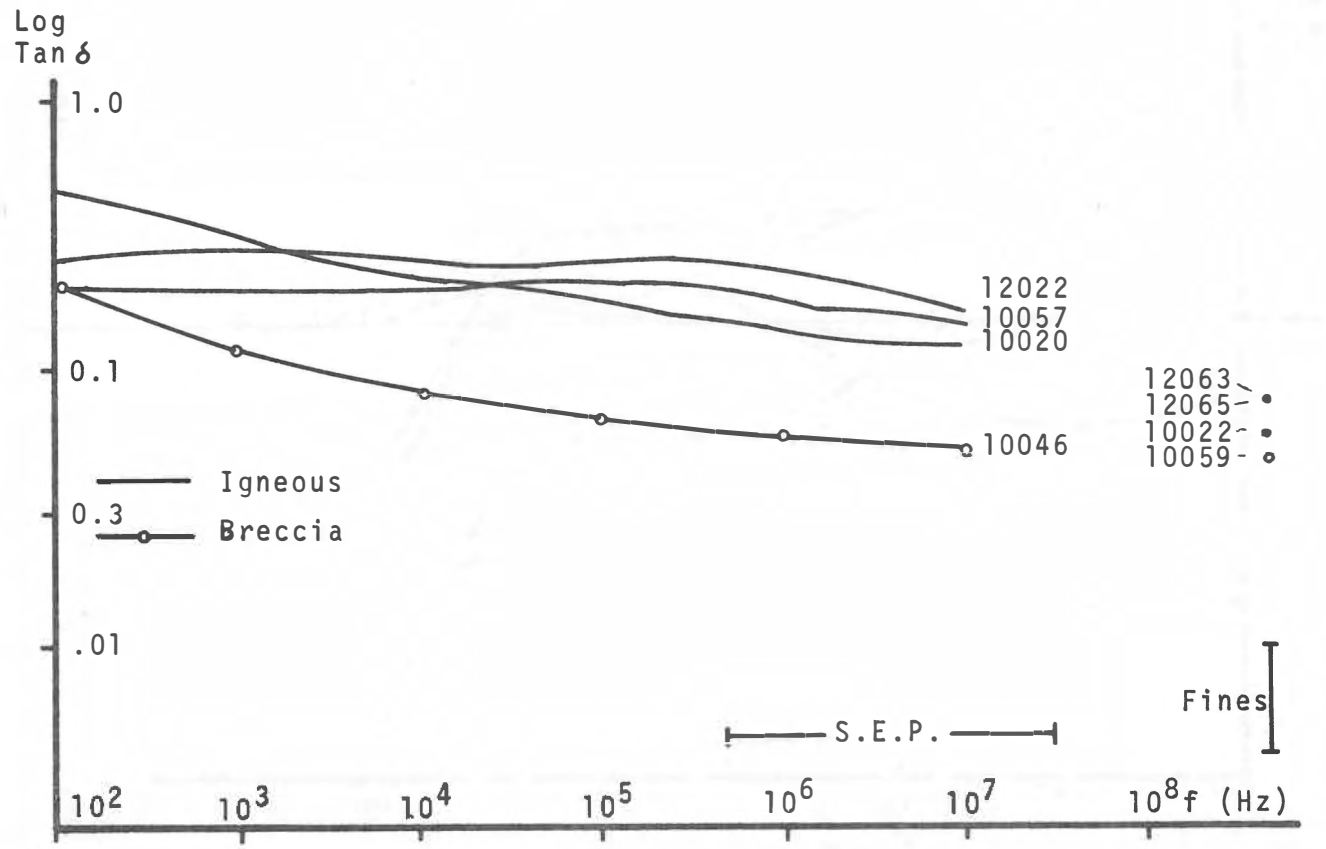

Loss Tangent vs. Frequency at 298°K

FIGURE 2-10: SUMMARY OF DIELECTRIC MEASUREMENTS ("DRY")
LUNAR SAMPLES

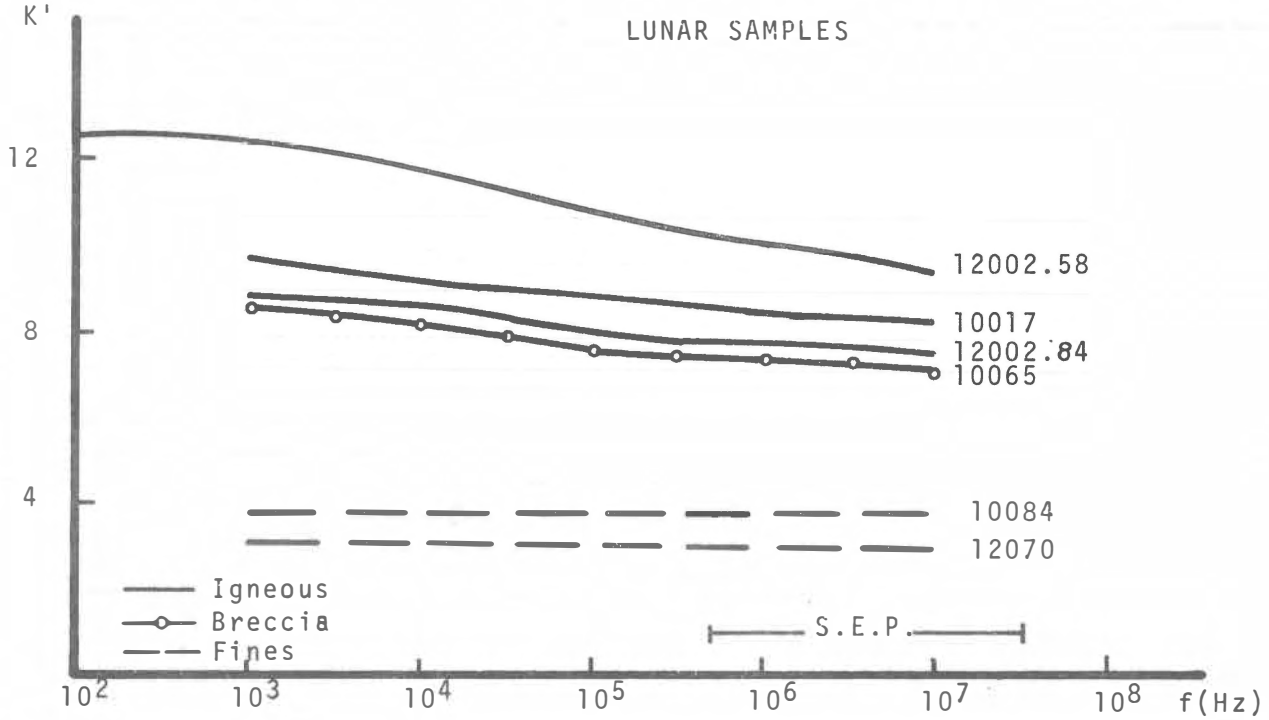

Dielectric Constant vs. Frequency at 298°K

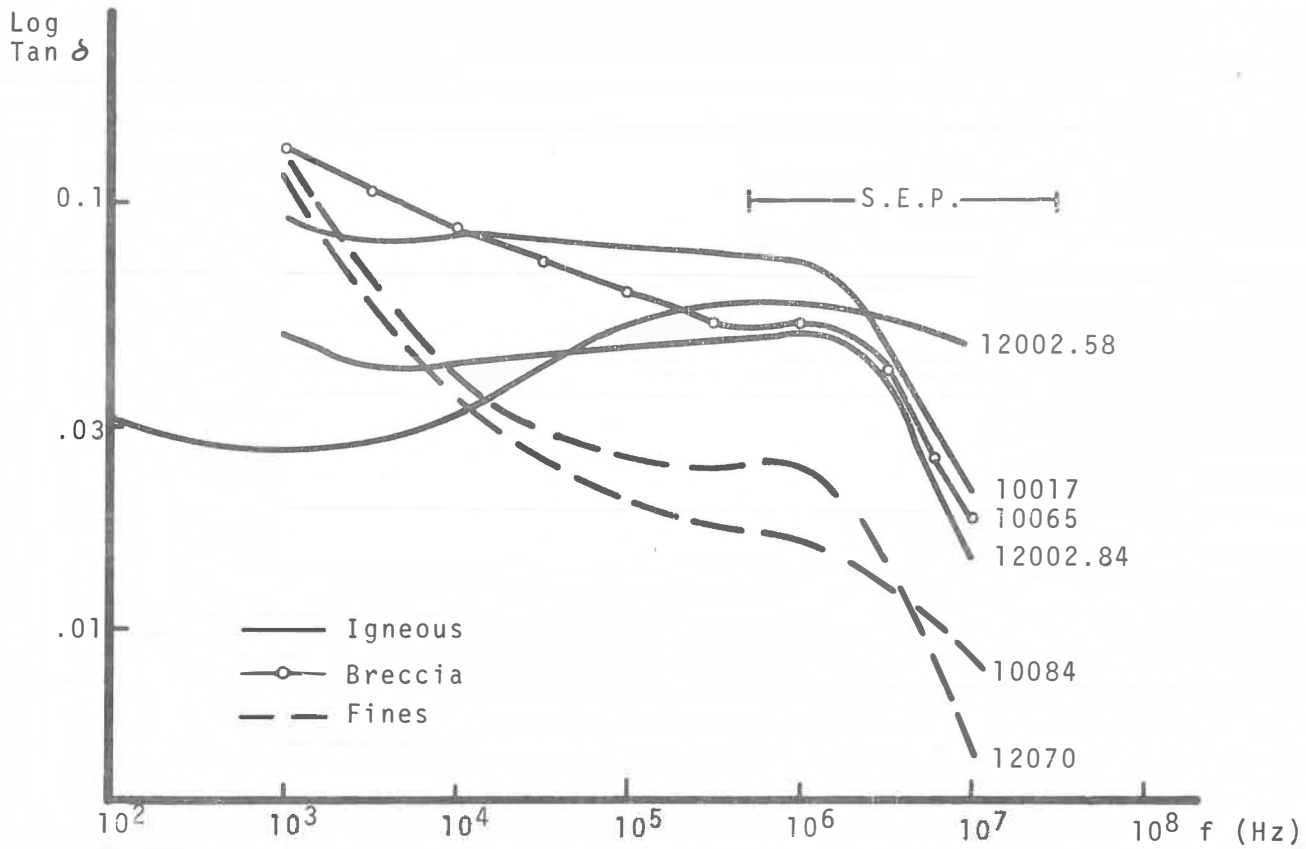

Loss Tangent vs. Frequency at 298°K

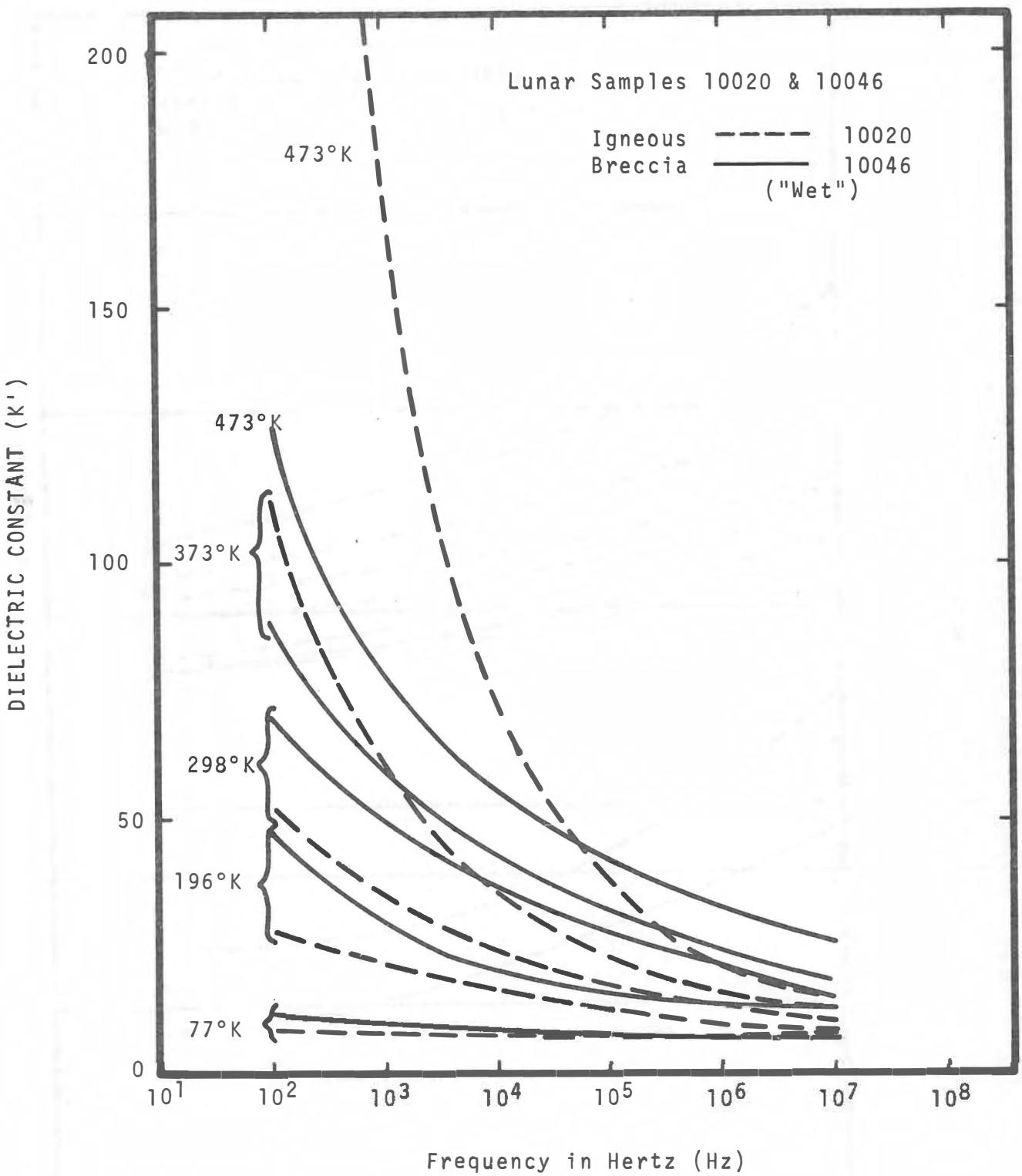

FIGURE 2-11: AFTER CHUNG ET AL (1970)

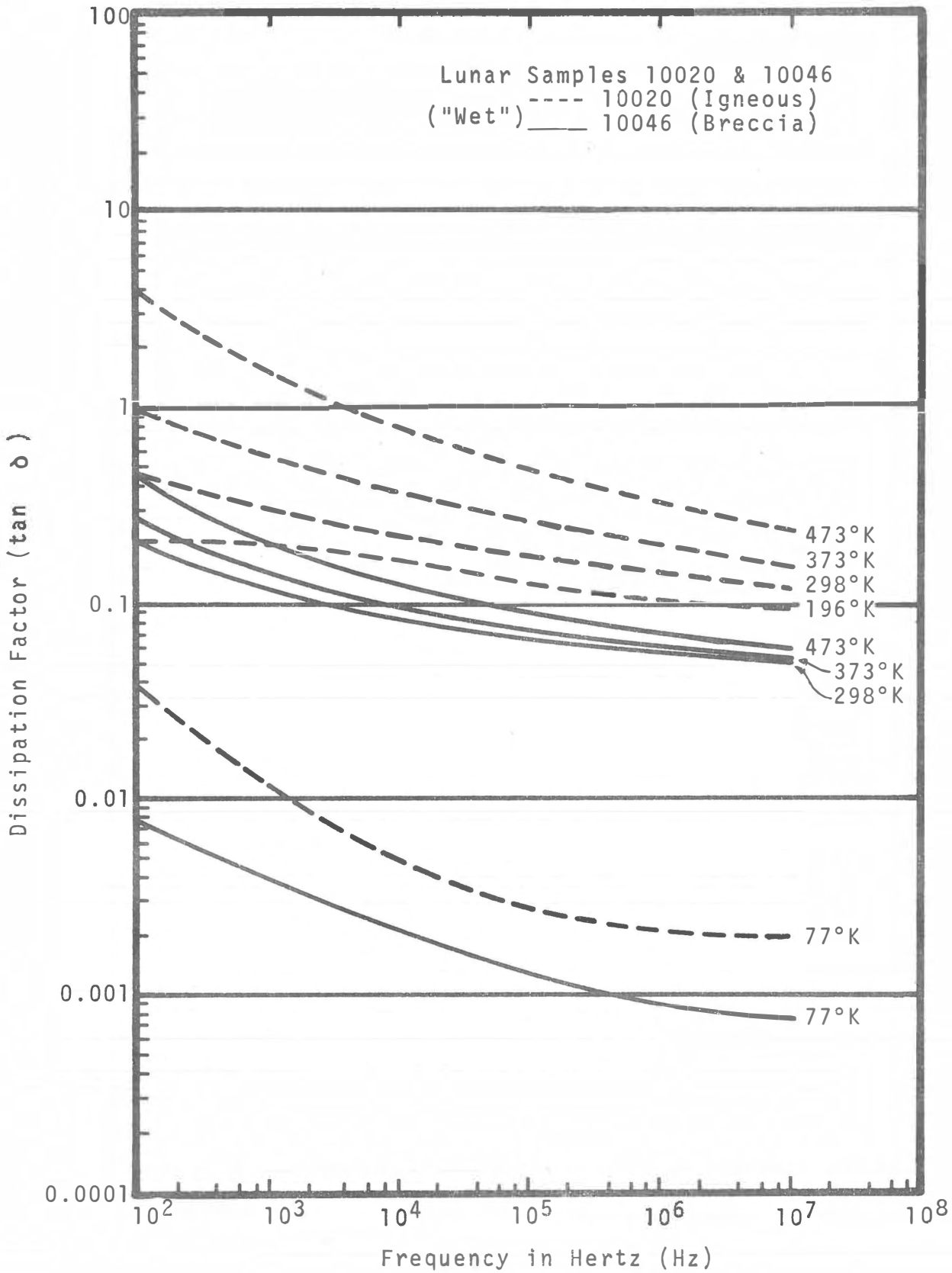

FIGURE 2-12: AFTER CHUNG ET AL (1970)

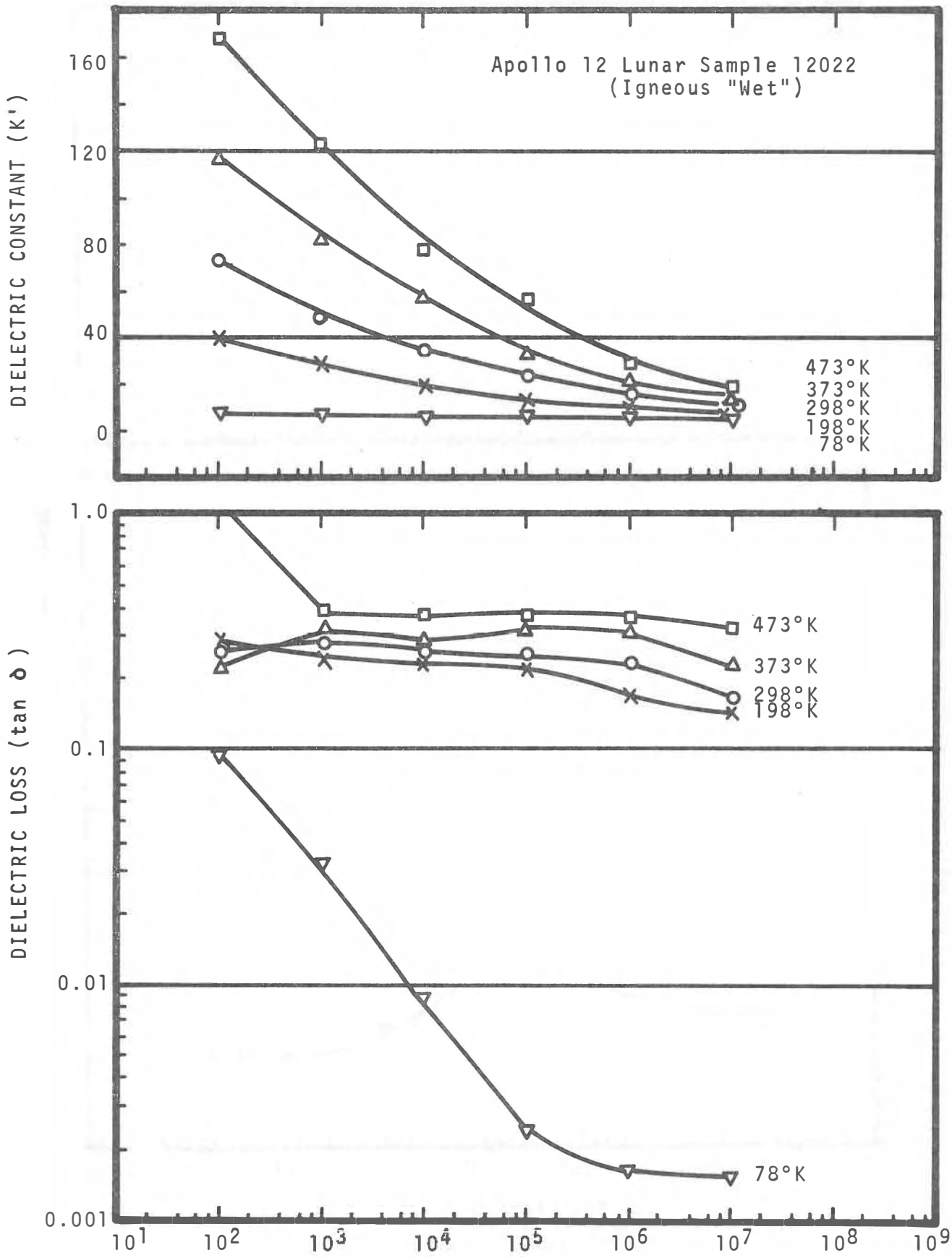

FIGURE 2-13: AFTER CHUNG ET AL (1971)

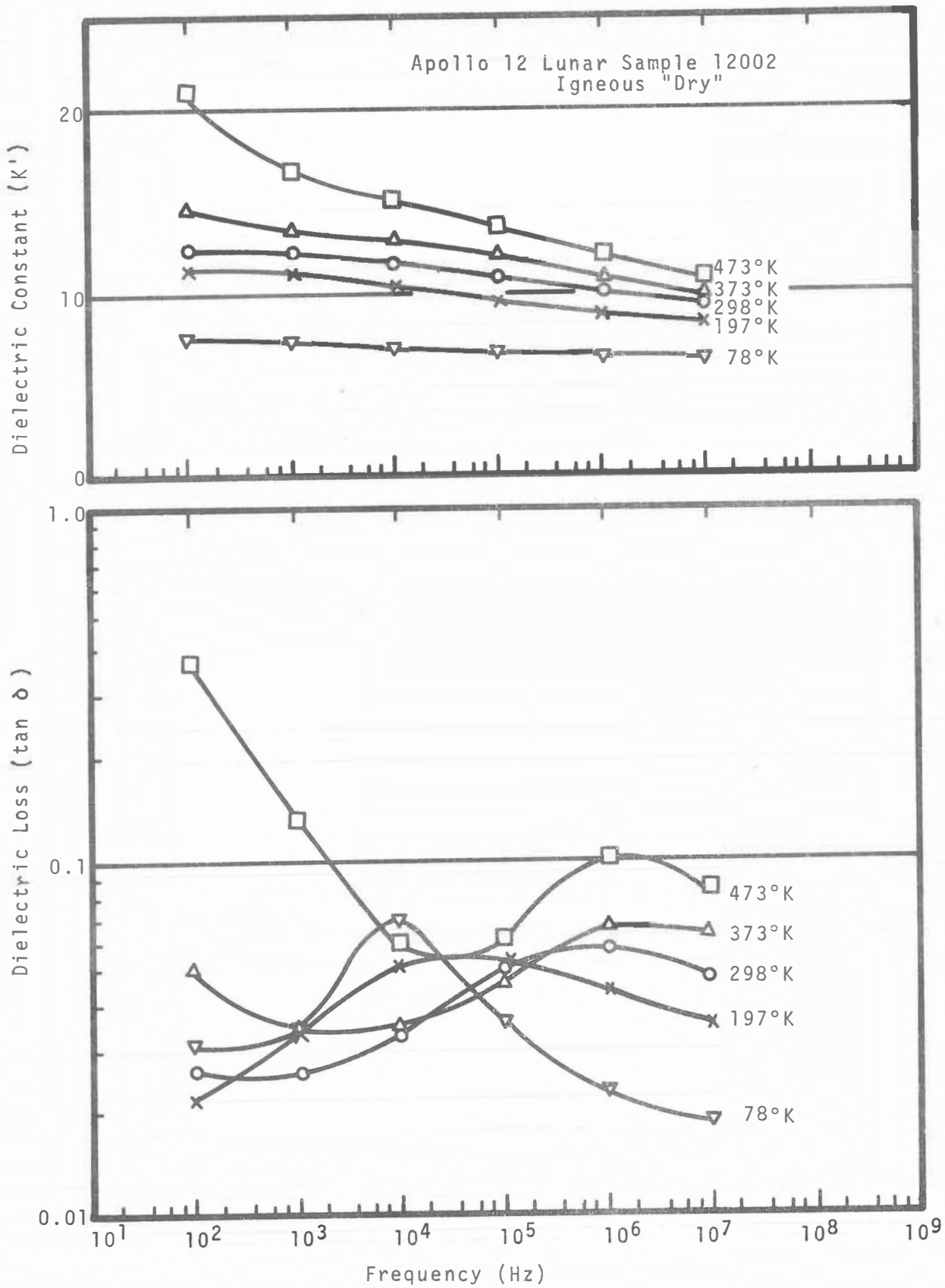

FIGURE 2-14: AFTER CHUNG ET AL (1971)

two workers, using similar techniques, on sample 12002 (Figure 2-10). There do not seem to be any systematic differences between the igneous and the breccia samples (contrary to Chung et. al., 1970), although differences might be expected, since the densities differ by about 20%. The fines have consistently lower K' and tan δ, and Gold et. al., have shown that these depend in a regular way on density, and that they agree with previous radiometric data.

Comparing Figures 2-5 to 1-8 with Figures 2-9 to 2-14, several conclusions can be drawn. First, although there is considerable variation among terrestrial basalts, the lunar samples have consistently higher dielectric constants and loss tangents than terrestrial rocks. Both Chung et. al., and Collett and Katsube have suggested that this is caused by the larger ilmenite content of the lunar material. Since ilmenite has a high dielectric constant (35 to 80, compared with 4 to 11 for the other minerals), and since it is fairly conductive, it may well account for the higher K' and tan δ. Chung et. al., have also stated that a Maxwell-Wagner type of effect contributes to the higher values, but they don't say why it would be more important in lunar material.

The second feature is that the lunar "wets" have considerably higher values for dielectric constant and loss tangent than the "drys". It seems clear that this is due to larger amounts

of residual water in the "wet" samples — by comparing Figures 2-11 and 2-13 with Figure 2-15, it appears that they could have absorbed about 0.8% water. The water would also account for the drastic change seen at 78°K. At this temperature the water is presumably frozen, although it is not frozen at 197°K because of a high dissolved-ion concentration.

Thirdly, there is a pronounced relaxation loss peak observed for all the "dry" samples (seen about 1 MHz at room temperature). It is likely that this is due to very small amounts of residual moisture, even in these samples, although none of the authors mentions this. However, Chung is now satisfied that none of his samples was baked sufficiently to remove all traces of water (private communication from A. R. von Hippel). Although great care was taken to avoid moisture contamination, the dry nitrogen in which the samples were stored passes over open dunk tanks in the NASA Lunar Receiving Laboratory (D. W. Carrier, private communication).

The significance of this is that the contamination may mask all other effects. Several studies have been made on the effects of small amounts of water on the dielectric properties of rocks (see St. Amant, 1968; Saint-Amant and Strangway, 1970; Parkhomenko, 1967). These studies show that water is absorbed very easily by rocks, and is very difficult to remove—often requiring baking in a good vacuum, for several days, at temperatures of 200°C. or higher. Although all the "dry" lunar samples

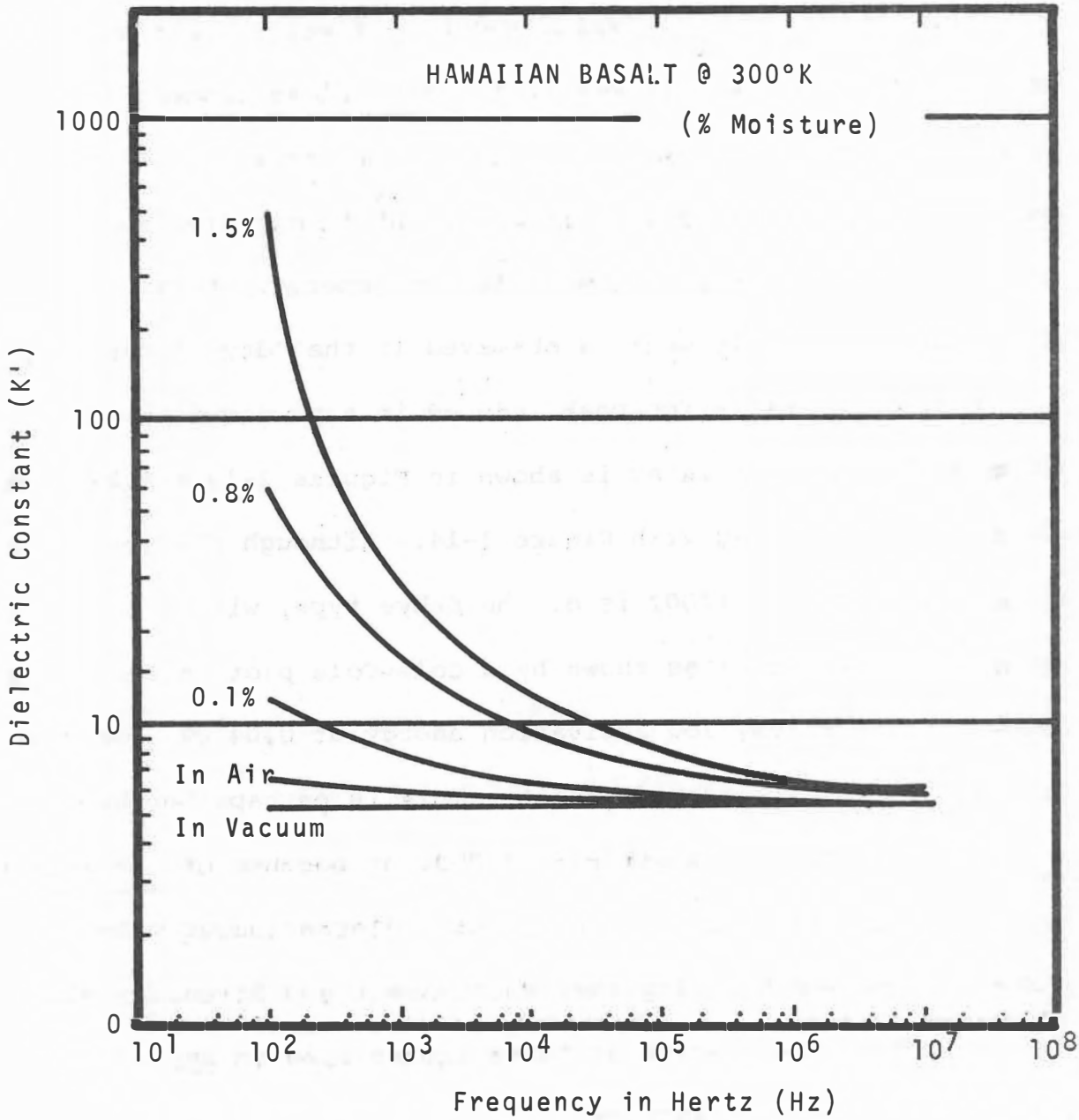

FIGURE 2-15: EFFECT OF SMALL AMOUNTS OF WATER ON A TERRESTRIAL BASALT (AFTER CHUNG ET AL, 1970)

were exposed to the atmosphere (except possibly 10017), none of them went through this type of baking.

The addition of very small amounts of water has the effect of raising the dielectric constant and the loss tangent in a fairly uniform way if there is enough of it present. In tiny amounts it is not clear what it does, but it may give a Debye-type relaxation with very low activation energy. These two phenomena are exactly what is observed in the "dry" lunar samples.

A typical relaxation peak induced in a powdered basalt by the addition of 0.5% water is shown in Figures 2-16 and 2-17, which can be compared with Figure 1-14. Although the relaxation peak of sample 12002 is of the Debye type, with a small spread in frequencies as shown by a Cole-Cole plot in Figure 2-18), it has a very low activation energy of 0.04 ev, compared to 0.8 ev for the powdered basalt. This is perhaps because there is less than 0.5% water in 12002, or because of the smaller pore space of the solid sample giving a discontinuous water phase. It is worth noting that Saint-Amant and Strangway did not see a Debye relaxation at these frequencies in <u>any</u> of their solid <u>dry</u> terrestrial samples.

Therefore, it is very likely that water has masked all other effects in the measurements of dielectric properties of lunar samples. This gives unrealistically high values for both the dielectric constant and the loss tangent. Any relaxation

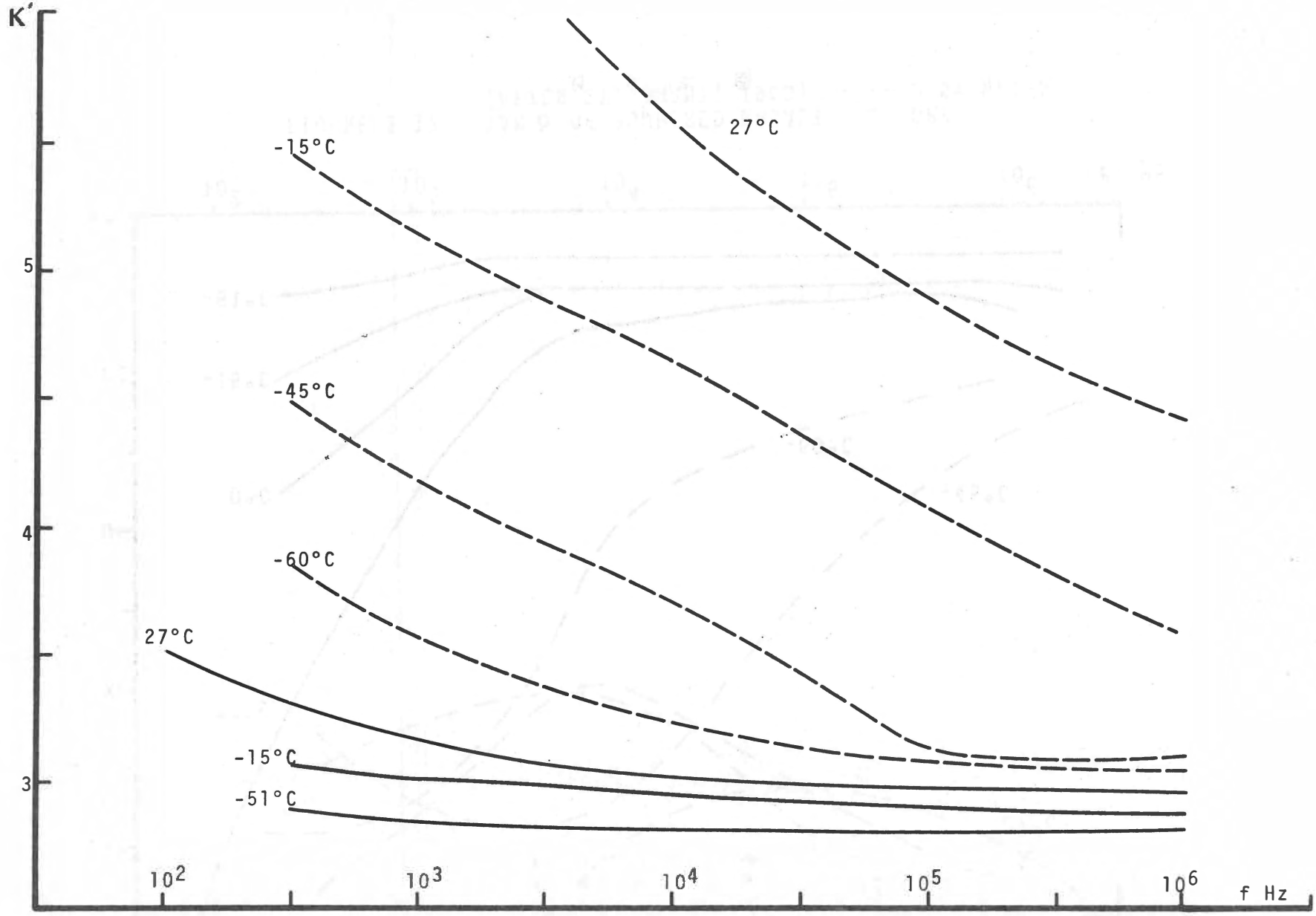

FIGURE 2-16: DIELECTRIC CONSTANT OF POWDERED BASALT, ___ DRY, --- 0.5% WATER, (AFTER ST. AMANT, 1968)

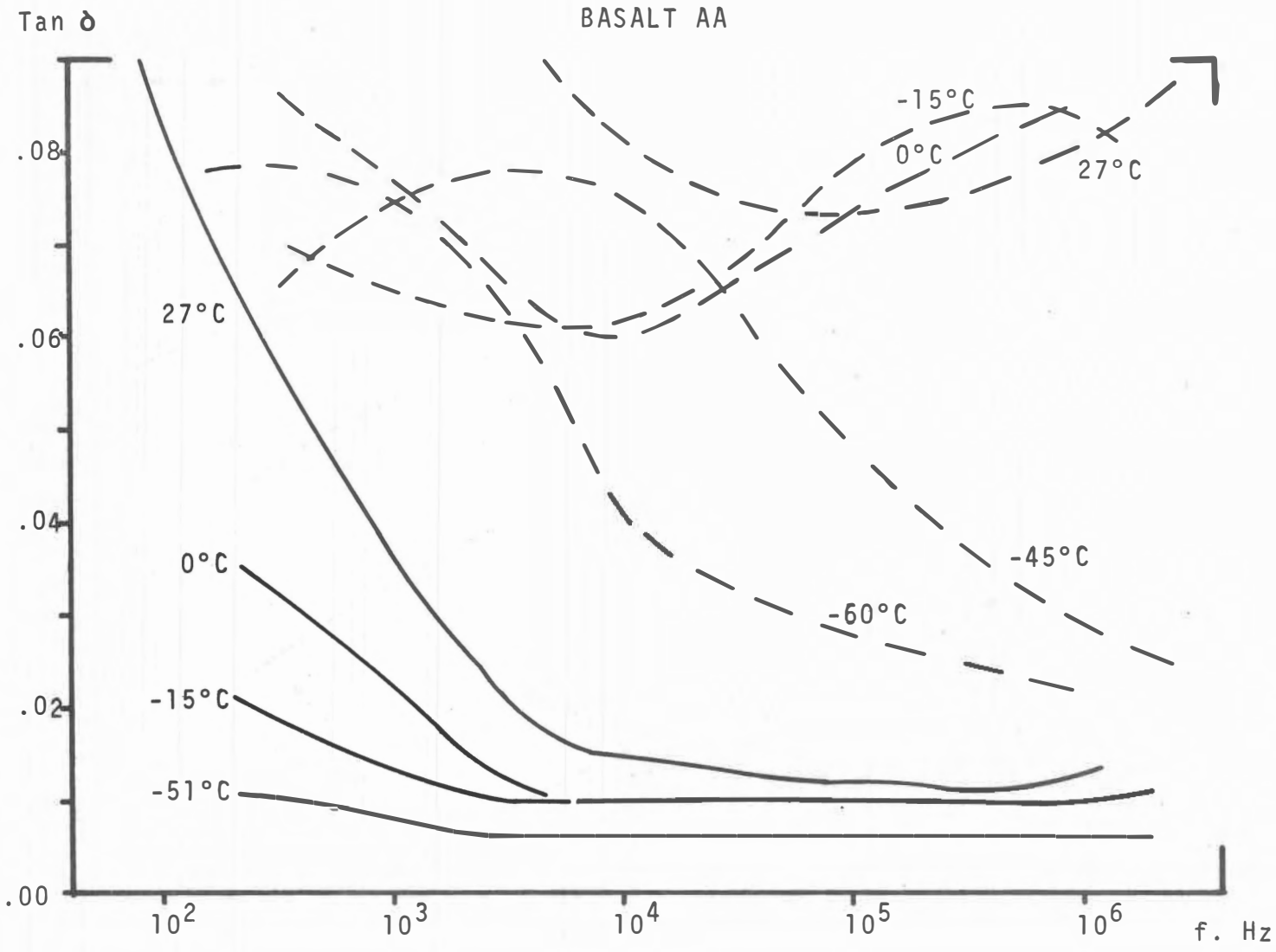

FIGURE 2-17: TAN δ OF POWDERED BASALT ——— DRY
(AFTER ST. AMANT, 1968) ---- 0.5% WATER

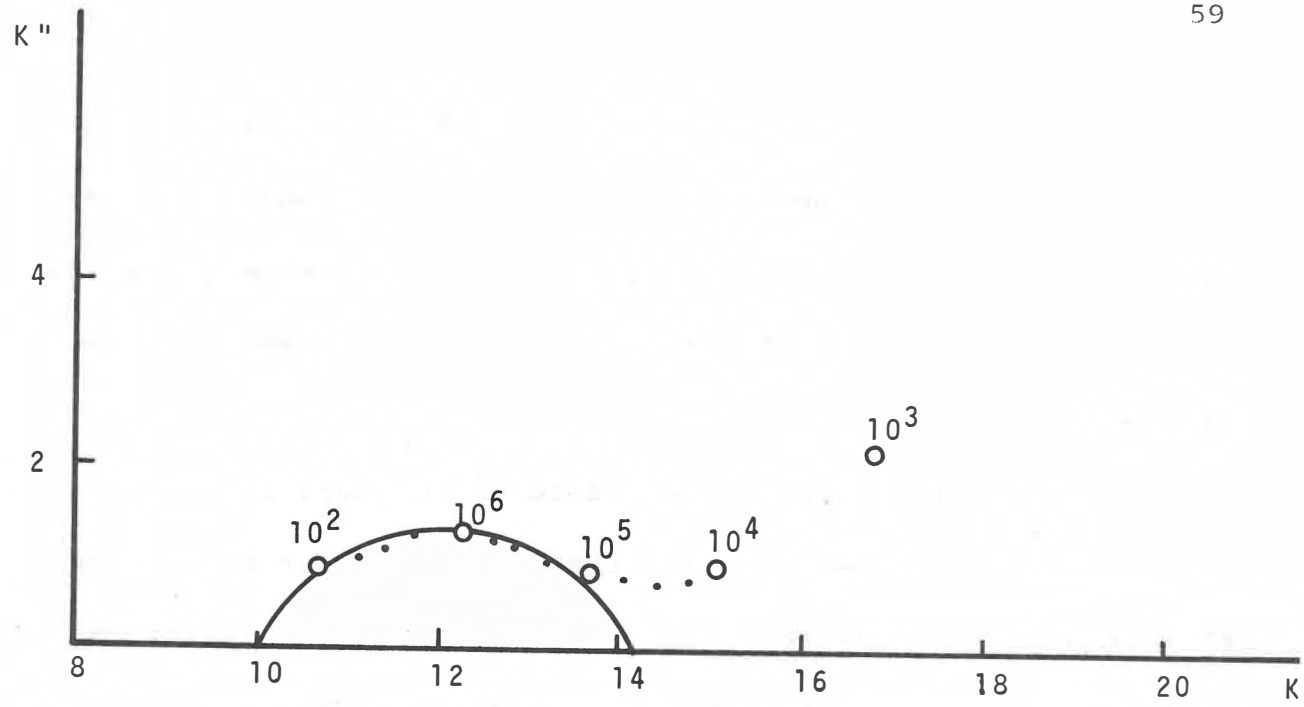

Cole - Cole Plot for Igneous Sample 12002.58 at 473°K

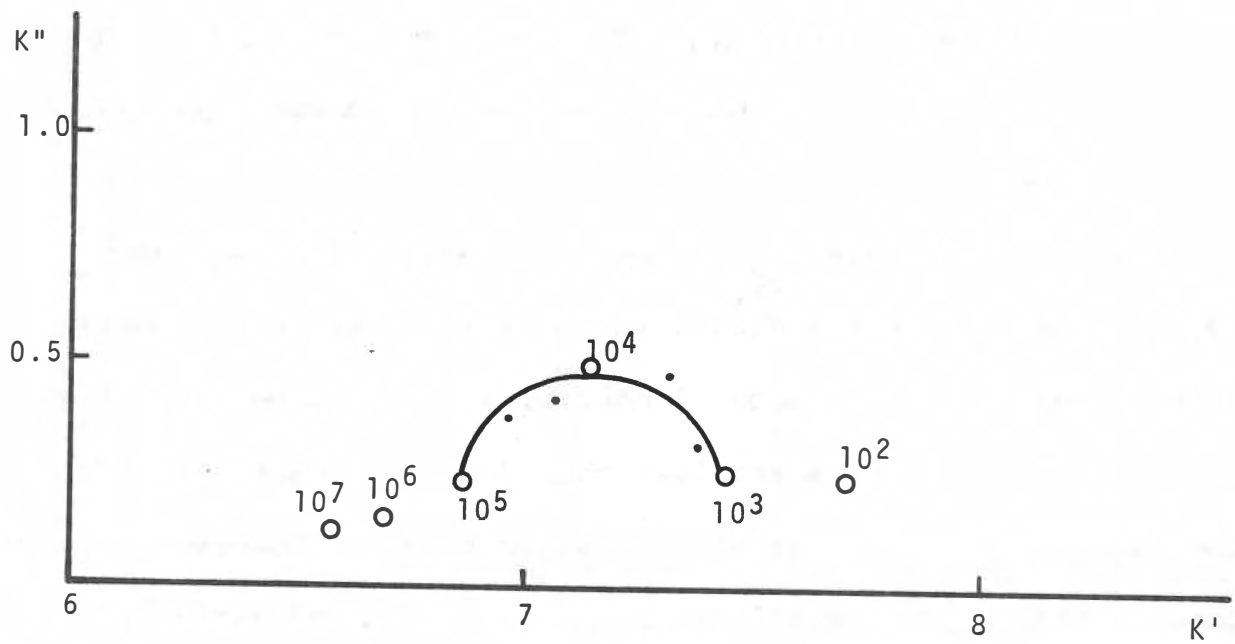

Cole - Cole Plot for Igneous Sample 12002.58 at 78°K

FIGURE 2-18: COLE - COLE PLOTS OF SAMPLE 12002, FROM DATA OF CHUNG ET AL (1971)

phenomena may have been obscured (although more measurements on powders will be necessary to confirm this). Only by more fastidious attention to the possibility of water-contamination, or by more prolonged baking of the samples, will this problem be resolved.

Although it is likely that residual moisture is very important in the lunar results, there may be other mechanisms at work as well. Certainly the large amounts of ilmenite may be important. There might be greater Maxwell-Wagner effects at grain boundaries because of imperfections caused by the much greater radiation bombardment on the moon (suggested by D. W. Strangway). This could be tested by radiating terrestrial samples before and after dielectric measurements. Also, magnetic losses may be important on the moon (Strangway et. al., 1970c: Olhoeft, 1970).

Eddy currents are also a possible source of losses and would not appear in the dielectric measurements. For ilmenite, with a conductivity of about 1 mho/m., a relative permeability of about 1, and grain sizes less than 700 μm. (Cameron, 1970), the maximum absorption is at 10^{12} Hz or higher. However, Cameron also reports small amounts (0.5 - 1.5%) of native iron uniformly disseminated throughout a number of lunar samples. Although this is not sufficient to raise the bulk conductivity significantly, eddy currents may be present. Substituting iron's conductivity of 5×10^{6} mhos/m., relative permeability

of 1000, and grain sizes of 30 μm. or smaller into the induction number (given in Section 2.2), eddy current loss could be significant at frequencies of 0.5 MHz and greater.

Therefore, it seems that the available data on the dielectric properties of lunar samples is inconclusive. Work needs to be done on very well dried samples, over a wide range of temperatures, in order to fully understand the dielectric mechanisms involved. No temperature-dependent measurements have been made on powders or fines; these typically would give more information than solid samples. Finally, experiments to discover any magnetic losses, eddy currents, or radiation effects should be undertaken.

2.4 Dielectric Properties of Ice

A geological area that would reasonably analogue the lunar surface was required in order to test the feasibility of the interference method. Although most terrestrial rocks have intrinsically high resistivities of 10^{12} to 10^{17} Ω-m. (giving the dielectric properties described in the last section), the presence of pore water decreases the resistivity to 10 to 10^{9} Ω-m. (Grant and West, 1965, p. 393). In fact it is difficult to find large areas with resistivities higher than 10^{4} or 10^{5} Ω-m. From calculations like those shown in Figure 1-8, it was decided that a loss tangent of 0.03 or less was needed to test the interferometry method. This implies a D.C. conductivity of 10^{-5} to

to 10^{-7} mhos/m. for the frequencies used, even if there were no other effective loss mechanisms (see Figure 2-19).

Four types of geological region have very high resistivities: (i) salt areas, (ii) permafrost regions, (iii) occasional areas of fresh volcanics, and (iv) ice sheets. However, even the most arid areas do get some rain, and this results in a slightly moist, extremely ion-rich, layer near the surface with a very high conductivity. Similarly, frozen regions have very ion-rich pore water, which does not completely freeze at temperatures as low as -50^{o}C. This again leaves a conductive surface layer with highly variable resistivities (Ogilvy, 1970). Neither of these types of regions have been fully studied. Some volcanic regions have resistivities up to 10^{4} or 10^{5} Ω-m. (e.g. Zohdy and Jackson, 1969), but they are local, poorly mapped, and highly variable (A. A. R. Zohdy, private communication to D. W. Strangway).

However, ice has a very high resistivity — from 10^{5} to 10^{7} Ω-m. (Röthlisberger, 1967; Röthlisberger and Vögtli, 1967). Moreover, the very pronounced relaxation frequency of water molecules at 10^{10} Hz is found at about 10^{4} Hz in ice, and EM pulse soundings have been made by various groups (e.g., Evans, 1963; Jiracek, 1967; and Harrison, 1970). Since glaciers are fairly homogeneous, and have been mapped by several techniques, it was decided to conduct field tests on a glacier. The dielectric properties of ice and snow have been studied by various workers

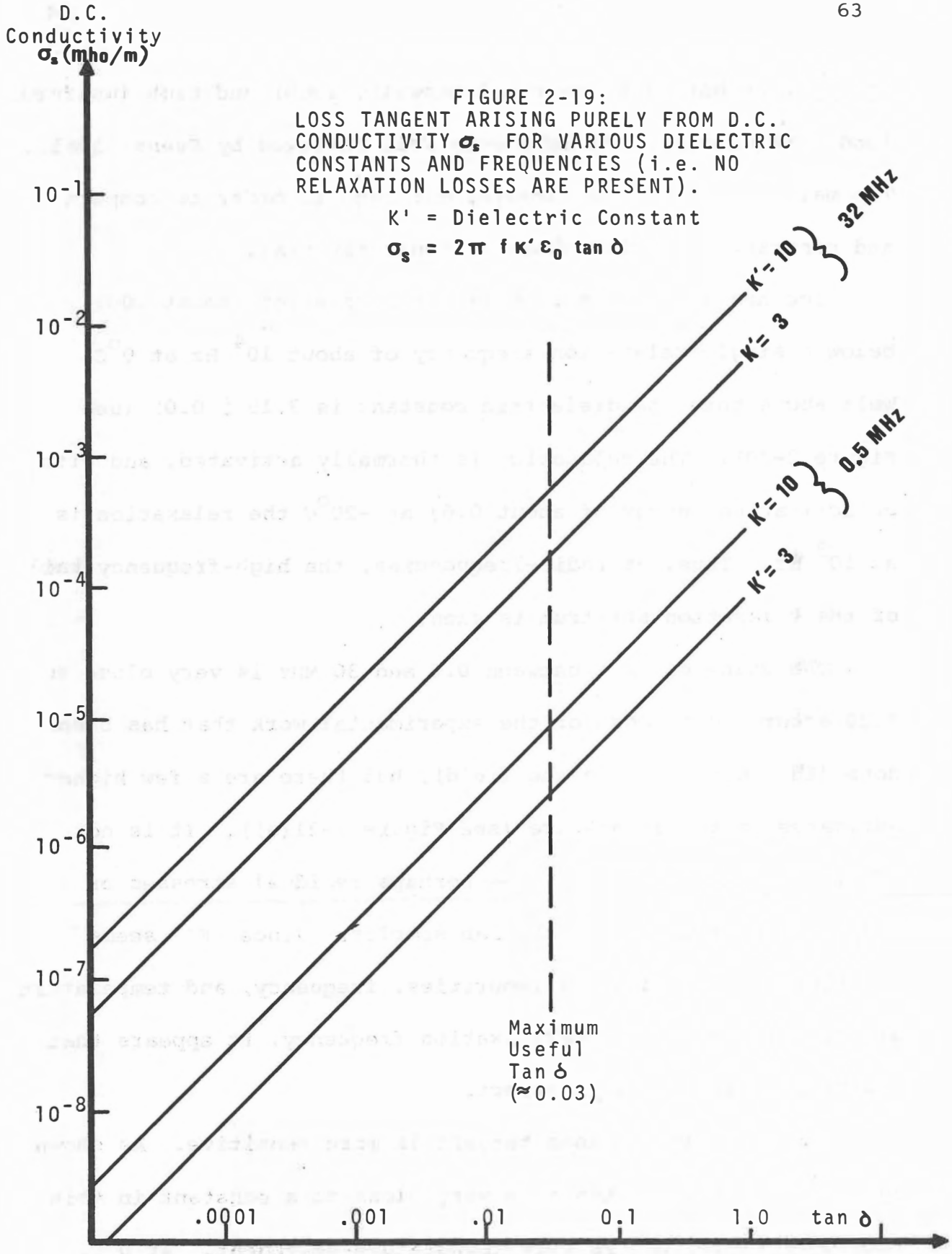

FIGURE 2-19:
LOSS TANGENT ARISING PURELY FROM D.C. CONDUCTIVITY σ_s FOR VARIOUS DIELECTRIC CONSTANTS AND FREQUENCIES (i.e. NO RELAXATION LOSSES ARE PRESENT).

K' = Dielectric Constant

$\sigma_s = 2\pi f K' \varepsilon_0 \tan \delta$

in situ, at both low (Watt and Maxwell, 1960) and high (Walford, 1968) frequencies, and have been well reviewed by Evans (1965). The main points will be brought out here in order to compare and contrast them with those of lunar material.

Ice has a high static dielectric constant (about 100), below a single relaxation frequency of about 10^4 Hz at 0°C. Well above this the dielectric constant is 3.15 ± 0.05 (see Figure 2-20). The relaxation is thermally activated, and with an activation energy of about 0.6; at -20°C the relaxation is at 10^3 Hz. Thus, at radio-frequencies, the high-frequency tail of the relaxation spectrum is seen.

The value of K' between 0.5 and 30 MHz is very close to 3.20 according to most of the experimental work that has been done (including work in the field), but there are a few higher estimates in the literature (see Figure 2-21(a)). It is not clear what these are due to — perhaps residual stresses or temperature gradients in the lab samples. Since K' seems relatively independent of impurities, frequency, and temperature at this distance from the relaxation frequency, it appears that the higher values are incorrect.

The value of the loss tangent is more sensitive. As shown by Figure 2-21(b), $f \tan \delta$ is very close to a constant in this frequency range, but is very temperature-dependent. At 0°C, $f \tan \delta = 0.25$ or 0.30, but at -10°C this has dropped to about

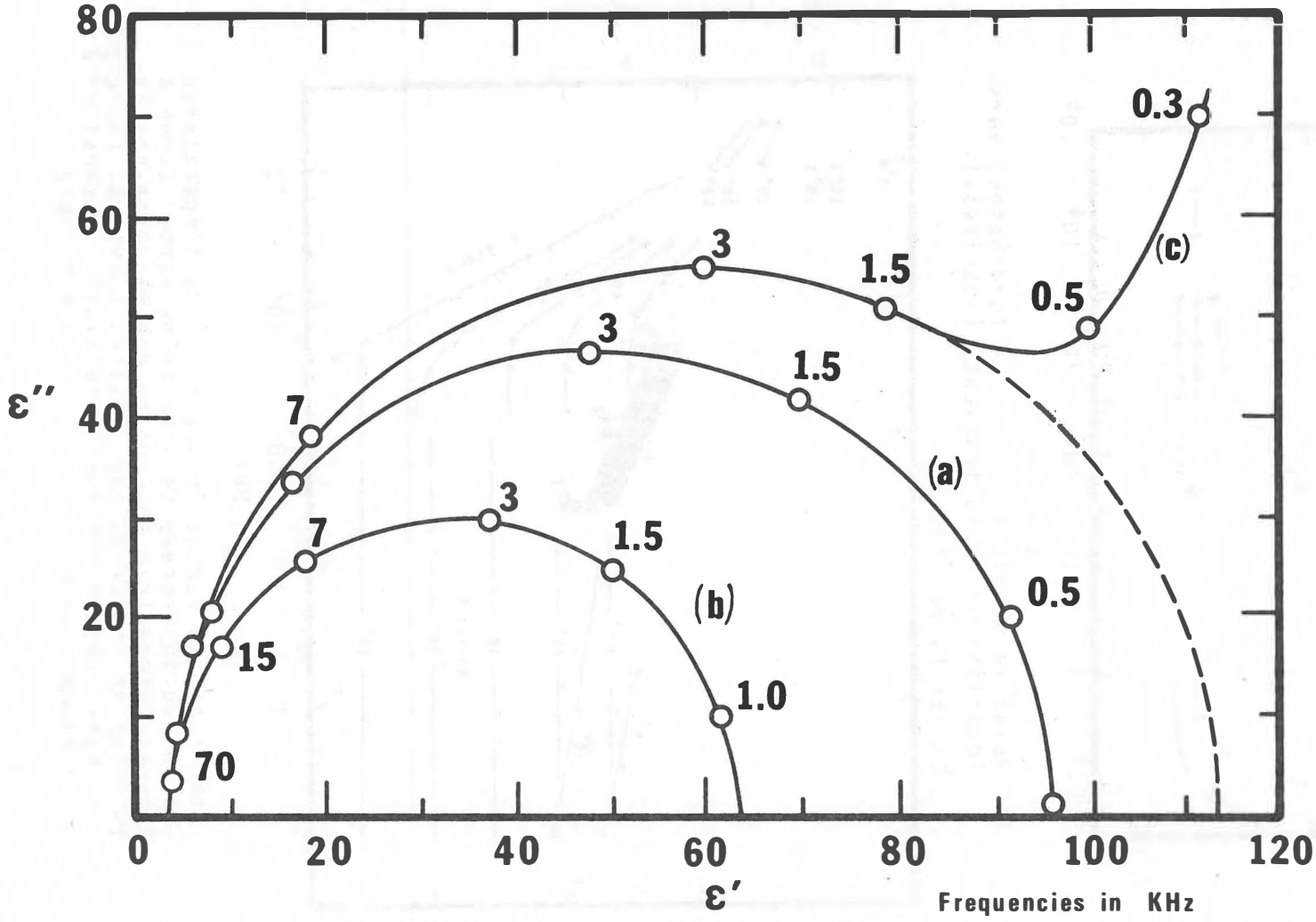

FIGURE 2-20

Cole-Cole Plot For Ice At - 10.8°c.
a. Pure Ice, b. Crack Perpendicular To Field
c. With Impurities, (After Evans, 1965)

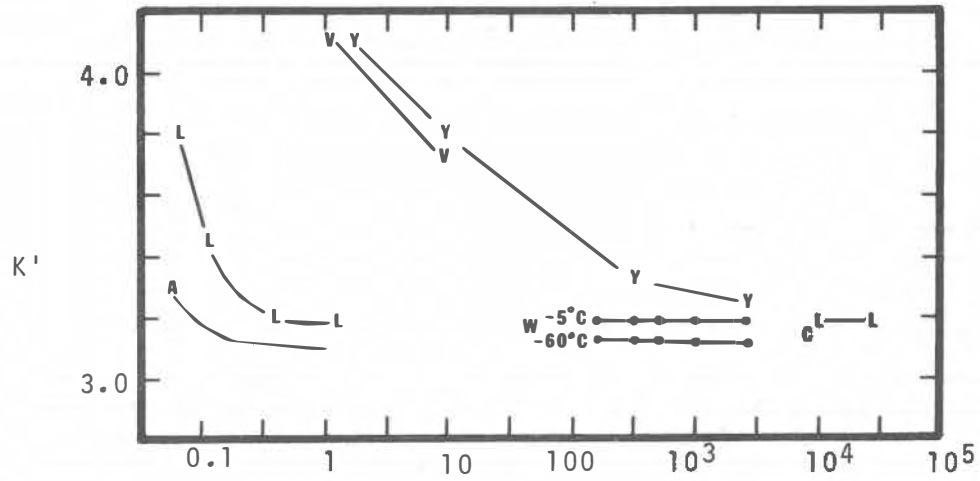

(a) Relative permittivity of ice (ordinates) versus logarithm of radio-frequency (abscissae). (after Evans, 1965)

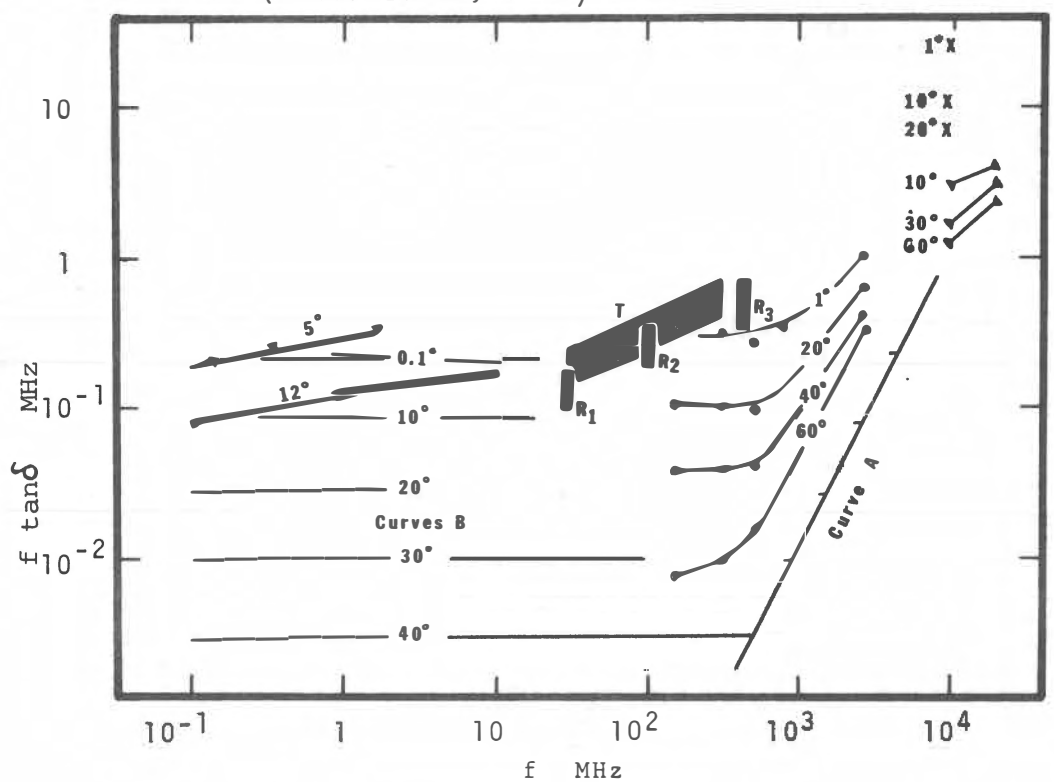

(b) f tan δ of ice versus frequency. Ice temperatures are marked in degrees Celsius below zero. Curve A: Expected dielectric absorption due to resonance absorption at infra-red wavelengths, Curves B: Expected dielectric absorption due to relaxation absorption at lower radio-frequencies (after Walford, 1968).

Figure 2-21: DIELECTRIC CONSTANT AND LOSS TANGENT FOR ICE

0.10. Since most glaciers in the temperate latitudes are very close to the melting point throughout, this sensitivity should not manifest itself. The inverse-frequency dependence implies that losses increase proportionally to the distance rather than to the number of wavelengths that a wave travels. Therefore, an expected maximum depth for sounding (by any radio-frequency means) will apply to whatever wavelength used by that technique.

More troublesome to account for rigorously is the effect of impurities, inhomogeneities, cracks, water, and air bubbles on the loss tangent. Certainly these will increase the loss tangent. Walford (1968) has indicated that $f \tan \delta$ is proportional to the logarithm of impurity content. However, Watt and Maxwell (1960), show that at radio-frequencies the losses in glacial ice are not appreciably more than for pure ice. Water content and cracks probably vary from season to season; this has not been well studied to date (W. S. B. Paterson, private communication). The presence of water-ice boundaries indicates the possibility of Maxwell-Wagner effects and eddy-current losses in ice close to the melting point. These would be particular to a certain ice-water configuration, and do not appear to have been mentioned in the literature.

The major differences, then, between ice and expected lunar rock are the dielectric constant and the frequency-

dependent loss tangent of ice. Assuming that the relaxation peak seen in Figure 2-14 is due to water, and that the lunar material is fairly homogeneous, the major relaxation in lunar materials is expected at about 10 Hz or less. Therefore the K' of the rock at radio-frequency would probably be constant, although about four times higher than that of ice. The frequency-dependent loss tangent of ice limits the sounding depth through it. In lunar material this would not be expected, and some other factor would limit the effective maximum depth of sounding on the moon (e.g., galactic noise, which also increases with wave-length). However, in general ice provides a good analogue of the dielectric behaviour expected from lunar surface material.

CHAPTER THREE: DESCRIPTION OF THE ATHABASCA GLACIER TRAVERSE EXPERIMENT

3.1 The Athabasca Glacier

The Athabasca Glacier in Alberta, Canada, was chosen for the experimental work carried out during 1970. It is one of the most accessible glaciers in the world, being less than a a mile from the Banff-Jasper (or "Glacier") Highway, in Canada's Jasper National Park, and it has been extensively studied for many years. It is also a relatively safe glacier to work on. Calgary International Airport is 200 miles away (see Figure 3-1), and excellent access highways (see Figure 3-2), are maintained throughout the year by the National Parks Service.

Of course, as important as accessibility in the choice of a test site was accurate and complete information on the nature and depth of the ice. A gravity survey of the Athabasca has been conducted by Kanasewich (1963); siesmic and drilling studies have been made by Paterson and Savage (1963); and electromagnetic and resistivity soundings have been run by Keller and Frischknecht (1960, 1961). Their results are shown in Figures 3-3 to 3-5 respectively.

The Athabasca is one of several glaciers flowing from the 150 square mile Columbia Icefield. It is a valley glacier, about 6 Km. long and 1.1 Km. wide throughout its length. There

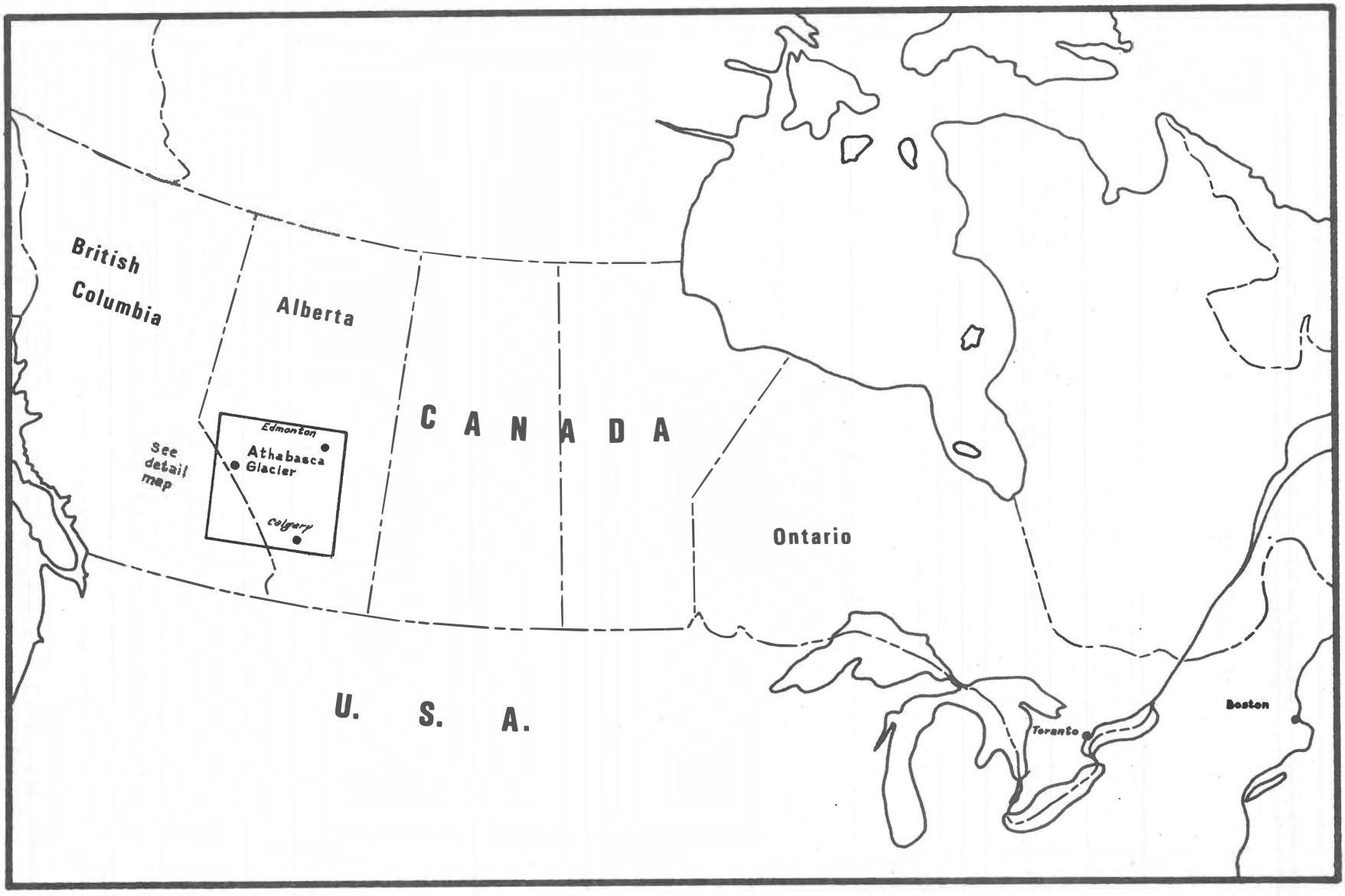

General Location Map

FIGURE 3-1

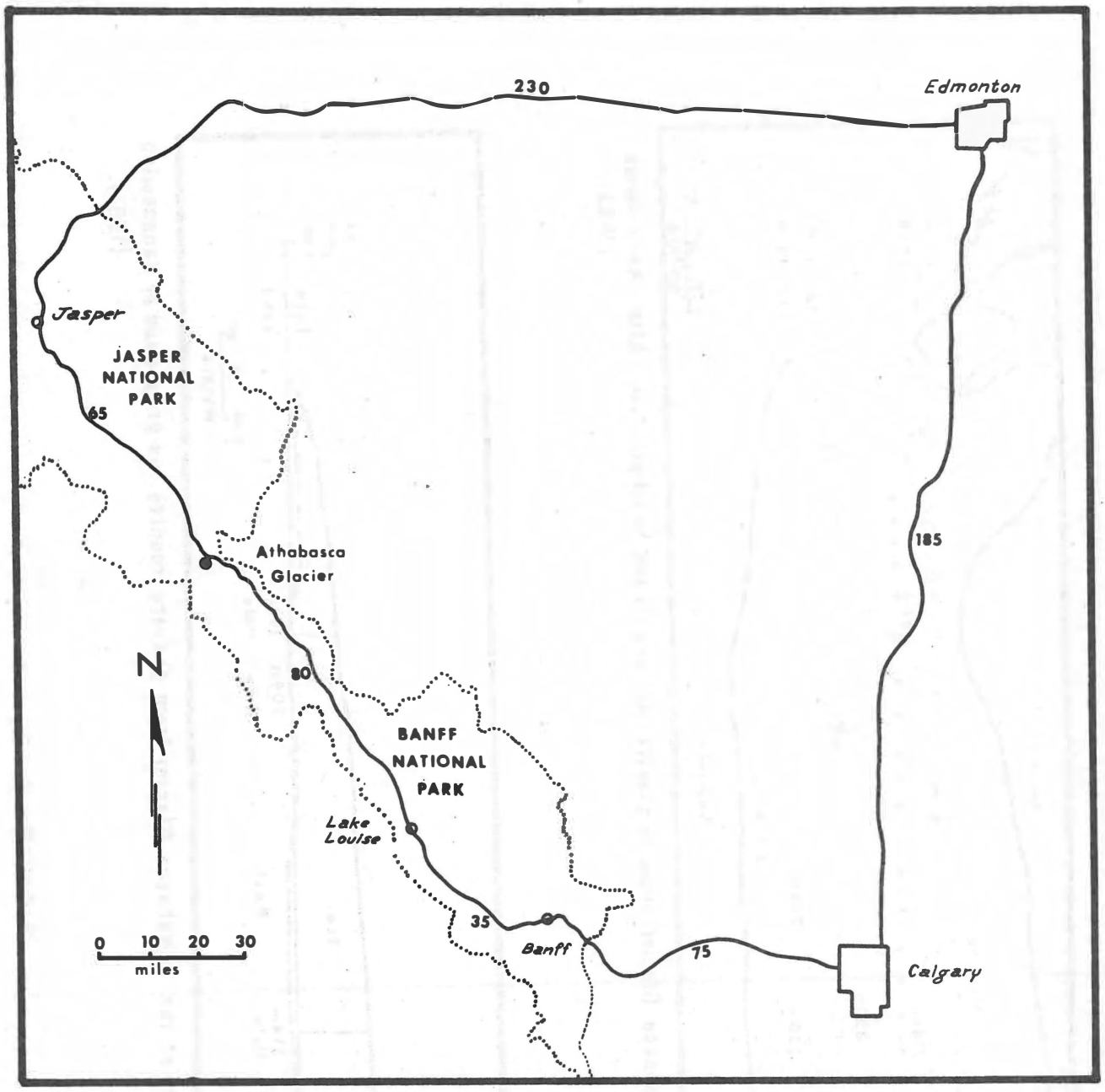

Athabasca Glacier Location Map

Highway distance shown in miles

FIGURE 3-2

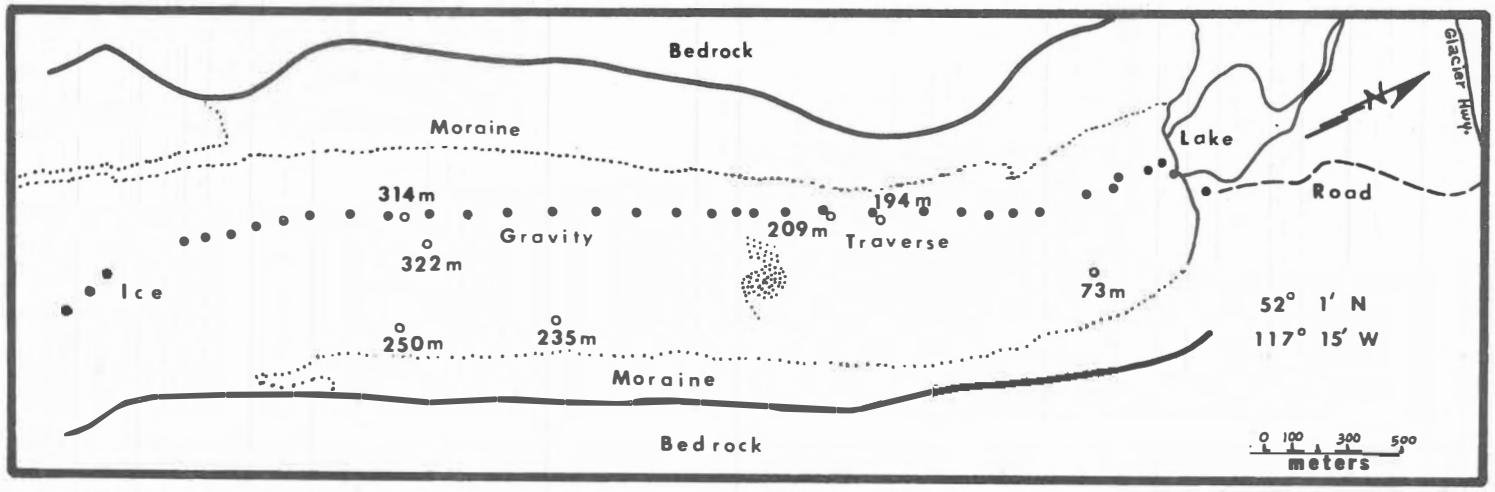

Sketch map of the Athabasca Glacier showing gravity stations (•) and boreholes (o). After Kanasewich (1963)

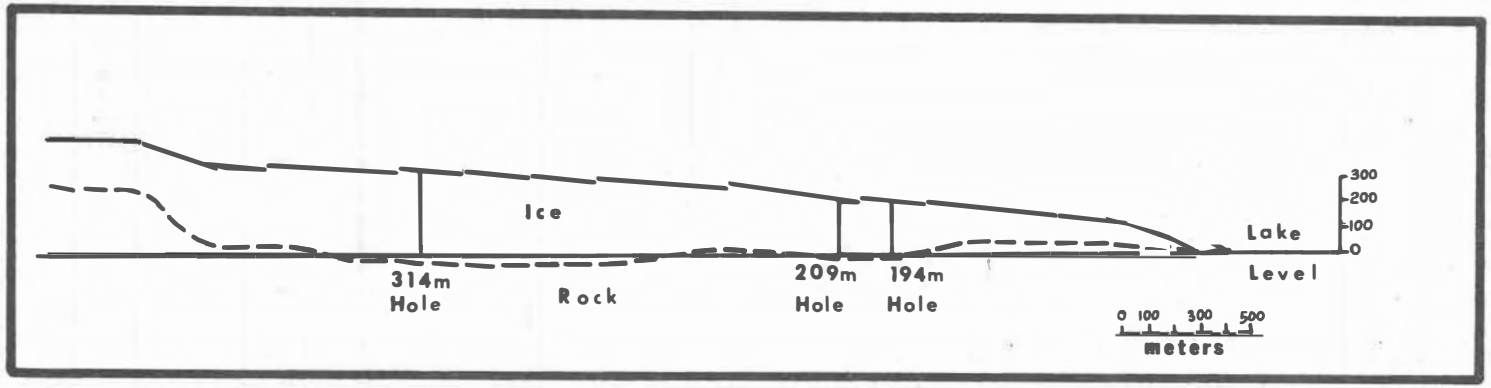

Longitudinal profile of the Athabasca Glacier from gravity results as proprosed by Kanasewich (1963).

FIGURE 3-3

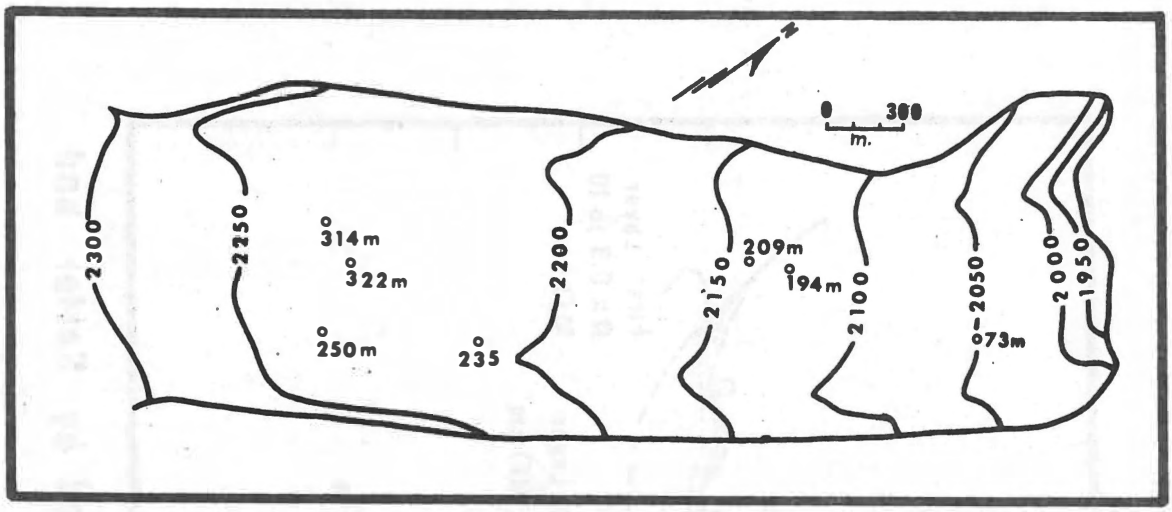

Contour map of the Athabasca Glacier after Paterson and Savage 1963

Elevation above sea level in m. **Boreholes shown ∘**

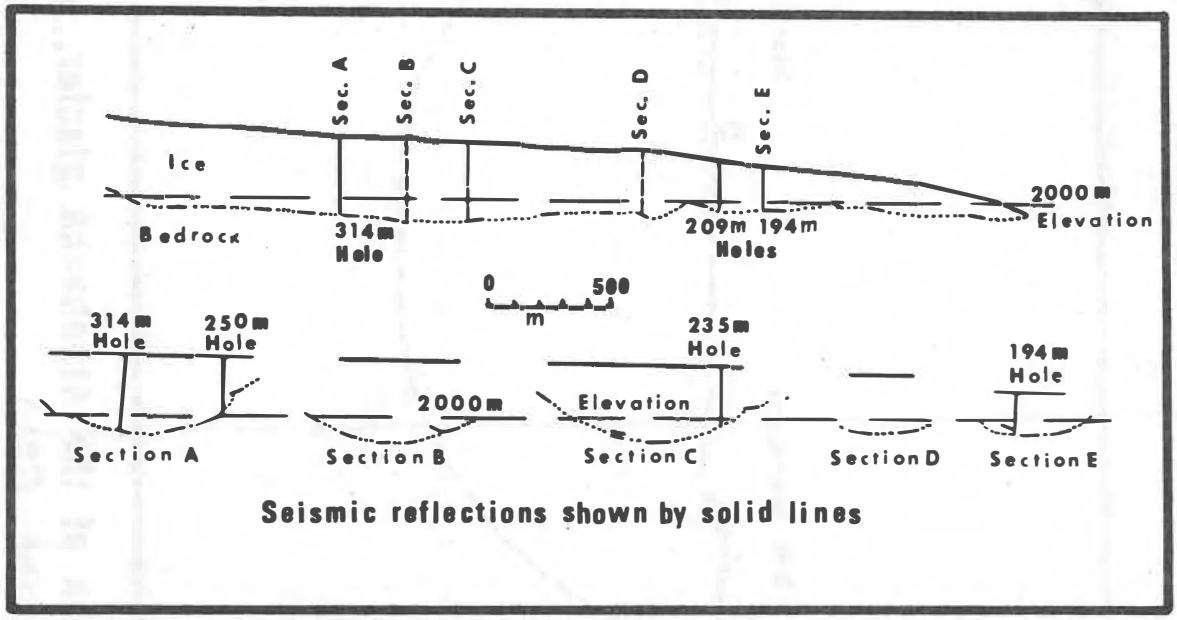

Longitudinal and transverse sections of the Athabasca Glacier, proposed from seismic and drilling results by Paterson and Savage 1963

FIGURE 3 – 4

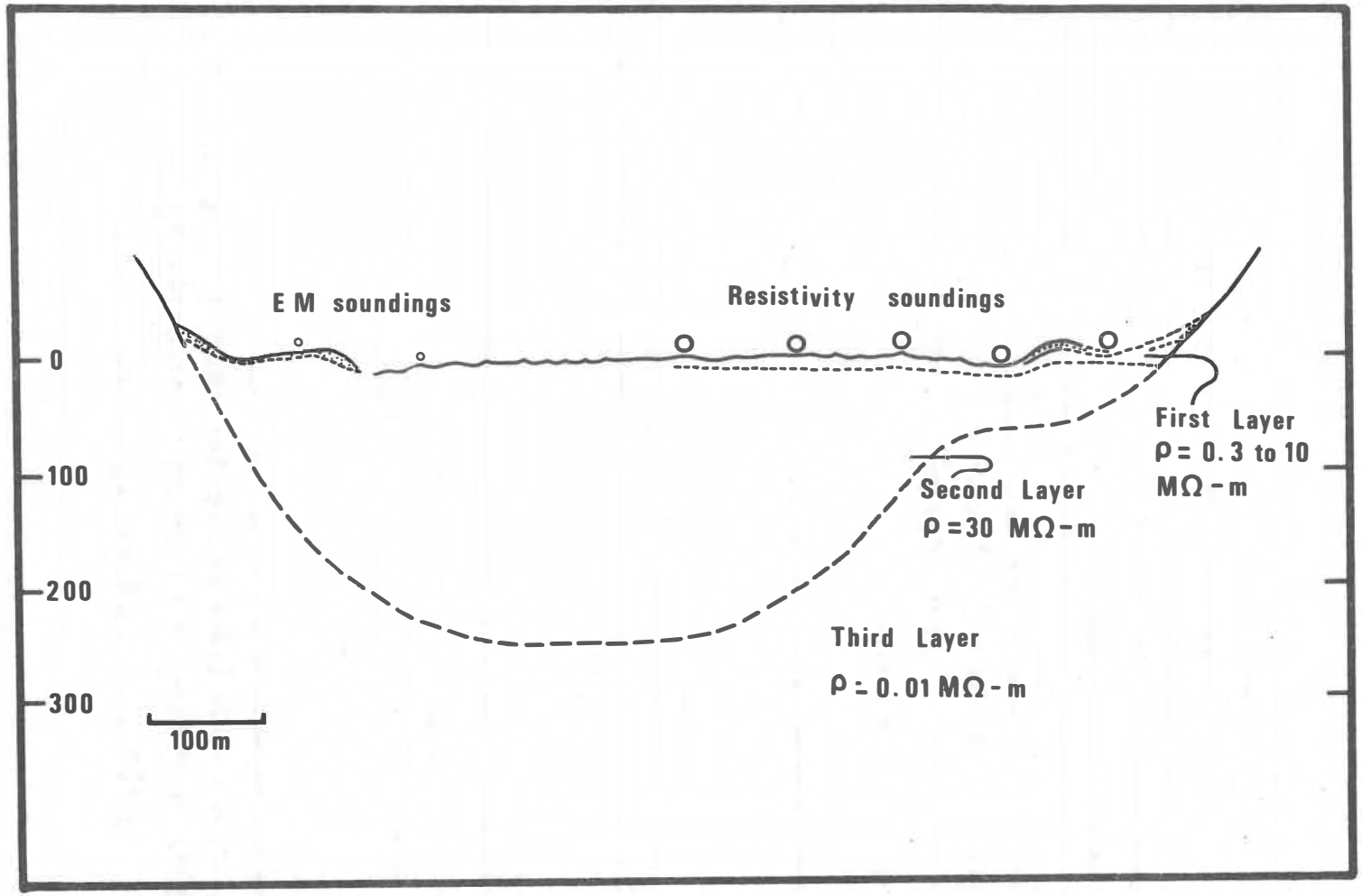

Cross-section of the Athabasca glacier, as postulated by Keller and Frischknecht ('61)

FIGURE 3-5

are three major icefalls, and all work was done on the 3.8 Km. section between the toe and the first icefall. The ice surface varies considerably in roughness. In spring the surface is covered with wind-packed snow that fills in all crevasses. However, during the summer large crevasses (tens of meters across) open up and the surface is covered with hummocks several meters high, and a network of water drainage ravines. Work is then restricted to the less broken-up areas. The glacier rises continuously from the toe to the icefall, with a slope of some 3^{o} to 5^{o} except near the terminus where it drops off very steeply

Two physical properties were especially important for the interferometry experiment. The resistivity of the ice had to be very high, and the depth had to be 200 meters or less, with as simple a geometry as possible. Keller and Frischknecht (1961) measured the resistivity to be 0.3 M Ω-m. for the first 10 to 30 meters, and 30 M Ω-m. for the bulk of the ice. This was confirmed by Watt and Maxwell (1960), who got high-frequency loss tangents in agreement with the estimates given in Section 2.4. Although Watt and Maxwell feel there is some change in electrical properties with depth, there is considerable scatter in all the published results. Both groups worked during the summer, when large amounts of melt-water may have contributed to anomolous readings. Ron Goodman has recently measured the resistivity of the ice, and found it to be between 10^{5} and 10^{7} Ω-m. (private communication). It is also a clean glacier, with

very little surface debris.

The depth was considered to be adequate for this experiment. From Annan's theoretical calculations (see Chapter One), it was decided that when the depth became greater than $0.2/\tan \delta$, there was not enough energy reflected to give interpretable interference patterns. Using the value for tan δ given in Section 2.4 for ice at $0^{o}C$, it is found that 200 meters is a rough maximum to which ice at 0^{o} can be sounded by the interferometry technique. Since the depth of the Athabasca varies from less than 100 m. near the toe and the edges, to over 300 m. near the icefall, this condition was fulfilled. The geometry of the ice was not ideal, however. The glacier valley is basically parabolic, with high lateral moraines, and mountains on either side. Thus, reflections from the sides and from unusual angles of the bottom may be a problem. Moreover, there is some indication that the ice is not homogeneous, but contains caverns and hollows even at depth (Ron Goodman, private communication).

The reflectivity of the bottom is very good. Watt and Maxwell measured the DC resistivity of the surrounding soils to be about 10^{3} to 10^{4} Ω-m., in agreement with Keller and Frischknecht's value. It appears that the underlying rock contains considerable moisture, and thus provides an excellent reflector.

3.2 Experimental Equipment and Procedure

Three sets of experiments were run on the Athabasca during 1970: (1) a test of the feasibility of the interference technique, from mid-March to mid-April; (ii) an unsuccessful test of an azimuth-determining system for the S.E.P. Experiment, during September; and (iii) a careful determination of the radiation patterns of various transmitting dipole lengths, from late October to mid-December. A preliminary report of the first experiment was issued on its completion (Johnston et. al., 1970), and the results presented here constitute a final report. Brief discussions of the second and third experiments are given by Rossiter (1971).

The basic experiment is shown in Figure 3-6. A multiple-frequency transmitter fed a ribbon-wire half-wave dipole antenna lying on the surface of the ice. The receiving coil was held on the snow surface in the appropriate position. A standard communications receiver was located a short distance away in a small sled, which was pulled by a skidoo. Traverses were made by moving the receiver away from the transmitter, on a line orthogonal to the transmitting dipole. Readings were taken about every 1/6 of a free-space wavelength of the frequency being used. Traverses were continued to 20 wavelengths, or until the received signal was too small to detect.

The position of the transmitter (000 m.) and traverse

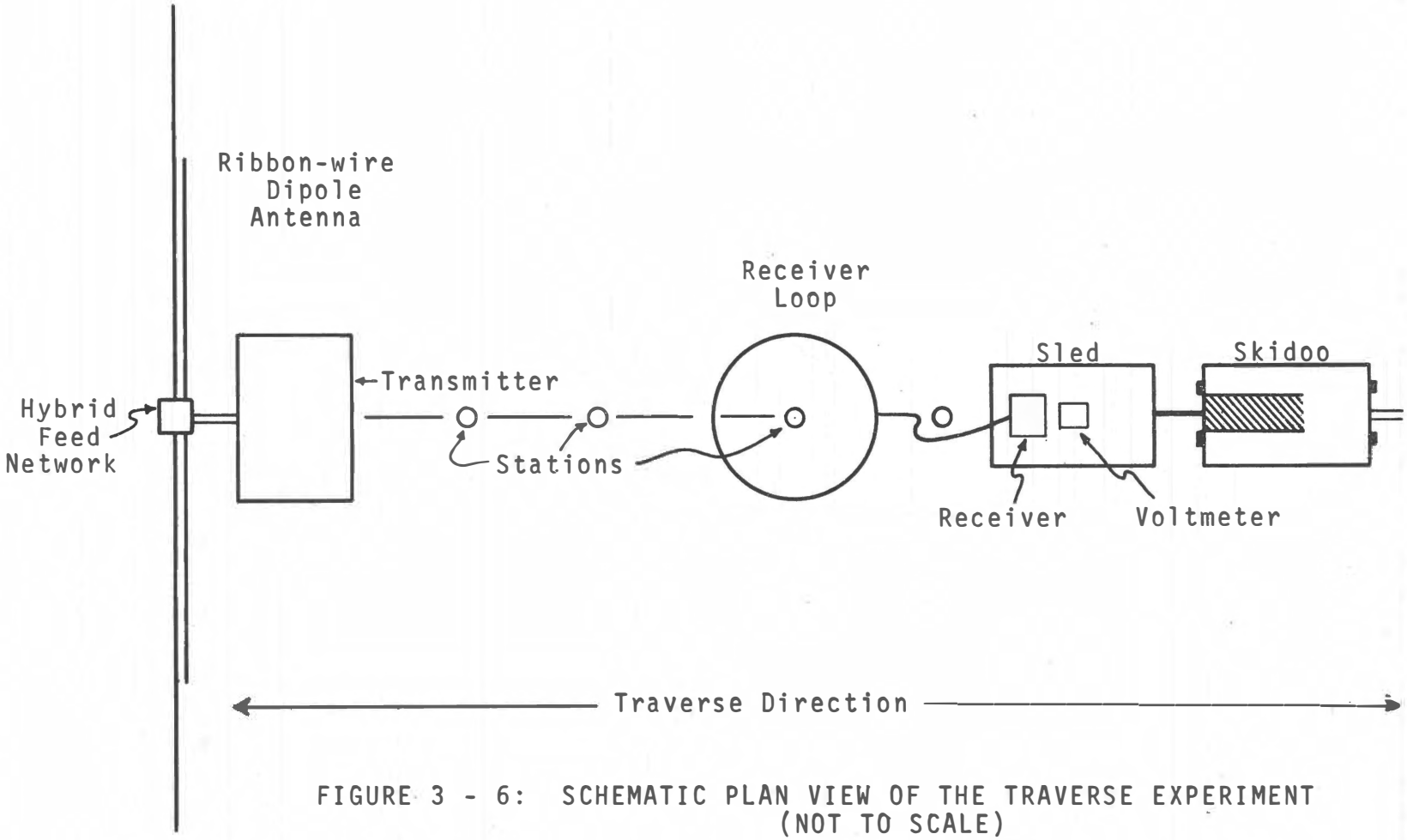

FIGURE 3 - 6: SCHEMATIC PLAN VIEW OF THE TRAVERSE EXPERIMENT
(NOT TO SCALE)

line (000 m. to 1500 m.) is shown on a depth-contour map of the glacier (Figure 3-7). The line was chained, and small markers left at station intervals. The majority of the traverses were made away from the toe; for a few, the transmitter was placed at the far end of the line (1500 m.), and the traverses run toward the toe.

The equipment was fairly simple, battery operated, and it performed well. The 1-Watt multiple-frequency crystal-controlled transmitter was built by the Center for Space Research at M.I.T. It fed a several-inch long lead to a Merrimack HSM-110 hybrid feed network. This split the current into the ribbon-wire transmitting dipole, consisting of multiple strands of No. 22 wire which were spread out on the ice surface (tuning is described below).

The receiver was a standard Galaxy R530 communications receiver with phase-lock loop tuning. It was fed by a Singer single-turn loop antenna (or in one case by a half-wavelength electric dipole antenna). The loops were electrostatically shielded; a 1 meter loop was used for the 2, 4, and 8 MHz traverses, and a 1/3 meter loop for the 16 and 24 MHz runs. Approximately 3 m. of shielded coaxial cable led from the loop to the receiver. The receiver output was read on a Hewlett-Packard HP427A voltmeter; these units had been calibrated in a cold chamber before leaving for the glacier. The sensitivity

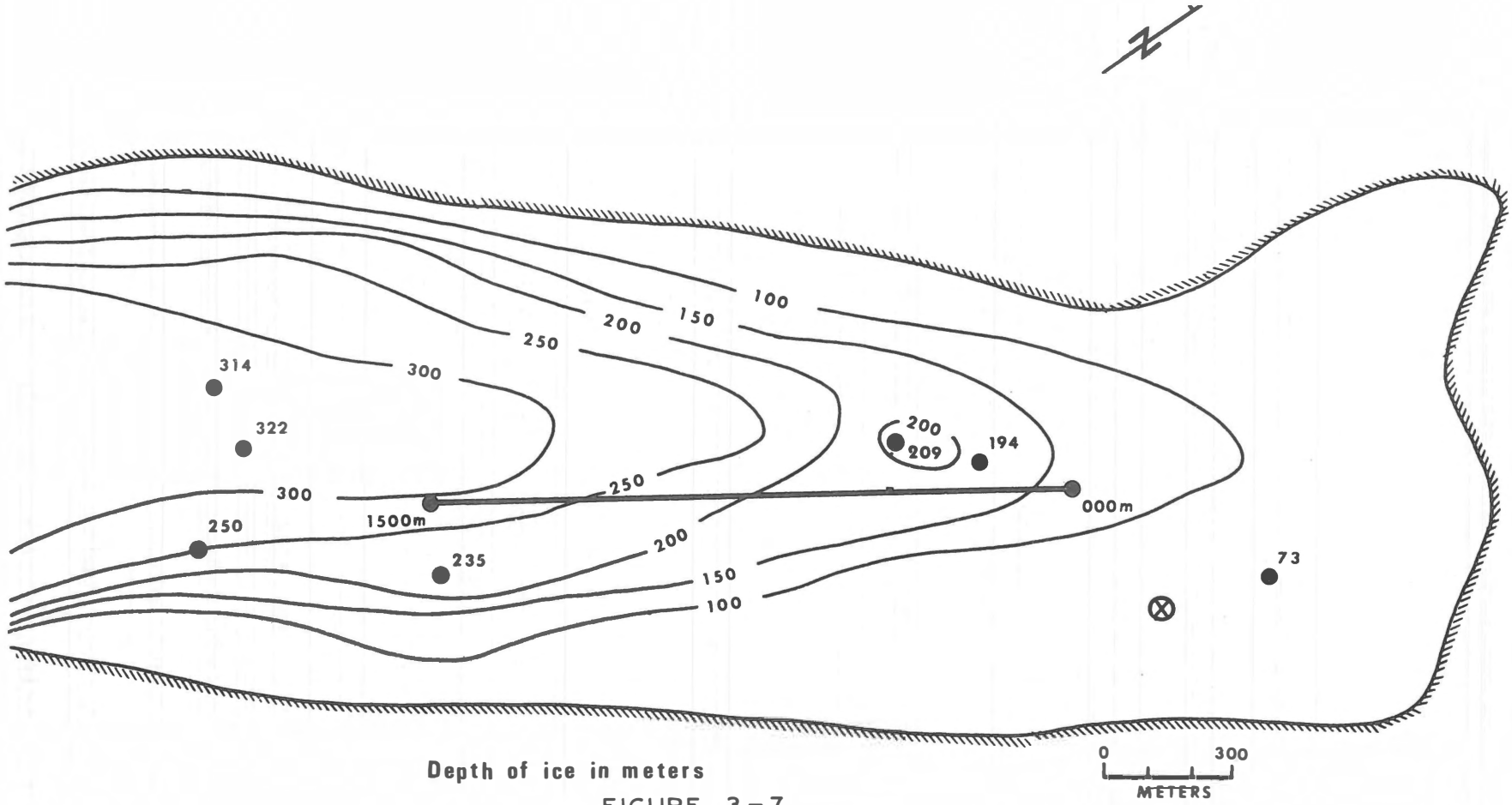

FIGURE 3-7

Contour Map of Depth of Athabasca Glacier From Seismic And Drilling Data of Patterson And Savage (1963)

● Boreholes with depth of ice

Interferometry Traverse Line

⊗ Transmitter site for rotating beam and radiation patterns

of the receiver was approximately 1 microvolt, or about 0.1 microvolt/m. magnetic field strength for the antennas used.

The transmitting antenna was a rather unique attempt to arrange eight half-wave dipoles in a single, small light-weight antenna. It consisted of ten strands of wire bonded together to form a ribbon. This was spread out on the ice surface to a length of 37 m. on either side of the transmitter, for a total length of $\lambda/2$ for the lowest frequency, 2MHz. Each elemen was trimmed to about 90% of the free-space wavelength of one of the frequencies, to compensate for the detuning associated with the shorter EM wavelength in ice.

The 2 MHz element was then connected to the feed, and trimmed until it radiated maximum power from the transmitter. The 4 MHz element was added to the network, and trimmed for maximum output power. The tuning of the 2 MHz antenna did not appear to change. This process was continued until all the elements were connected. The shorter dipoles needed to be trimmed to about 75% of their free-space wavelength, indicating that some detuning was due to the capacitance of the other wires.

Although the ribbon-wire antenna seemed to perform well, and the radiated power was much as expected, later experiments indicate that there may be significant re-radiation by several of the dipoles. Since the antenna lengths are in multiples

of two, the longer dipoles are resonant lengths of all higher frequencies. The radiation patterns for dipoles of various resonant lengths are radically different (see, for example, Kraus, 1950, p. 407). These patterns, some of which have major lobes off the orthogonal to the dipole, may well decrease the observed power along the traverse line. The position of these lobes may also contribute to spurious reflections from the bottom of the glacier. Evidently, then, the point dipole approximation may not be valid for the higher frequencies, which were measured in the near-field of the longer dipoles.

The only problems associated with the equipment were lead problems from the loop to the receiver, and fine-tuning of the receiver. The amount of pick-up by the shielded lead is unknown, but later experiments have indicated that the receiving loop should be rigidly mounted, and well grounded to the receiver. Traverses on which erratic signals were picked up, due to poor lead connections, are noted below as dubious. The receiver had to be fine-tuned to the transmitter at almost every station, and it was originally thought that the 2 KHz bandpass was too narrow. However, it appears that there was a small amount of oscillation in the transmitter, especially with fluctuations in temperature.

3.3 Data Reduction

A summary of the 21 traverses run is presented in Table 3-1. Frequencies of 2, 4, 8, 16, and 24 MHz were used. The vertical magnetic field (H_z) and the radial magnetic field ($H\rho$) were measured for each frequency, and in addition, the tangential magnetic field (H_ϕ), and the tangential electric field (E_ϕ), were measured for a few frequencies. Traverses run "forward" had the transmitter set-up at 000 m.; those marked "reverse" had it at 1500 m. (see Figure 3-7). The total length of the traverse is simply the number of data points times the distance between each reading. The output power was slightly over one watt for most of the traverses as measured by a power meter (individual power readings may be significantly in error, due to lead problems with the meter). The antenna calibration factor converts volts out of the loop antenna to the equivalent received electric field strength in volts/meter.

Data reduction was straight forward. At each station the receiver was fine-tuned, and the output was read from the portable voltmeter. This was recorded, and converted, using receiver calibration curves, to the equivalent receiver input. These values were then punched into computer format. Calibration of the data to take into account the antenna calibration factor, the conversion to magnetic field strengths, and normalization to one watt transmitted power, was made prior to plotting.

TRAVERSE NUMBER	FREQUENCY (MHz)	COMPONENT MEASURED	DIRECTION OF TRAVERSE	DISTANCE BETWEEN DATA POINTS (m)	NUMBER OF DATA POINTS	OUTPUT POWER (WATTS) (4)	ANTENNA CALIBRATION FACTOR v → v/m
1	2	Hz	Forward	20	50	0.77	34.0
2	2	Hρ	Forward	20	60	0.77	34.0
3	4	Hz	Forward	10	131	0.96	30.7
4	4	Hρ	Forward	10	144	0.96	30.7
5	4	Hz	Reverse	10	85	1.13	30.7
6	4	Hρ	Reverse	10	85	1.13	30.7
7	4	HΦ	Reverse	10	85	1.13	30.7
8	8	Hz	Forward	5	150	1.26	28.0
9	8	Hρ	Forward	5	150	1.26	28.0
10	8	Hz	Reverse	5	150	1.35	28.0
11	8	Hρ	Reverse	5	150	1.35	28.0
12	8	HΦ	Reverse	5	93 (1)	1.35	28.0
13 (2)	8	Hz	Forward	5	101	—	28.0
14 (2)	8	Hρ	Forward	5	101	—	28.0
15 (2)	16	Hz	Forward	3.33	117	1.35	51.0
16 (2)	16	Hρ	Forward	3.33	89	1.35	51.0
17	24	Hz	Forward	2	127	1.46	48.5
18	24	Hρ	Forward	2	127	1.46	48.5
19 (3)	24	Hz	Forward	2	125	1.34	48.5
20 (3)	24	Hρ	Forward	2	125	1.34	48.5
21	24	EΦ	Forward	2	120	1.34	—

NOTES: (1) Traverse Started at Station 58
(2) Dubious data
(3) Receiving loop carried on back, approximately 1 m. from ice surface
(4) This is a rough guide only to output power

TABLE 3-1: Spring Glacier Data — Summary of Traverses made

CHAPTER FOUR: DATA ANALYSIS AND INTERPRETATION

4.1 Basis of Interpretation

The primary aim of the experiment was not to develop an interpretational technique, but to demonstrate that the interferometry technique could give interpretable results. To do this, it was hoped that three different sets of data would be internally consistent, i.e., that the field data, linked with the published parameters of the Athabasca Glacier, would agree with the theoretical results compiled by Annan (1970) and Sinha (1971).

Although the theory is very complex, and of necessity approximate, some confidence has been developed in it. Annan got rough agreement between theory and scale-model results (see Chapter One). And the solutions by Sinha, for the H_z component, although calculated independently, are in virtually perfect agreement with Annan's. Further, the solutions for H_z computed by Sinha contain an extra term (i.e., second-order effects). In spite of this, they are virtually identical to Annan's solutions indicating that only first-order effects are significant.

One factor complicates the comparison between the Athabasca Glacier data and the theoretical curves. Referring to Figure 3-7, it can be seen that along the traverse line the depth of the ice is not constant, but increases fairly steadily. This gives perturbations from the theory for two reasons. First,

as the traverse progresses, the bulk of the energy reflected from the bottom sees a greater and greater depth of ice, and therefore a greater path length, and it arrives later. Secondly, if the bottom is relatively smooth, the angle of the reflection is altered so that the reflected signal is moved-out, as shown in Figure 4-1.

If the slope of the bottom is slight, the latter effect is more predominant than the former, and it might be expected that the interference pattern would not be greatly distorted, but that the peaks and troughs would be moved-out to greater distances from the transmitter. Similarly, if the slope were to decreasing thickness, the peaks and troughs would be moved-in. There is some scale-model evidence for this, shown in Figure 4-2. The model used was the same one described by Annan (1970), using dry sand as a dielectric, and an aluminum plate as a reflector. The depth of sand at the transmitter was 3 wavelengths, and the slope 1:40. In this case the slope is to decreasing thickness, and it can be seen that the resulting peaks and troughs do indeed move-in. The comparison with the corresponding theoretical curve is interesting as well. Although the peaks and troughs align well, the amplitudes are not in perfect agreement. This is thought to be caused by a discontinuity in the theoretical solutions which gives unrealistically high values for one peak of the theoretical curve (at 5.5 wavelengths in this case). Since the curve is scaled to this peak,

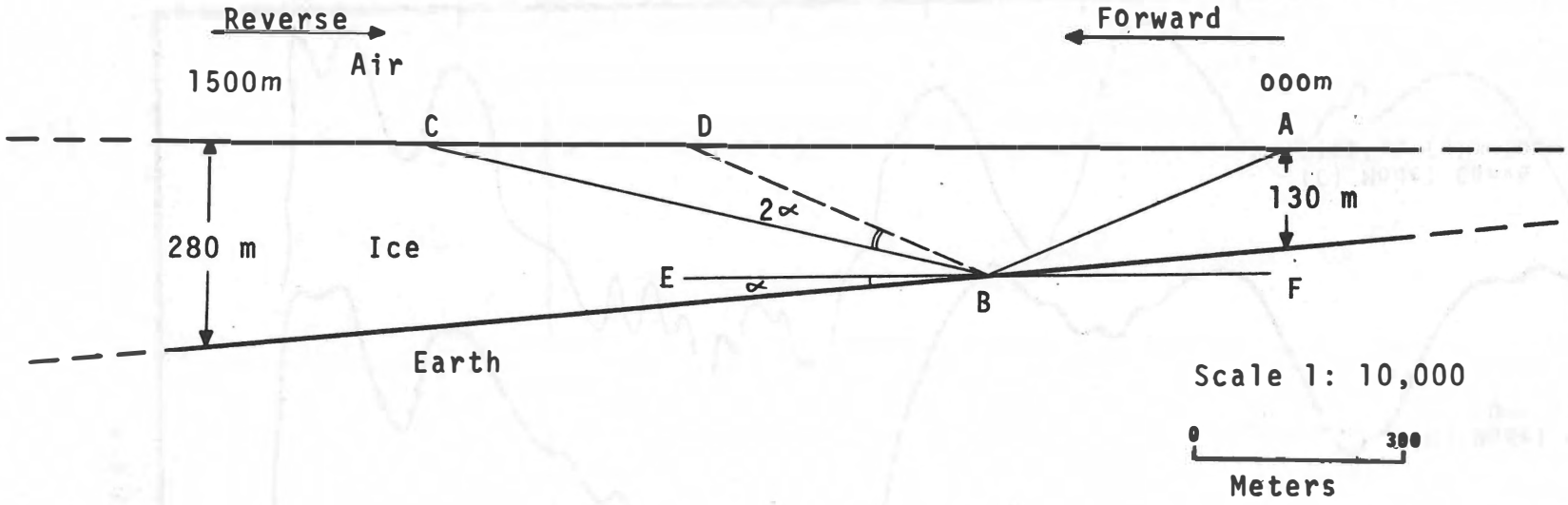

Athabasca Glacier Model

FIGURE 4-1: SIMPLIFIED INTERPRETATION OF ICE THICKNESS ALONG THE TRAVERSE LINE SHOWN IN FIGURE 3-7. MOVE-OUT OF REFLECTED WAVE ABC, COMPARED TO WAVE ABD REFLECTED FROM HORIZONTAL BOTTOM EBF, IS SHOWN.

FIGURE 4-2: COMPARISON OF THEORETICAL CURVE(A) SCALE - MODEL (B), AND SCALE - MODEL WITH BOTTOM INTERFACE SLOPING UPWARD AWAY FROM TRANSMITTER (C):

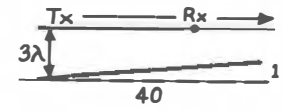

the rest of the amplitudes are also incorrect. This is a common feature in the theoretical results.

The slope of the bottom of the glacier, however, is quite a bit greater than 1:40. In fact, a choice of a "depth" becomes a moot point, since it varies significantly along the traverse. In order to give a more realistic picture to work from, three depths are shown in the following comparisons with theoretical curves. Also, it is reasonable to allow some move-out for forward curves (to increasing ice thickness), and some move-in for reverse traverses, so that the profiles are not symmetrical when reversed.

There is one additional complication in the Athabasca curves: the bottom is not likely to be a smooth reflector. This factor might contribute some scatter in the measured results In order to remove the effect of small random irregularities in the data, a 3-point running-average filter was applied. This converted each data point to the simple average of the three nearest data points. This type of filter seemed to successfully clarify the main points of the curves without introducing distortion. Scatter will be discussed further in Section 4.3.

4.2 Comparison to Theoretical Curves

In this section comparisons between theoretical curves for the various components and the Athabasca data are presented. The comparisons are <u>not</u> intended to show the best possible fits

of the measured curves to theoretical curves; however, after comparing the field data to many suites of curves as compiled by Sinha (1971), consistent fits much better than the ones presented here could not be made.

A summary of the comparisons made is given in Table 4-1. The values of the electrical parameters of ice used are those presented in Chapter 2, i.e., a dielectric constant of 3.2, and a loss tangent near 0.2/f, where f is the frequency in MHz. This is a bit lower than the published results, and indicates that the glacier ice is no more lossy than expected. The depths used are calculated from the model of the glacier shown in Figure 4-1, based on seismic and drilling data of Paterson and Savage (1963). The first depth given in Table 4-1 is calculated at the transmitter location. The second depth is calculated at the mid-point of the traverse, since, from geometrical optics, this is the approximate point from which the largest amount of energy is reflected at the end of the traverse. The theoretical curves actually shown are for depths that bracket the two calculated depths as well as possible.

The 2 MHz traverses (Figures 4-3 and 4-4), although very simple, were deceptively difficult to match perfectly to theory. They are reasonably close to something between 1.0 and 1.5 wavelengths, with a loss tangent of 0.100 or 0.150 (not shown). However, they are also very similar in nature to the half-space

Athabasca Glacier Traverse Number		Depth at Beginning of Traverse (2)	Calculated Depth at 1/2 Traverse Distance (2)	Depths shown in Theoretical curves (in wavelengths)			Shown in Figure Number
1		0.9	1.2	Half-space	1.0	1.5	4-3
2		0.9	1.3	Half-space	1.0	1.5	4-4
3		1.7	2.6	1.5	2.0	2.5	4-5
4		1.7	2.7	1.5	2.0	2.5	4-6
5		3.7	3.2	4.0	3.5	3.0	4-7
6		3.7	3.2	4.0	3.5	3.0	4-8
	(3)						
8		3.5	4.5	3.5	4.0	4.5	4-9
9		3.5	4.5	3.5	4.0	4.5	4-10
10		7.5	6.5	7.5	7.0	6.5	4-11
11		7.5	6.5	8.0	7.0	6.0	4-12
	(3)						
13	(1)	3.5	4.1	3.5	4.0	4.5	4-13
14	(1)	3.5	4.1	3.5	4.0	4.5	4-14
15	(1)	6.9	8.0	7.0	7.5	8.0	4-15
16	(1)	6.9	7.7	7.0	—	8.0	4-16
17		10.5	11.5	10.5	11.0	11.5	4-17
18		10.5	11.5	—	10.0	—	4-18
19		10.5	11.5	10.5	11.0	11.5	4-19
20		10.5	11.5	—	10.0	—	4-20
21		10.5	11.5	—	10.0	—	4-21

Notes: (1) Dubious data
(2) Calculated in wavelengths; from seismic data model (See Figure 4-1).
(3) HΦ (traverses 7 and 12) does not theoretically exist in this configuration

Table 4-1: Summary of Comparisons Between Theoretical and Athabasca Data

Figure 4-3: COMPARISON of THEORETICAL to FIELD DATA

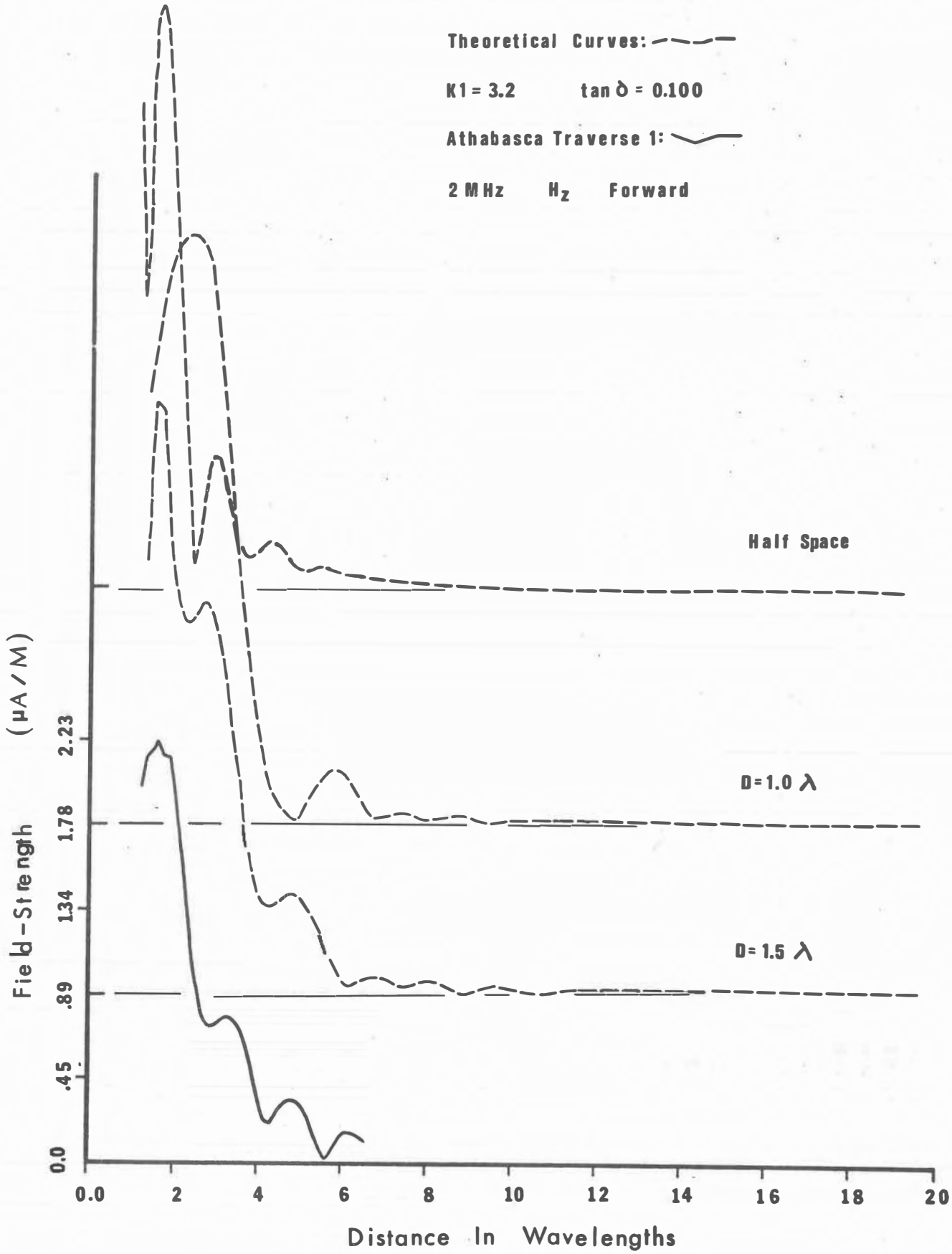

Figure 4-4: COMPARISON of THEORETICAL to FIELD DATA

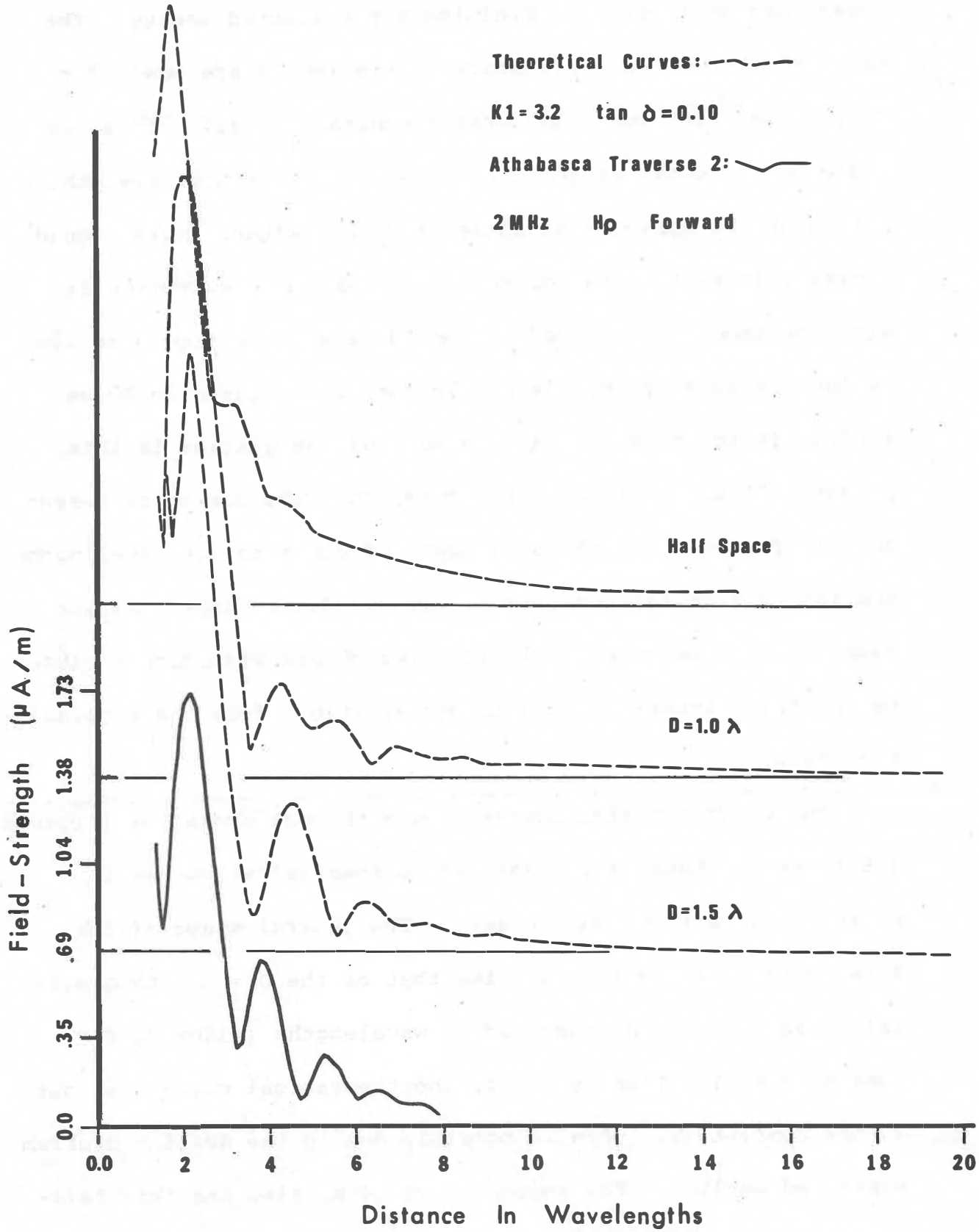

case, since even for the depth as low as 1 wavelength, the losses are sufficient to minimize any reflected energy. The match to theoretical half-space curves (which are exact for H_z), agrees best for a dielectric constant of 2.9. This low a dielectric constant for ice is unlikely — almost everything that might be expected to alter it (e.g., water, rocks) would increase it rather than decrease it. The only exception is air—the amount of trapped air would have to be from 5 to 10% (using the density vs. dielectric constant diagram in Evans, 1965). It is unlikely that the bulk of the glacier is this porous. It is concluded, therefore, that the curves represent an interference pattern for a depth of close to 1.0 wavelengths, and that the deviations from theory are due to approximations made in the theoretical solutions (which are significant close to the transmitter), or due to perturbations from the sloping interface.

The 4 MHz traverse curves show much more character (Figures 4-5 to 4-8). None of the matches to theoretical curves is perfect, but a trend can be seen. The general shape of the first curve (Figure 4-5) is like that of the D = 1.5 theoretical curve out to a distance of 10 wavelengths (allowing for some move-out). Then, however, the theoretical curve dies out almost completely. This is possibly due to the scaling problem mentioned earlier. The second curve (4-6) also has this deficiency. The reverse curves (Figures 4-7 and 4-8), are much

Figure 4-5: COMPARISON of THEORETICAL to FIELD DATA

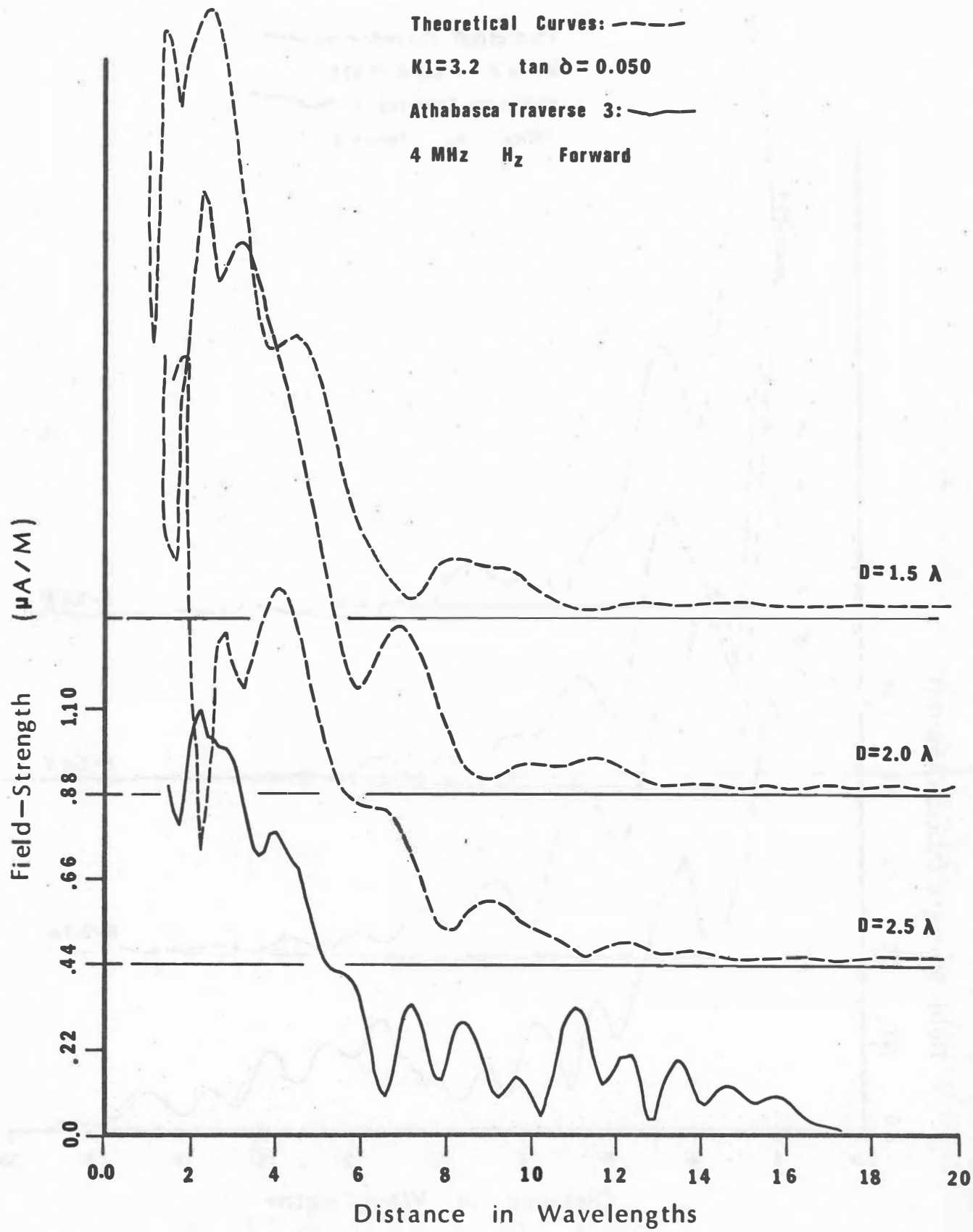

Figure 4-6: COMPARISON OF THEORETICAL TO FIELD DATA

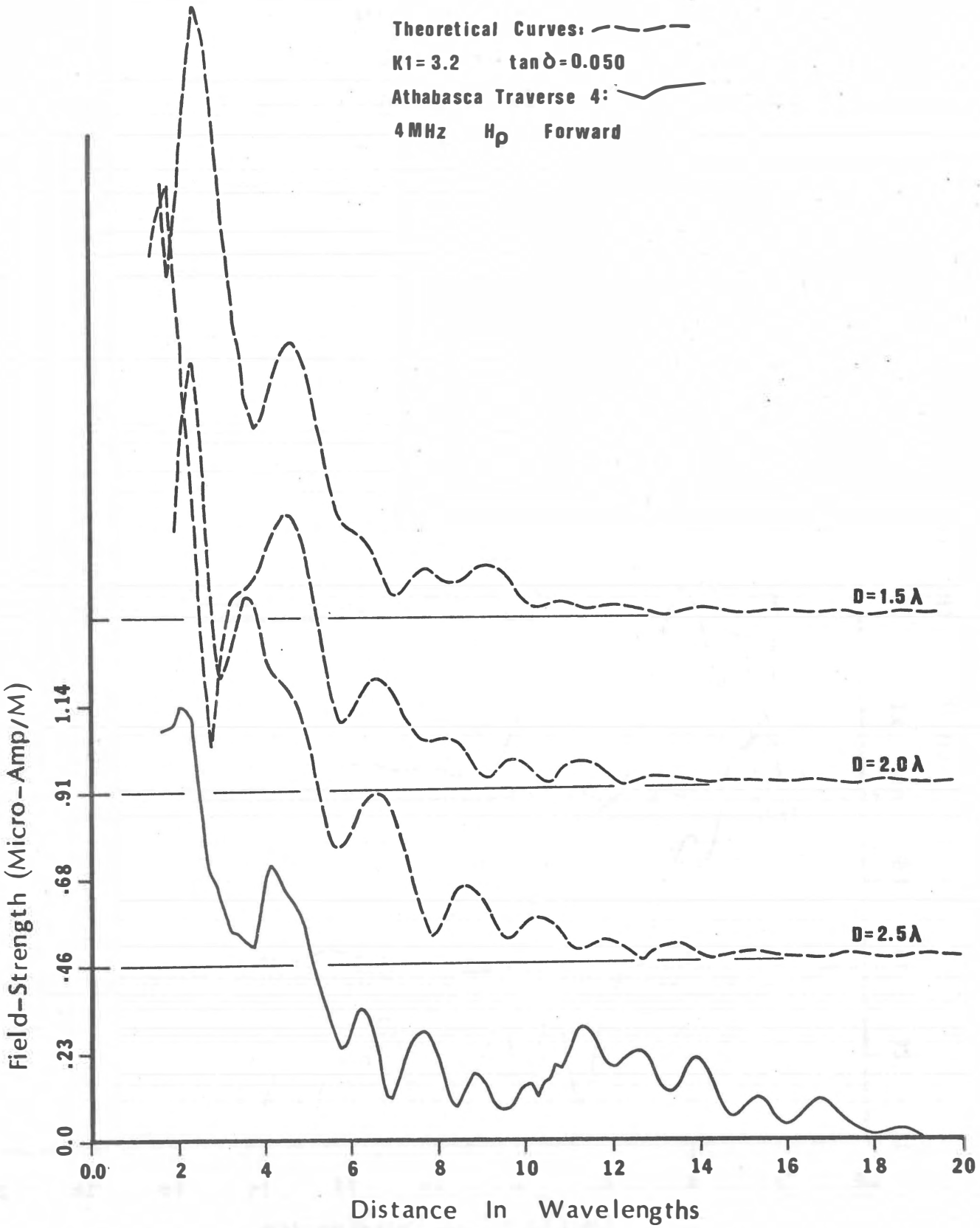

Figure 4-7: COMPARISON of THEORETICAL to FIELD DATA

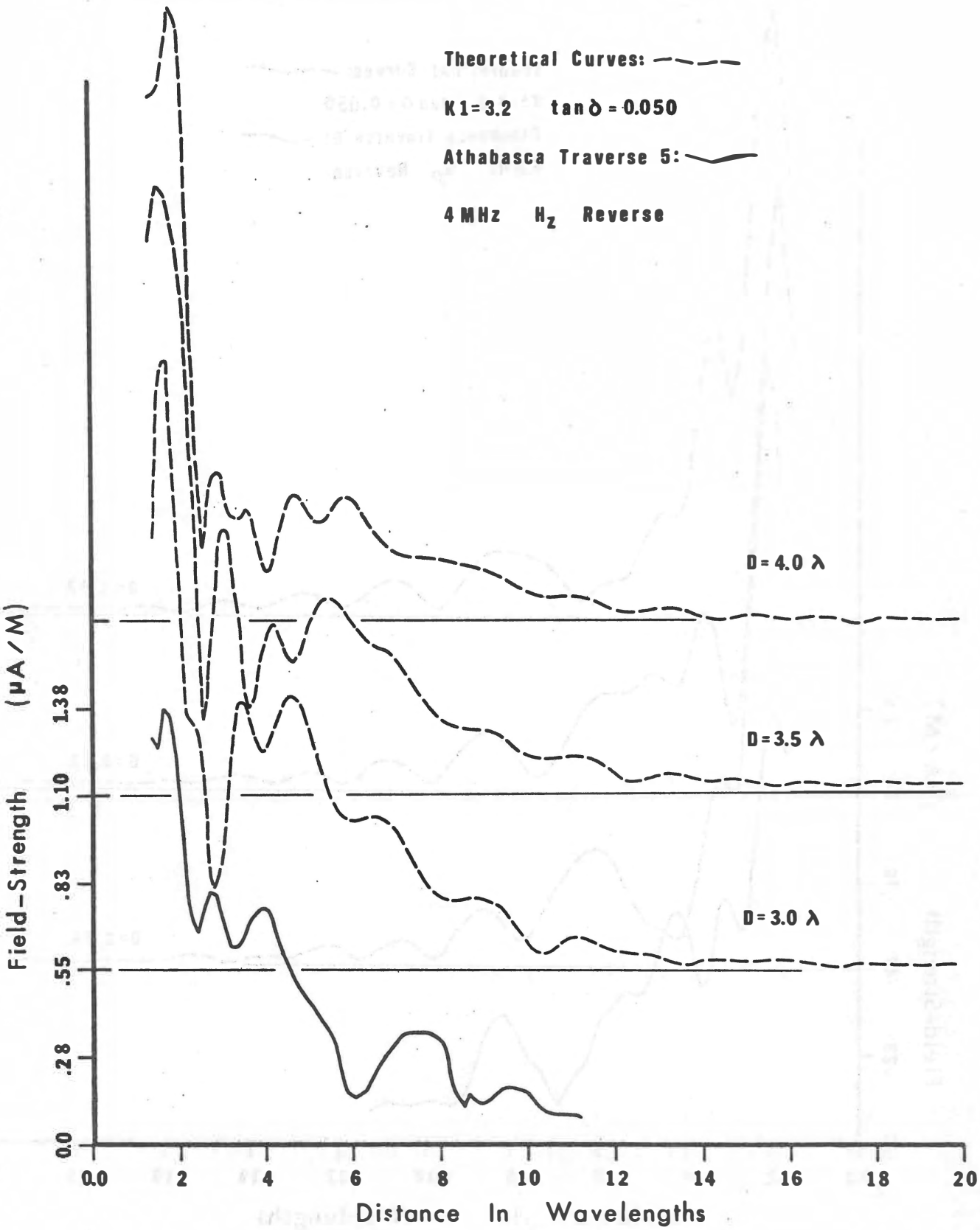

Figure 4-8: COMPARISON OF THEORETICAL to FIELD DATA

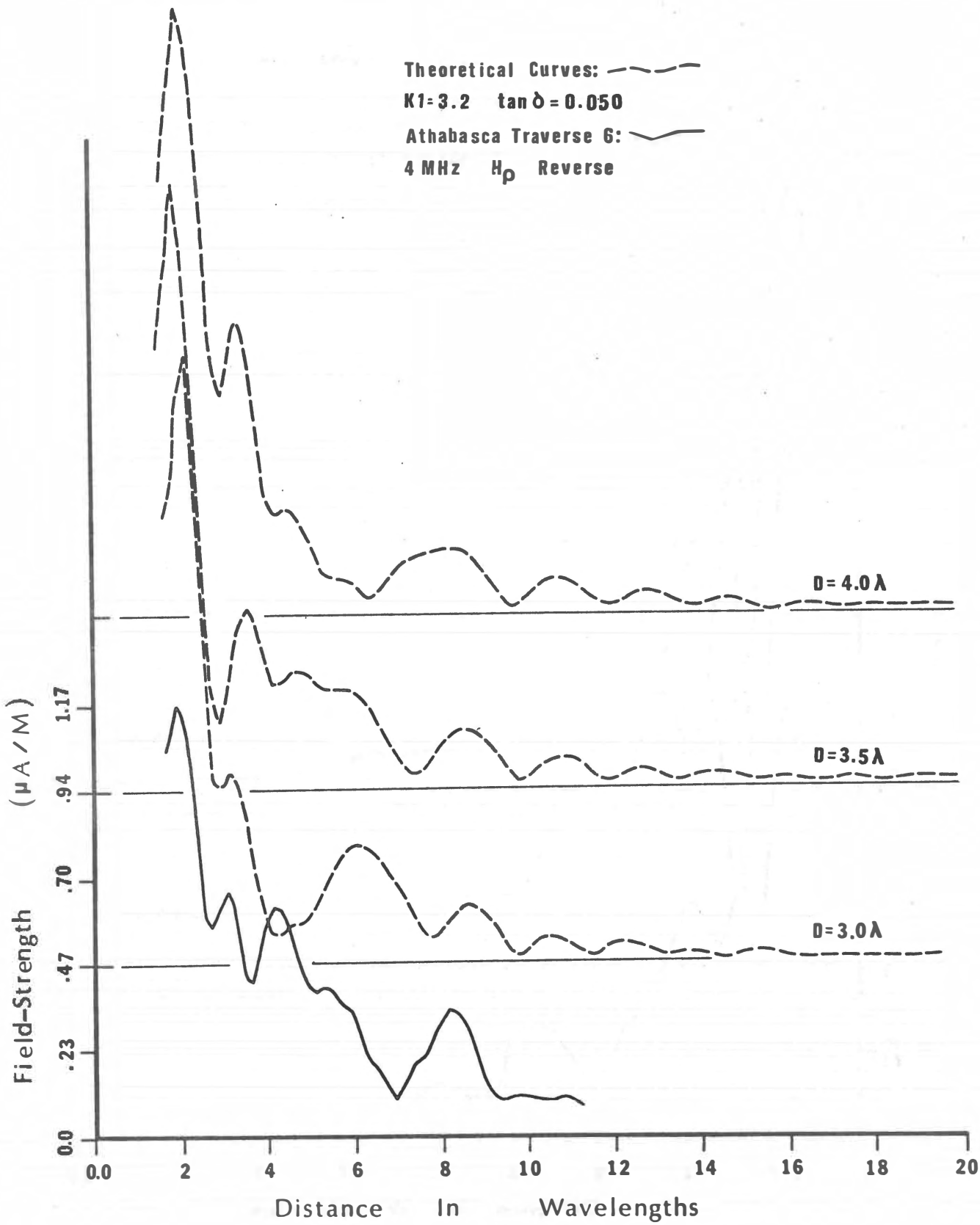

better. Allowing for some move-in, the match to the D = 3.5 and D = 3.0 curves is quite good, in both amplitude and position of the peaks.

The 8 MHz traverses give the best matches to theory (Figures 4-9 to 4-14). A good match of position and amplitude of the peaks can be made following a natural progression from top to bottom of the page, as one moves along the curve.

The 16 MHz curves (Figures 4-15 and 4-16), are not quite so clear. The high-frequency peaks seen in the theoretical curves seem to be obscured in the H_z curve, and the relatively large peak at 10 to 12 wavelengths appears to be too large. However, the H_ρ curve matches better, and it has a good general shape if a fair amount of move-out is allowed.

The 24 MHz curves show a distinct increase in the frequency of the interference peaks (Figures 4-17 and 4-18). In general the measured data are not nearly as smooth as the theoretical curves. This is not unexpected if any random scattering is present, and a greater measurement density should probably have been taken. However, there may also be more scattering at this frequency than at the others, since the waves, 12.5 meters long, are the same order of size as many scattering bodies. The experimental curves show a slowly declining amplitude, but not the increase towards the end of the traverse shown in the theoretical curves. There seems no reason to believe that this

Figure 4-9: COMPARISON OF THEORETICAL TO FIELD DATA

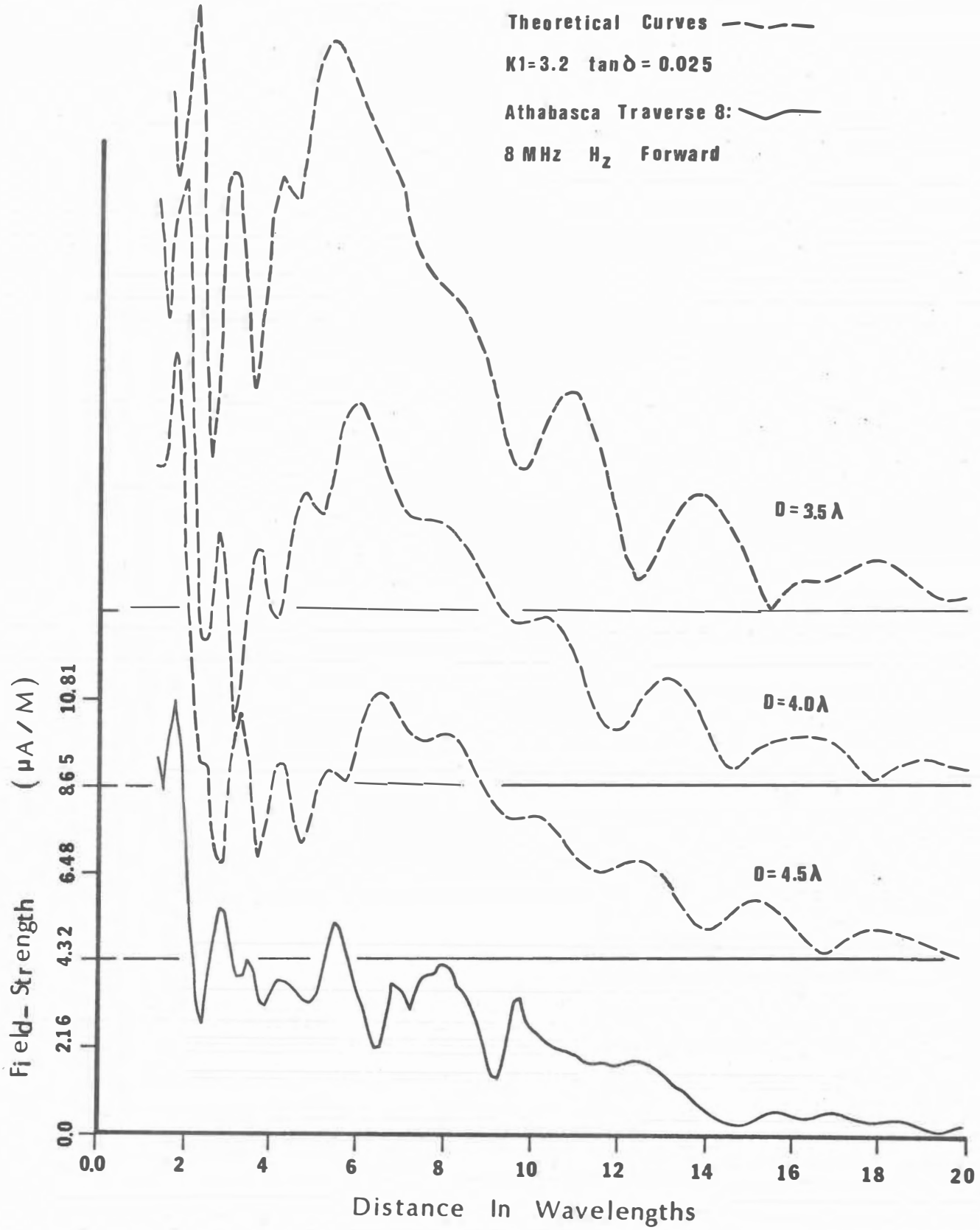

Figure 4-10: COMPARISON of THEORETICAL to FIELD DATA

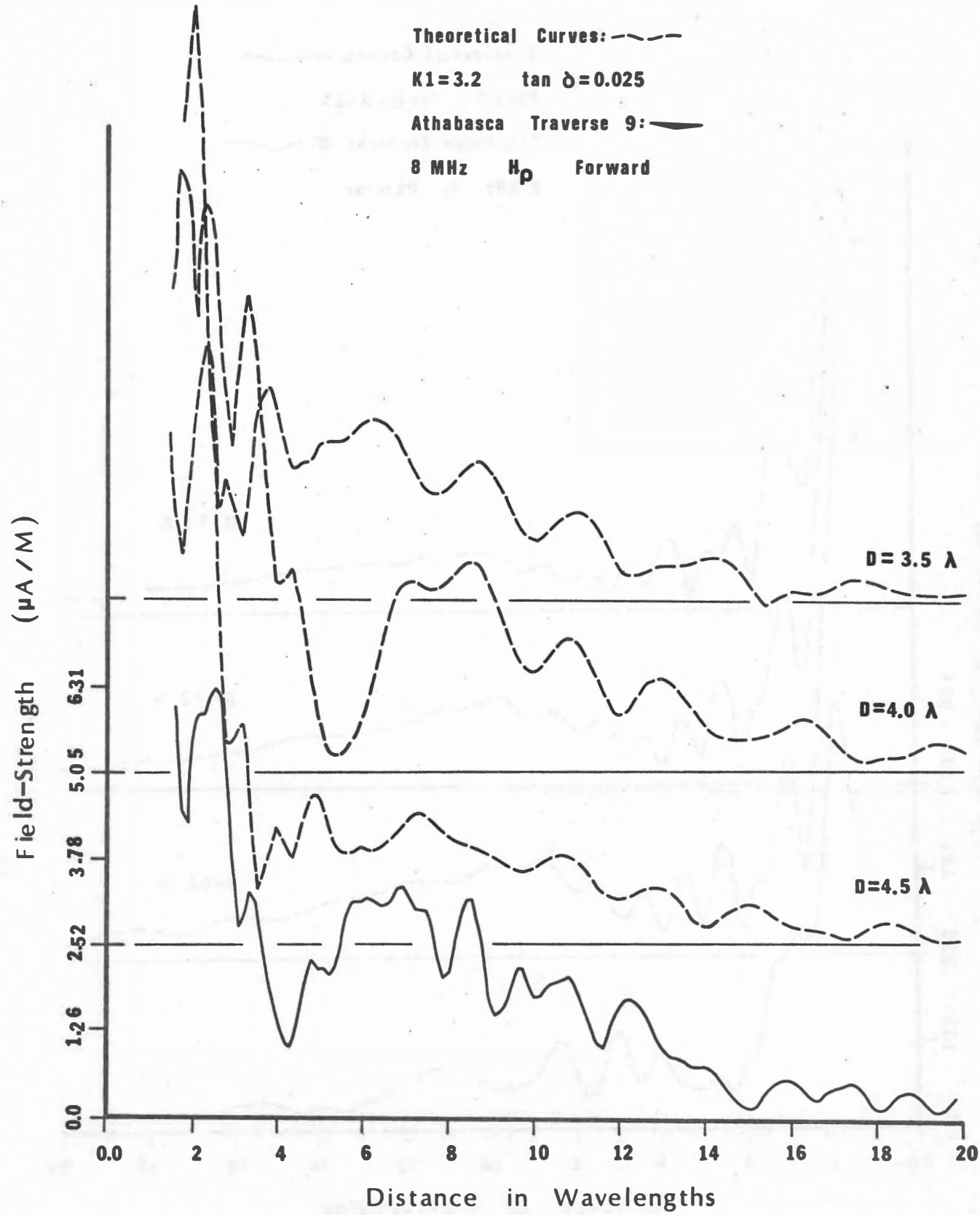

Figure 4-11: COMPARISON of THEORETICAL to FIELD DATA

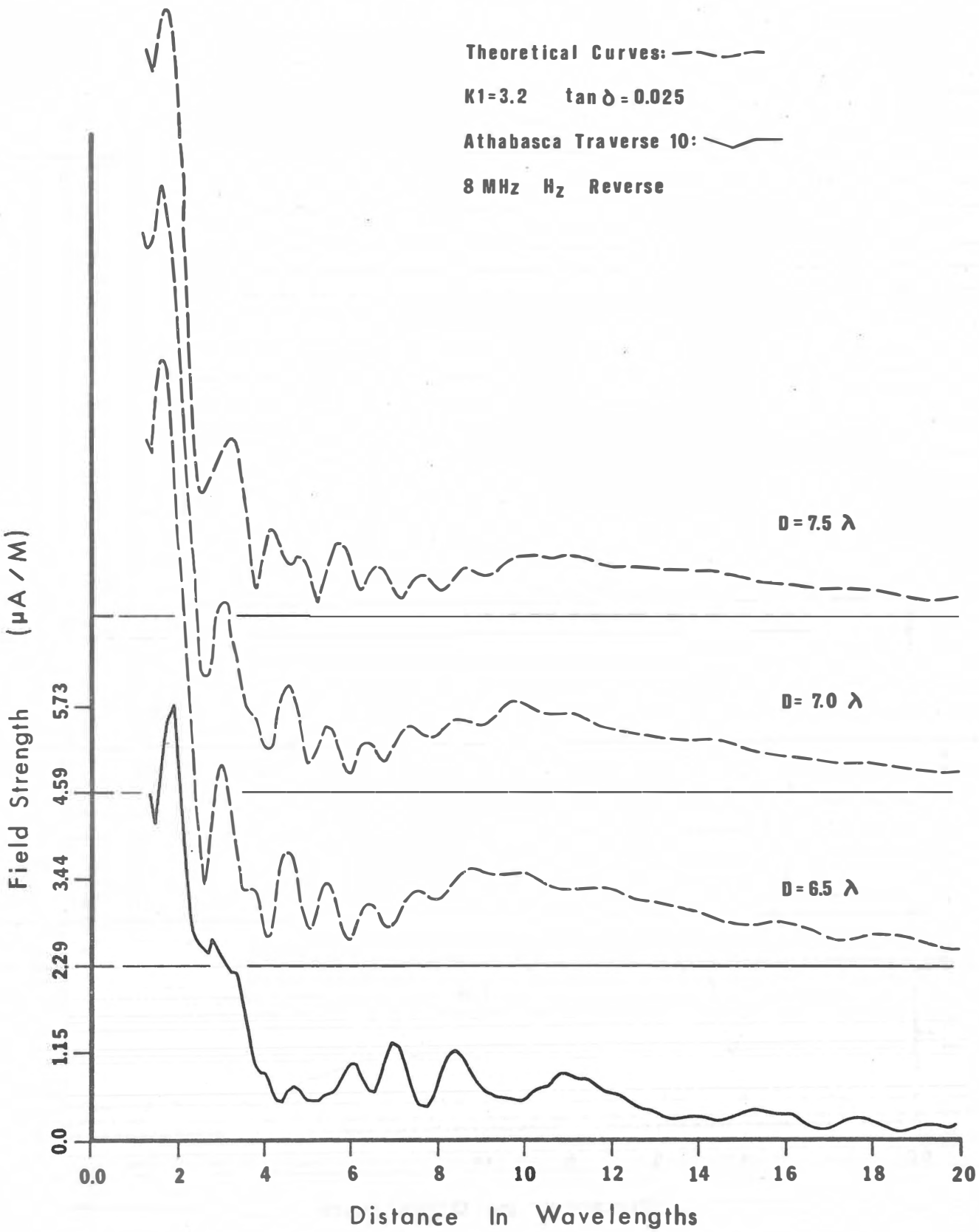

Figure 4-12: COMPARISON of THEORETICAL to FIELD DATA

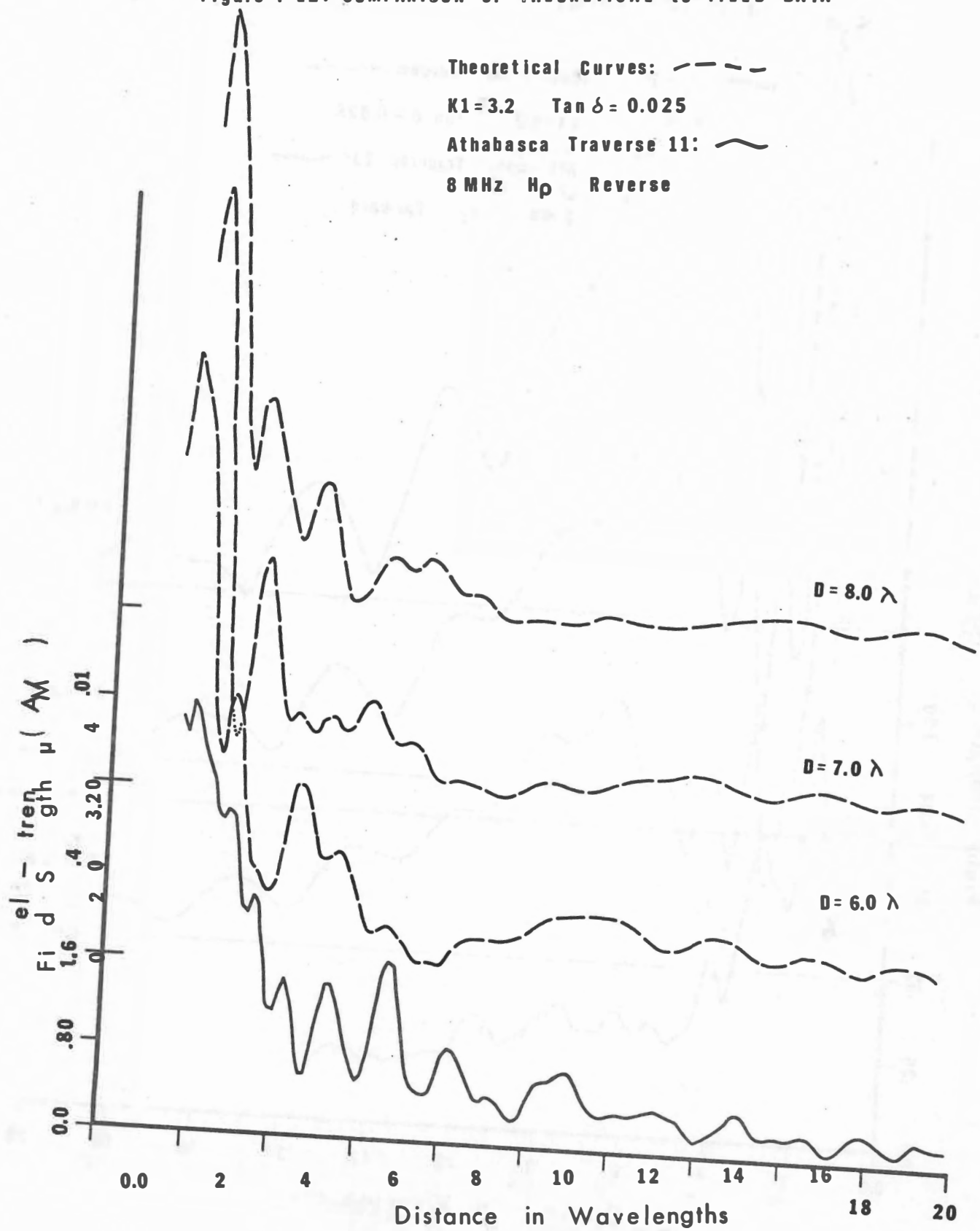

Figure 4-13: COMPARISON of THEORETICAL to FIELD DATA

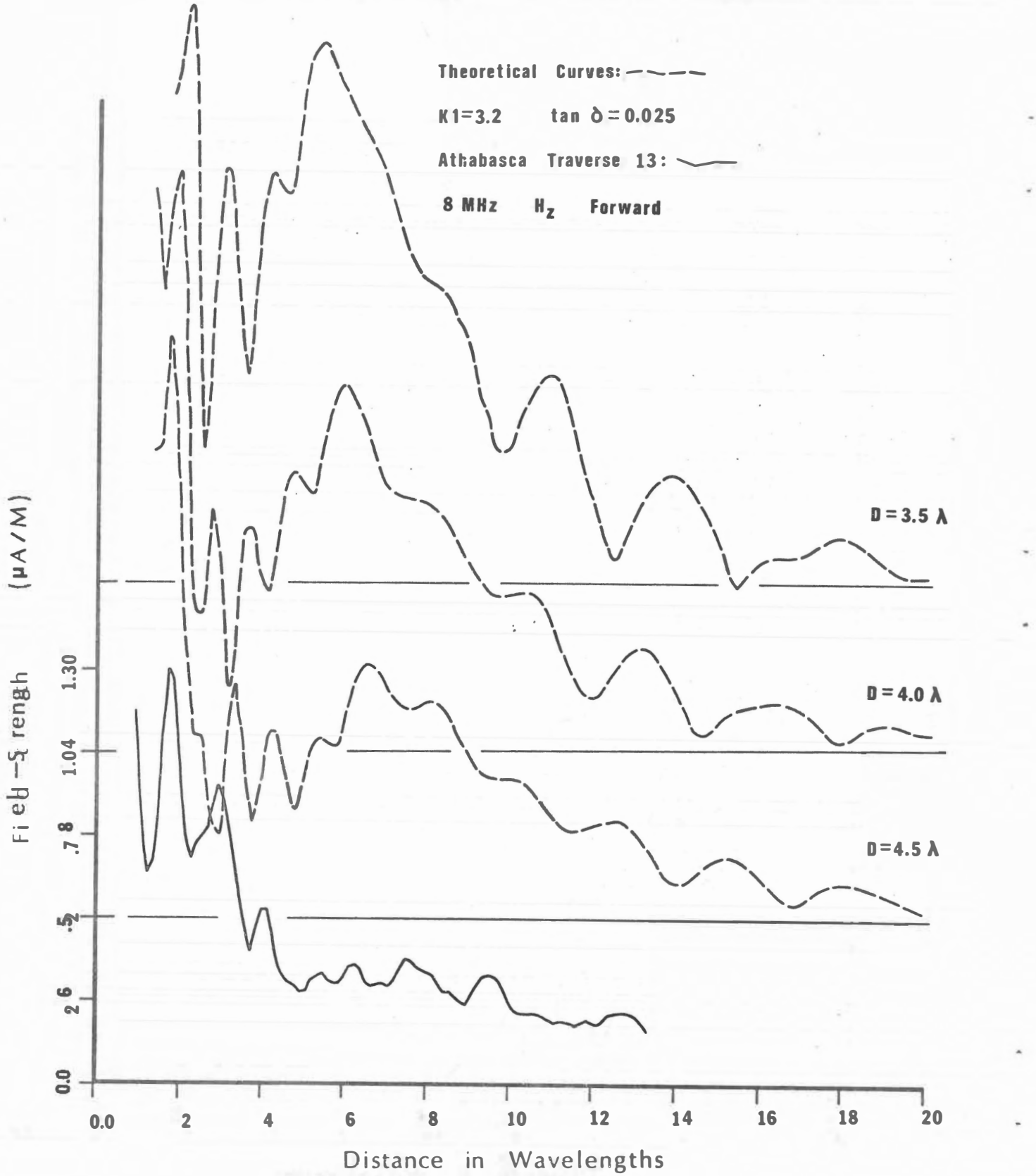

Figure 4-14: COMPARISON of THEORETICAL to FIELD DATA

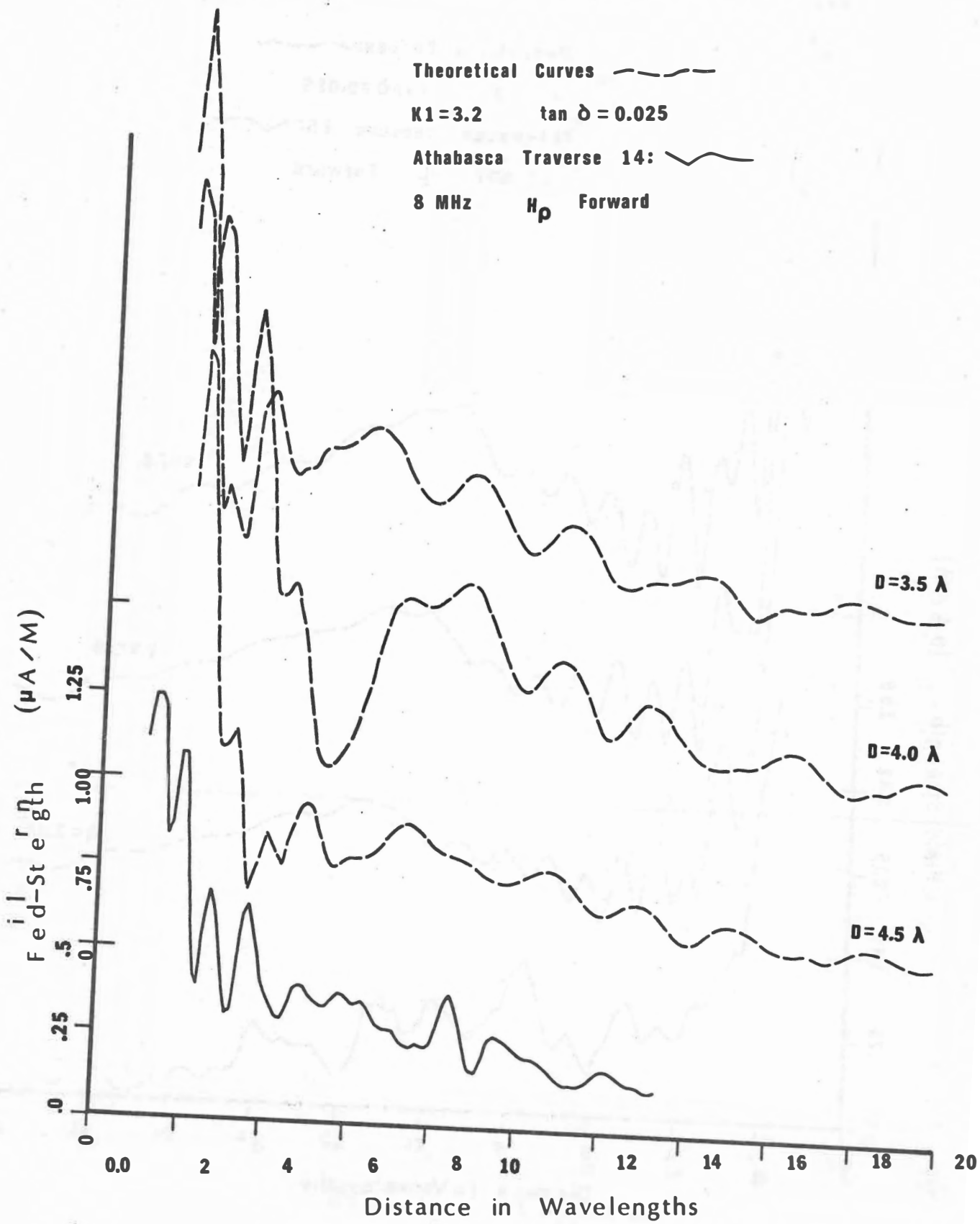

Figure 4-15: COMPARISON of THEORETICAL to FIELD DATA

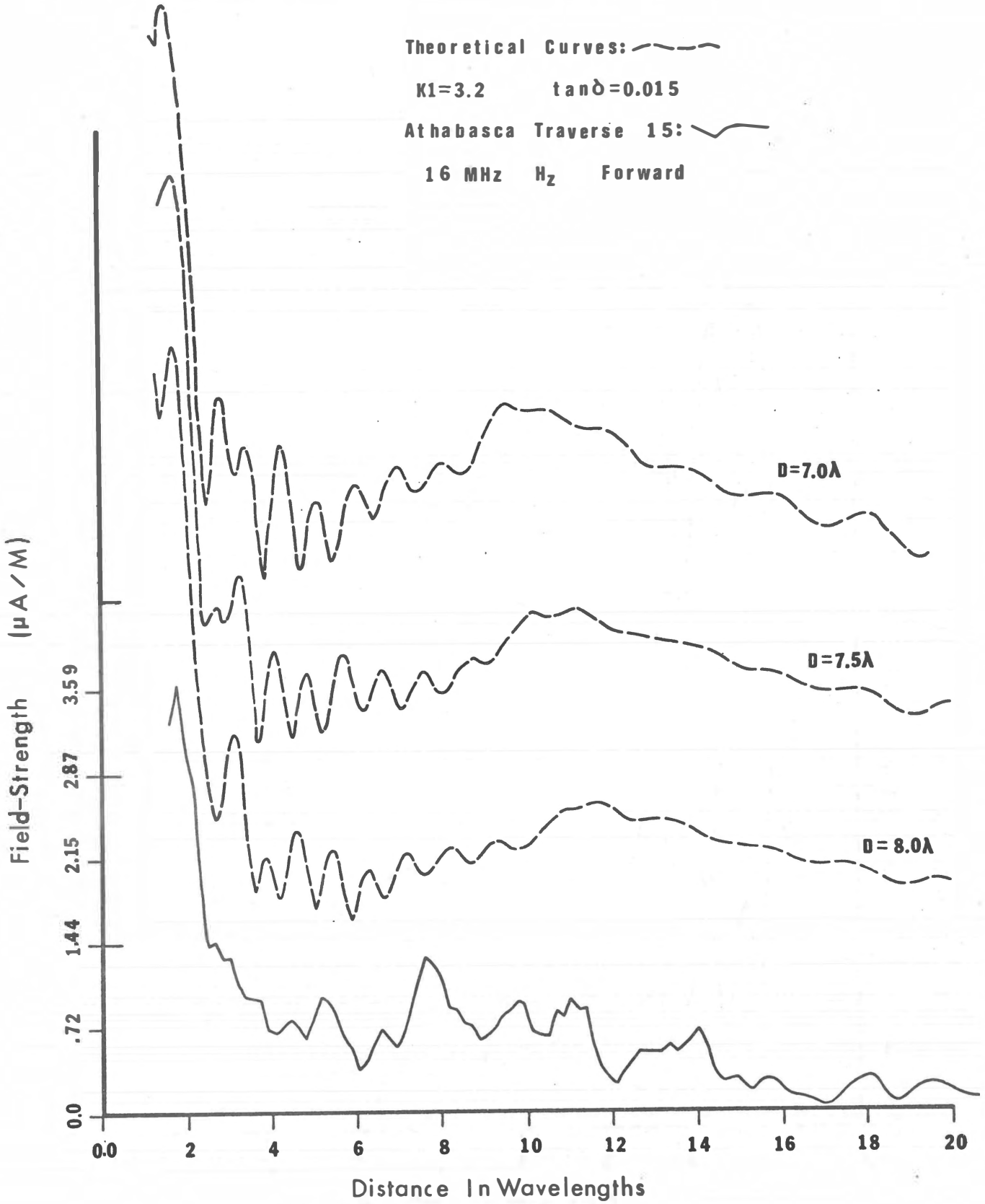

Figure 4-16: COMPARISON of THEORETICAL to FIELD DATA

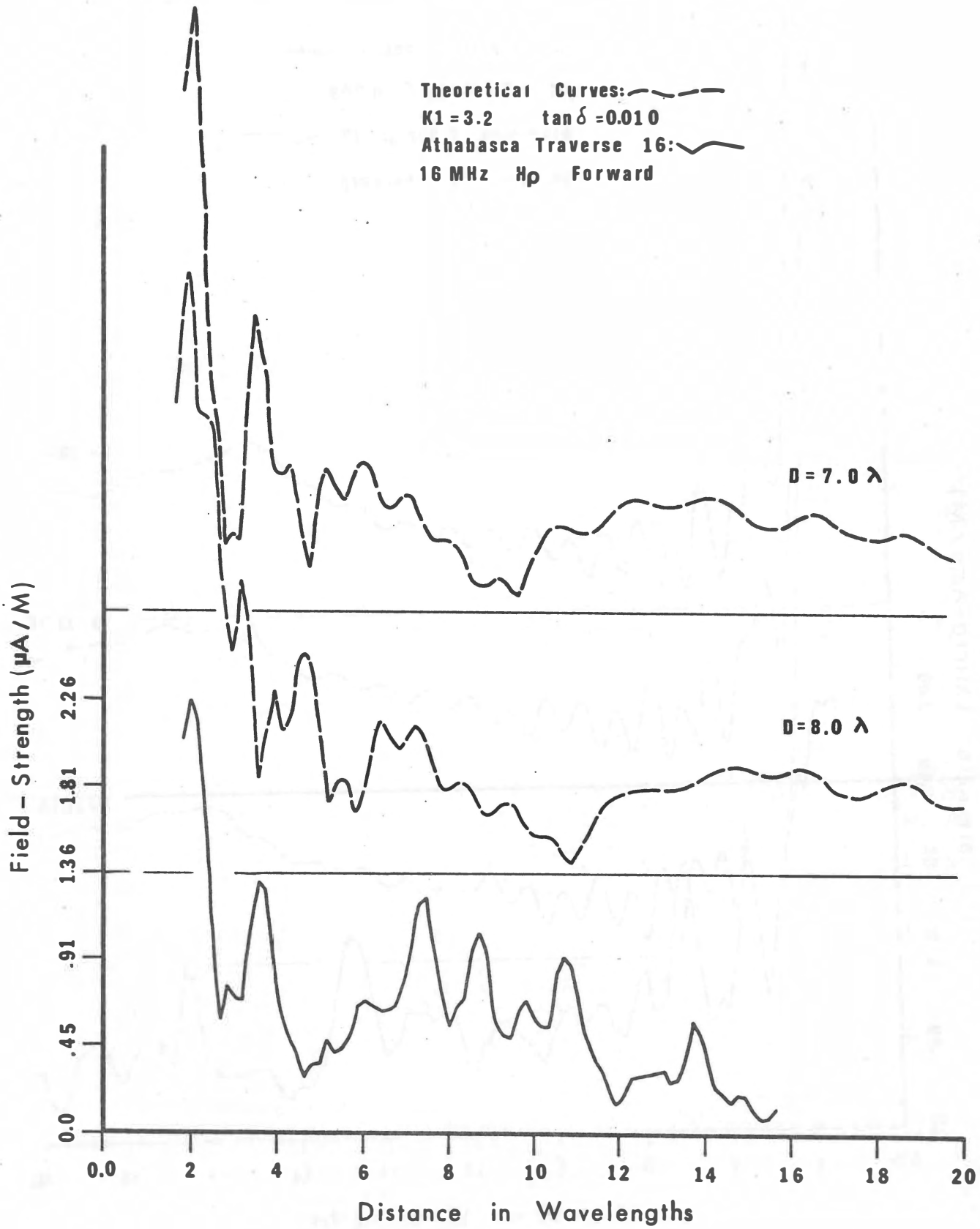

Figure 4-17 : COMPARISON of THEORETICAL to FIELD DATA

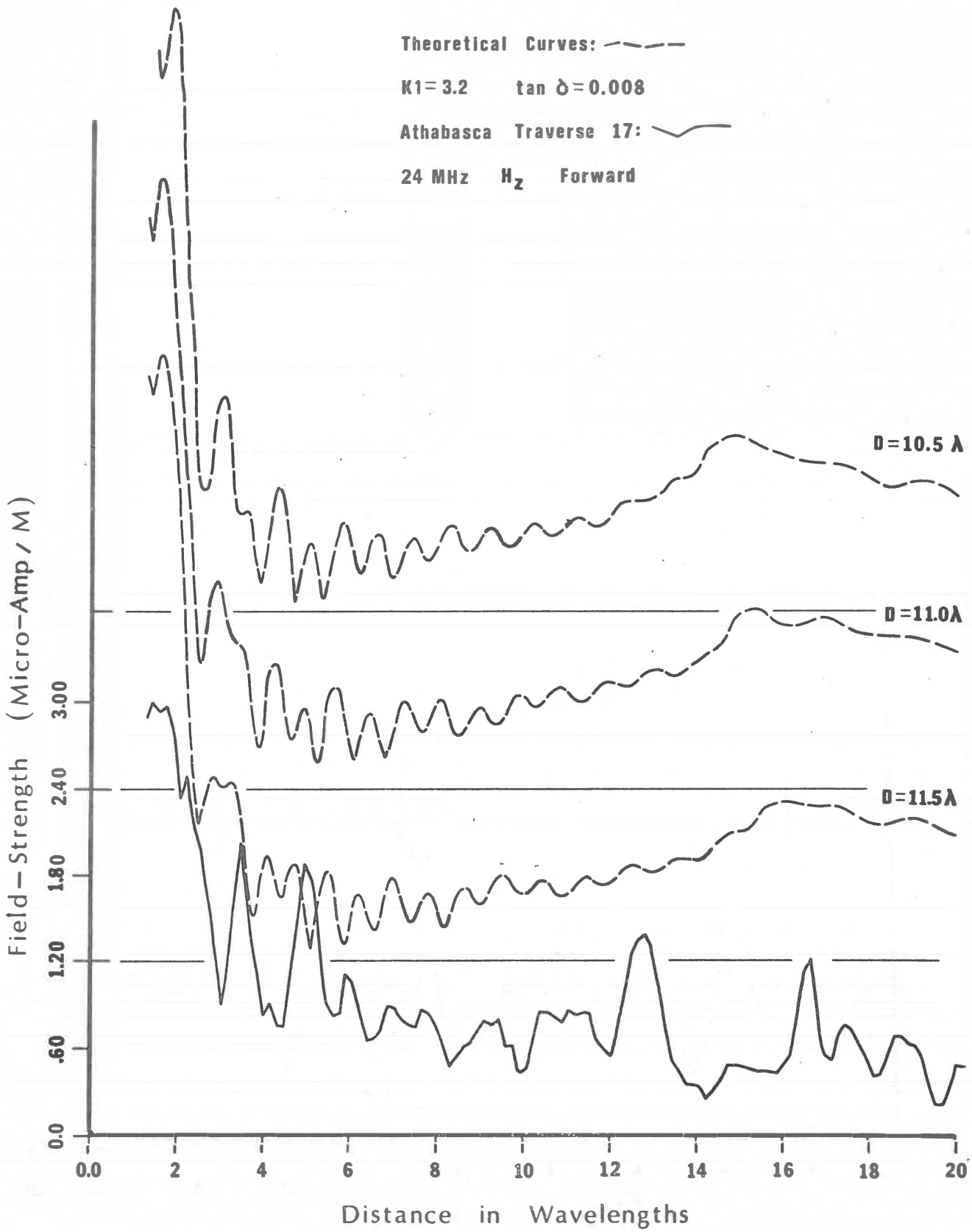

Figure 4-18: COMPARISON of THEORETICAL to FIELD DATA

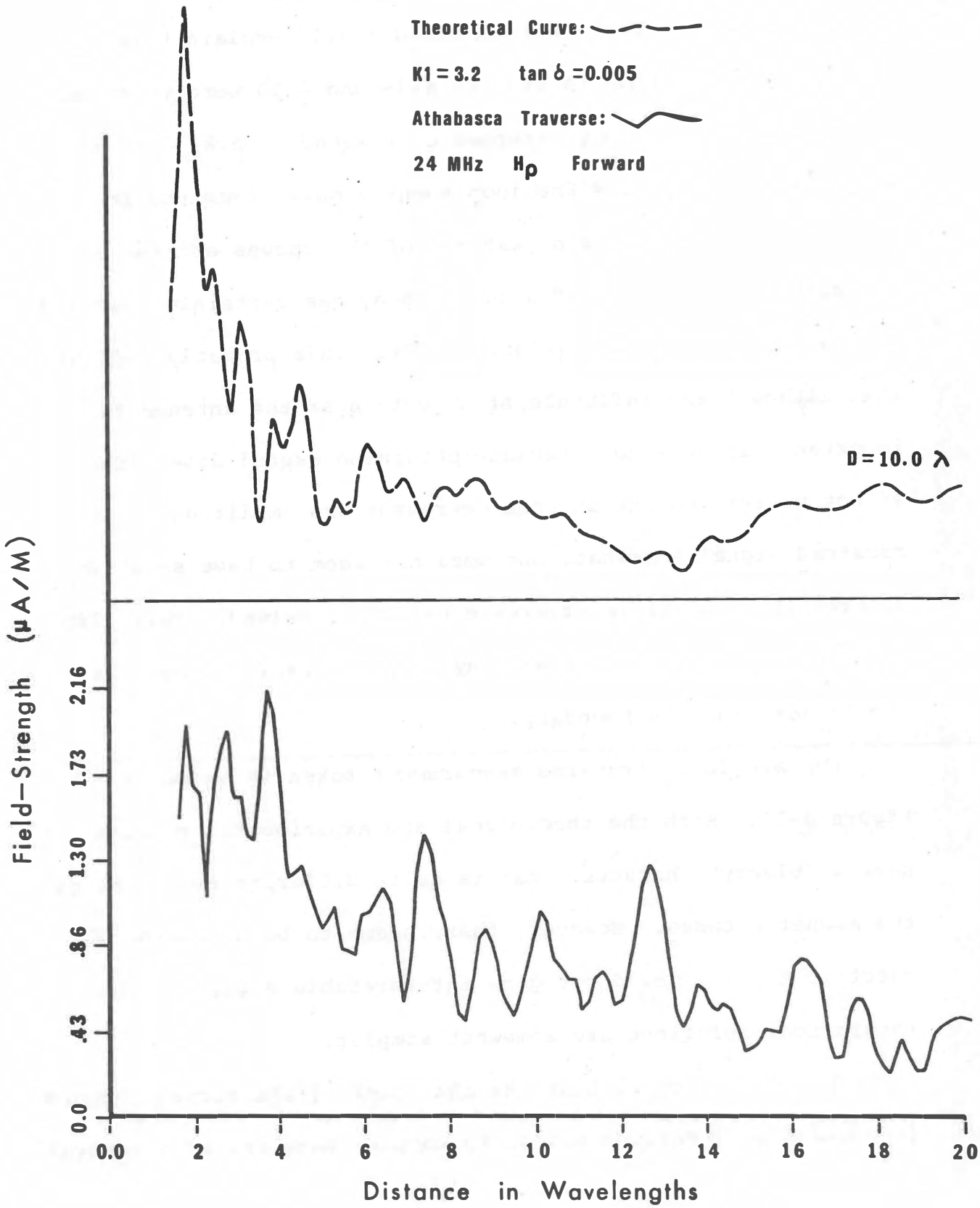

might not occur further than 20 wavelengths from the transmitter, and measurements into this region should have been made. The slope of the bottom could easily explain this.

The curves shown in Figures 4-19 and 4-20 were measured with the receiving loop strapped on someone's back, like a knapsack. This raised the loop about a meter from the ice surface ($\lambda/12$). The main features of the curves are the same, although the influence of a nearby body has certainly degraded the data in the H_ρ case (Figure 4-20). This probably indicates that although the influence of objects near the antenna is important, it does not preclude obtaining useful data. The effect of raising the antenna decreases the amplitude of the received signal somewhat, but does not seem to have severely altered the type of interference pattern received. This also needs more study, since there may be quite rapid changes in the fields near the boundary.

The single E_Φ traverse measurement taken is shown in Figure 4-21. Both the theoretical and experimental results have a "blocky" character that is quite different from that of the magnetic cases. However, there seems to be no reason why electric dipoles would not give interpretable data, and the theoretical solutions are somewhat simpler.

The conclusion is that the character of the curves changes from a few well-defined peaks, to complex patterns with several

Figure 4-19: COMPARISON of THEORETICAL to FIELD DATA

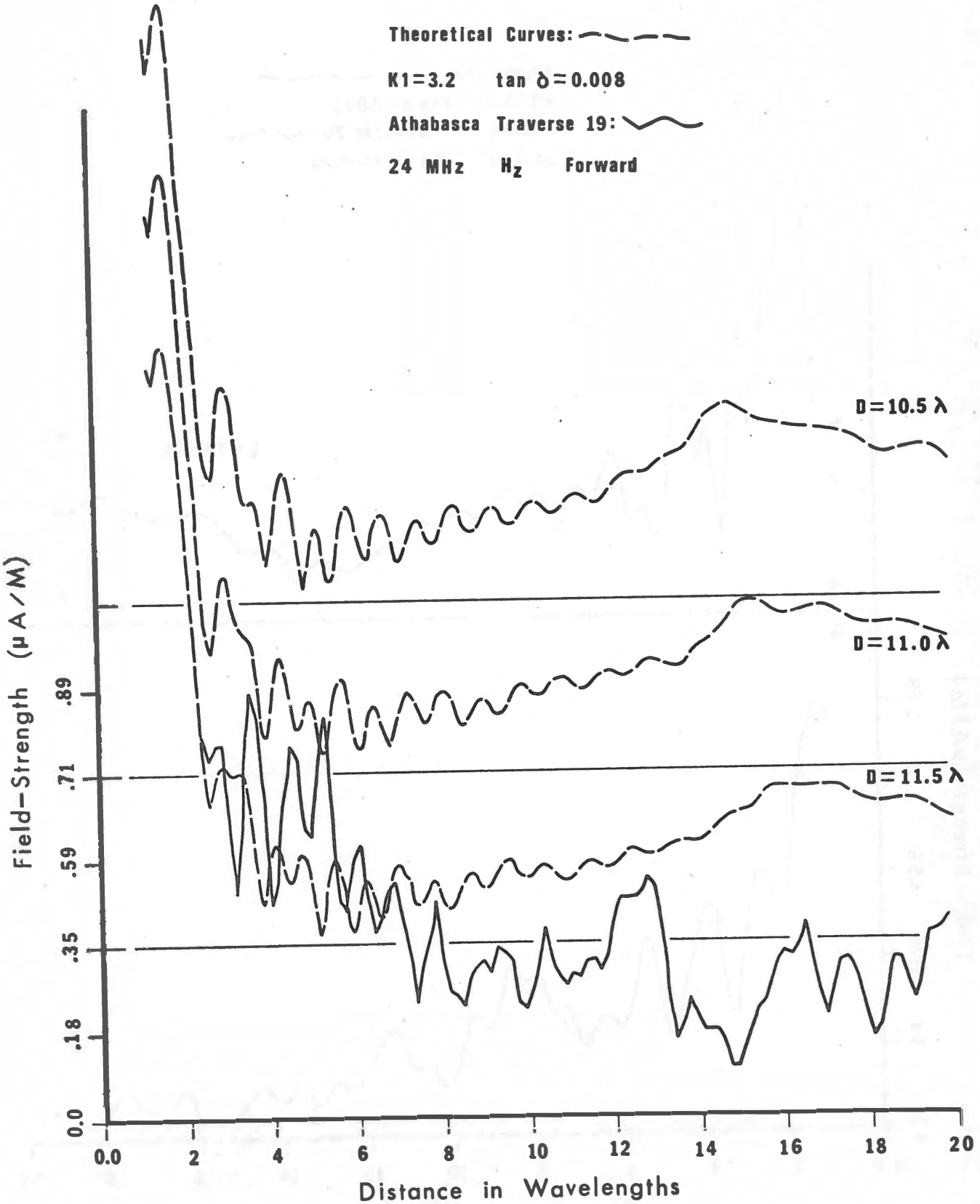

Figure 4-20: COMPARISON of THEORETICAL to FIELD DATA

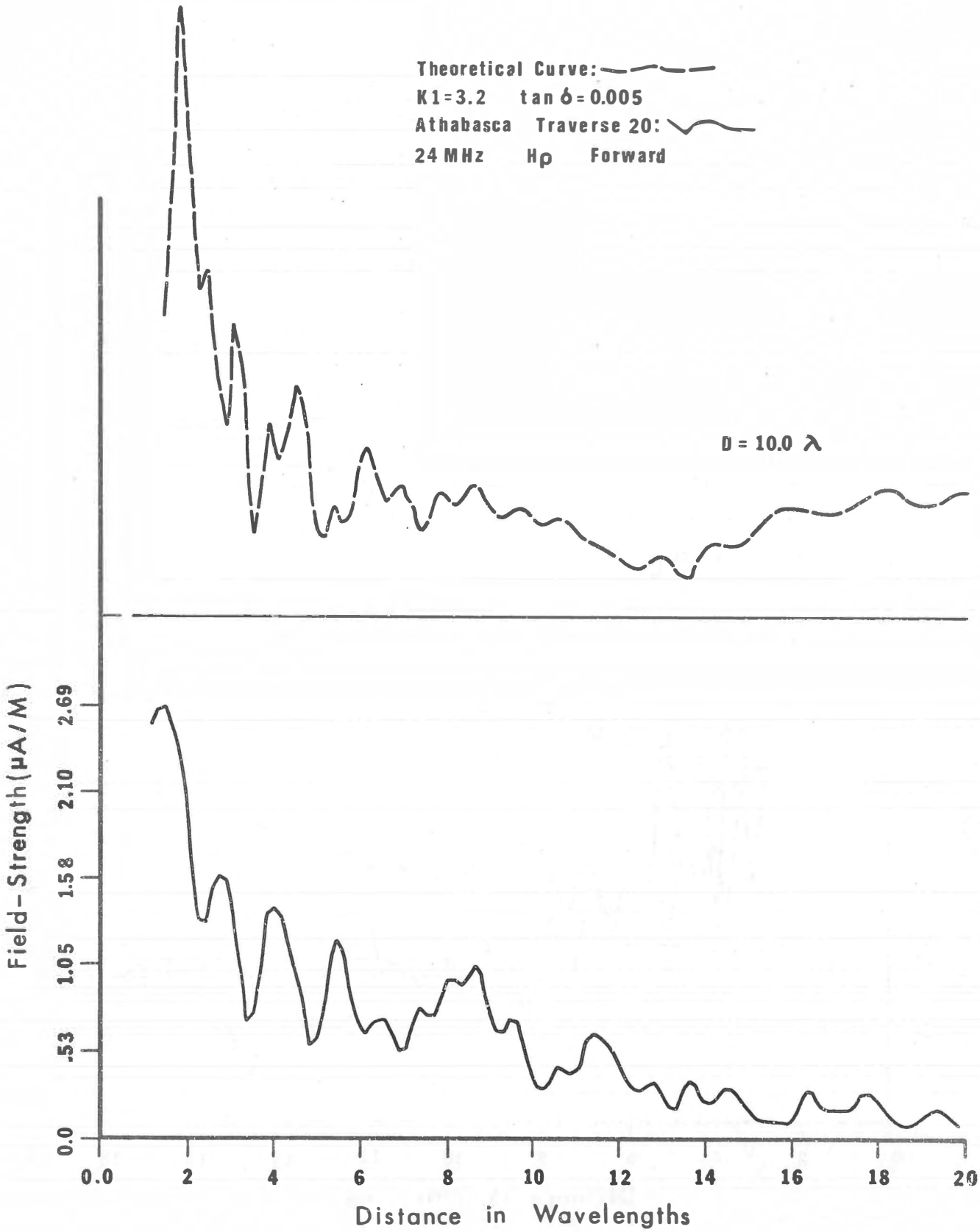

Figure 4-21: COMPARISON of THEORETICAL to FIELD DATA

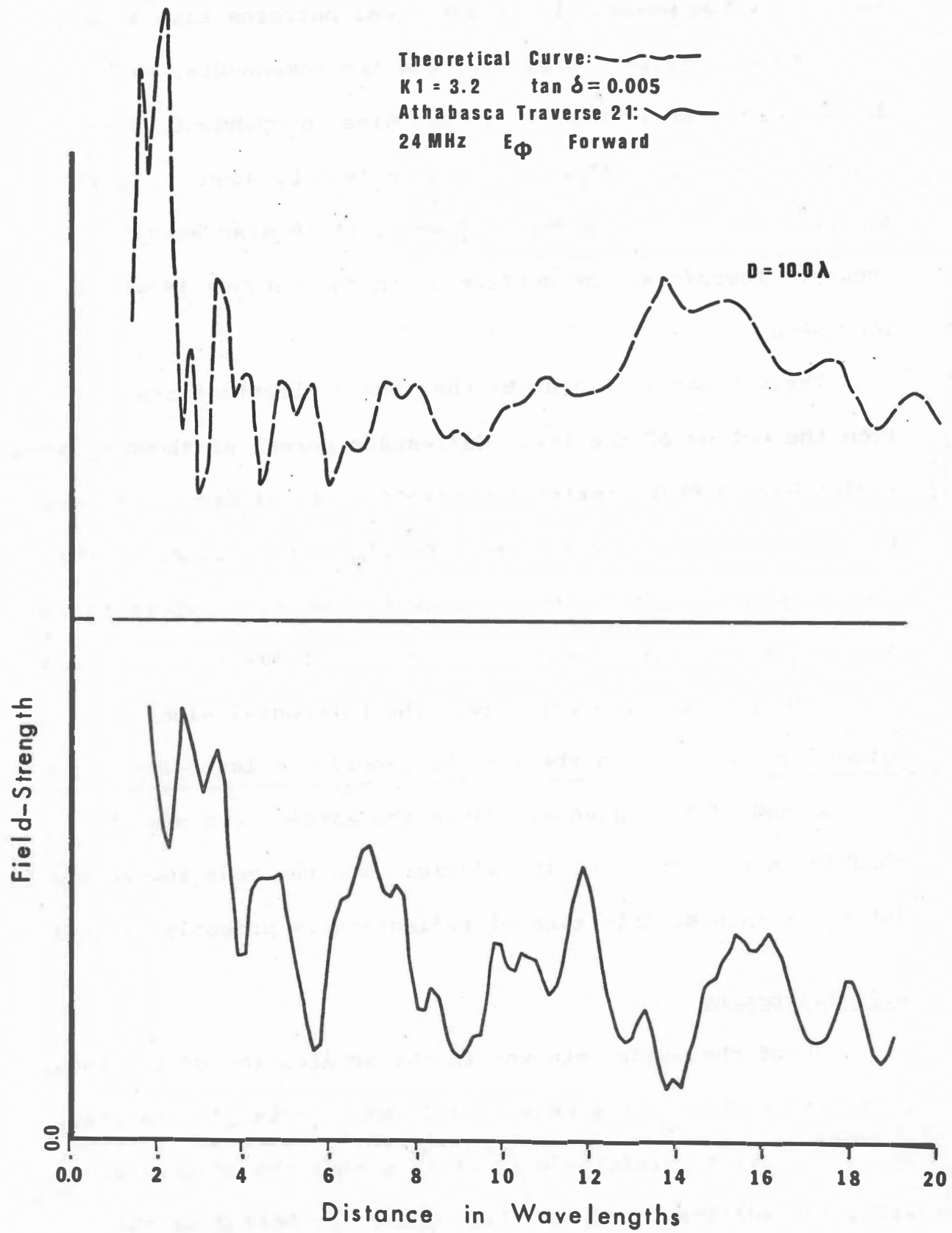

peaks of irregular amplitudes, to a high-frequency pattern, with few large peaks. The theoretical patterns also show this type of progression. Moreover, the two components, although different in their fine structure, give independent views of the same features. They are often offset by about $\lambda/2$, and although this is not understood well, it is also seen in the theory. Therefore, the confidence in the matches is greatly increased.

There seems little doubt that the reflections are coming from the bottom of the ice. Half-space curves as shown by Annan (1970) have a characteristic monotonic rate of decay. However, in the presence of a reflecting interface an increase in the amplitude of the interference peaks is common, as shown in the data collected. The possibility that the reflections are from nearby objects is also very low. The horizontal electric dipole couples well to the ice, but poorly to lateral objects off the end of the antenna. Since the antenna was placed roughly in the centre of the glacier with the ends toward the lateral moraines, this type of reflection is probably minimal.

4.3 Scattering

One of the major unknowns in the application of the interferometry method is how deleterious the effects of irregularities are. It is reasonable to believe that the effects of irregular surfaces (both at the top and the bottom of the

dielectric), inhomogeneities in the dielectric, reflections from unusual angles or positions, and the perturbations of the fields by objects near the transmitting or receiving antennas, could all contribute to extremely scattered data. In the absence of theoretical treatment or of careful scale-model evaluation of these problems, it is worth examining the field data for clues to their importance.

To a first approximation the data presented in Section 4.2 would indicate that any scattering present is not sufficient to destroy the general nature, at least, of the measured patterns. However, as mentioned earlier, filtering did enhance the main features of the curves. This is a possible method of reducing random irregularities, provided a high enough measurement density is taken.

After noticing that the maximum signal was not always in the z - ρ plane, two traverses were taken of the H_Φ component as well. These are shown in Figures 4-22 and 4-23. If there are no lateral reflections, there should be no H_Φ component. Both traverses show significant H_Φ, although they are both low in signal strength compared to the similar H_z and H_ρ traverses. There are two possible explanations. Either H_Φ is in a true null, and therefore gives an indication of the noise present in all components, or there are lateral reflections present. The first seems to apply to traverse 12, which shows irregular

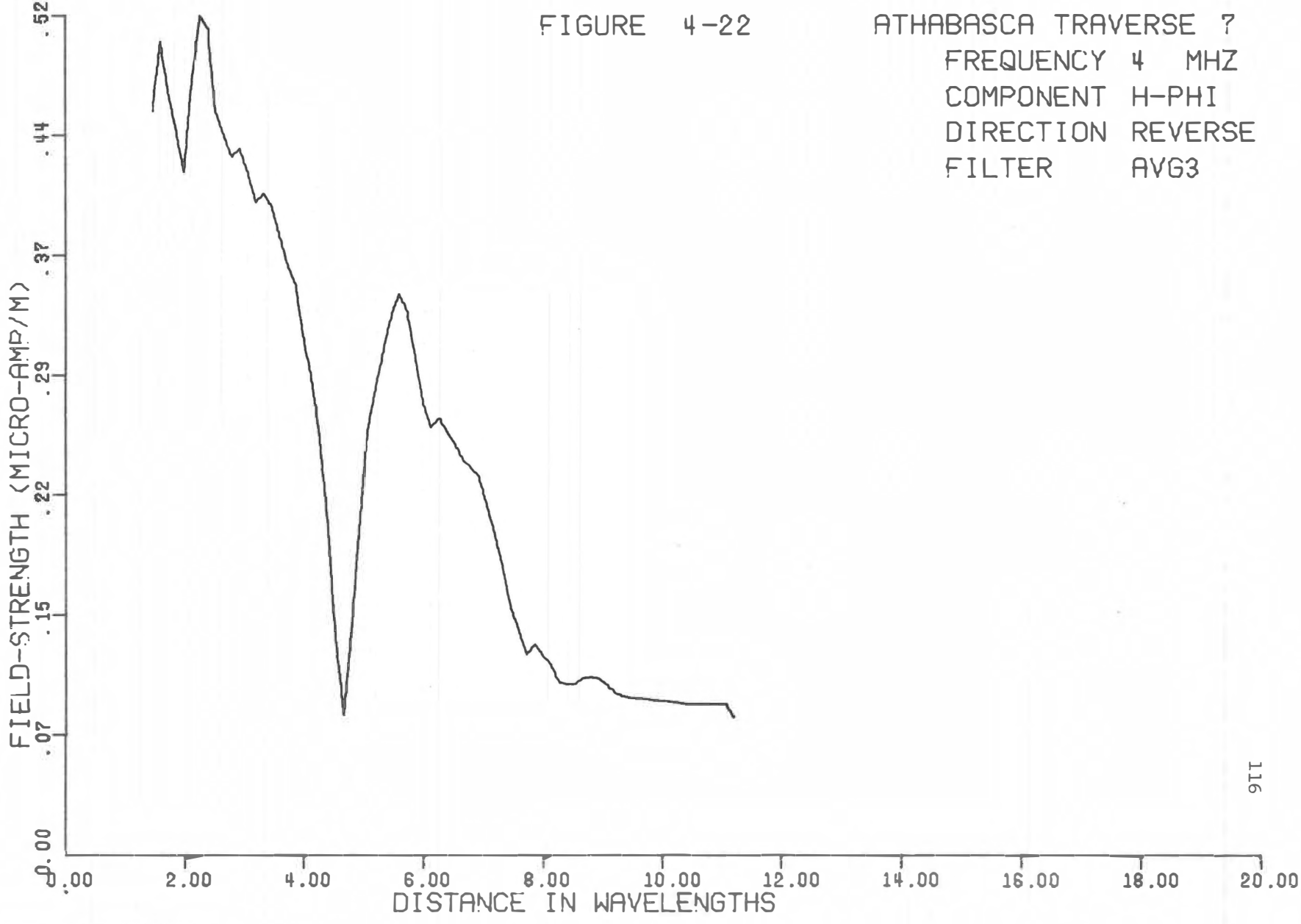
FIGURE 4-22
ATHABASCA TRAVERSE 7
FREQUENCY 4 MHZ
COMPONENT H-PHI
DIRECTION REVERSE
FILTER AVG3
FIELD-STRENGTH (MICRO-AMP/M)
0.00
.07
.15
.22
.29
.37
.44
.52
0.00
2.00
4.00
6.00
8.00
10.00
12.00
14.00
16.00
18.00
20.00
DISTANCE IN WAVELENGTHS

FIGURE 4-23

ATHABASCA TRAVERSE 12
FREQUENCY 8 MHZ
COMPONENT H-PHI
DIRECTION REVERSE
FILTER AVG3

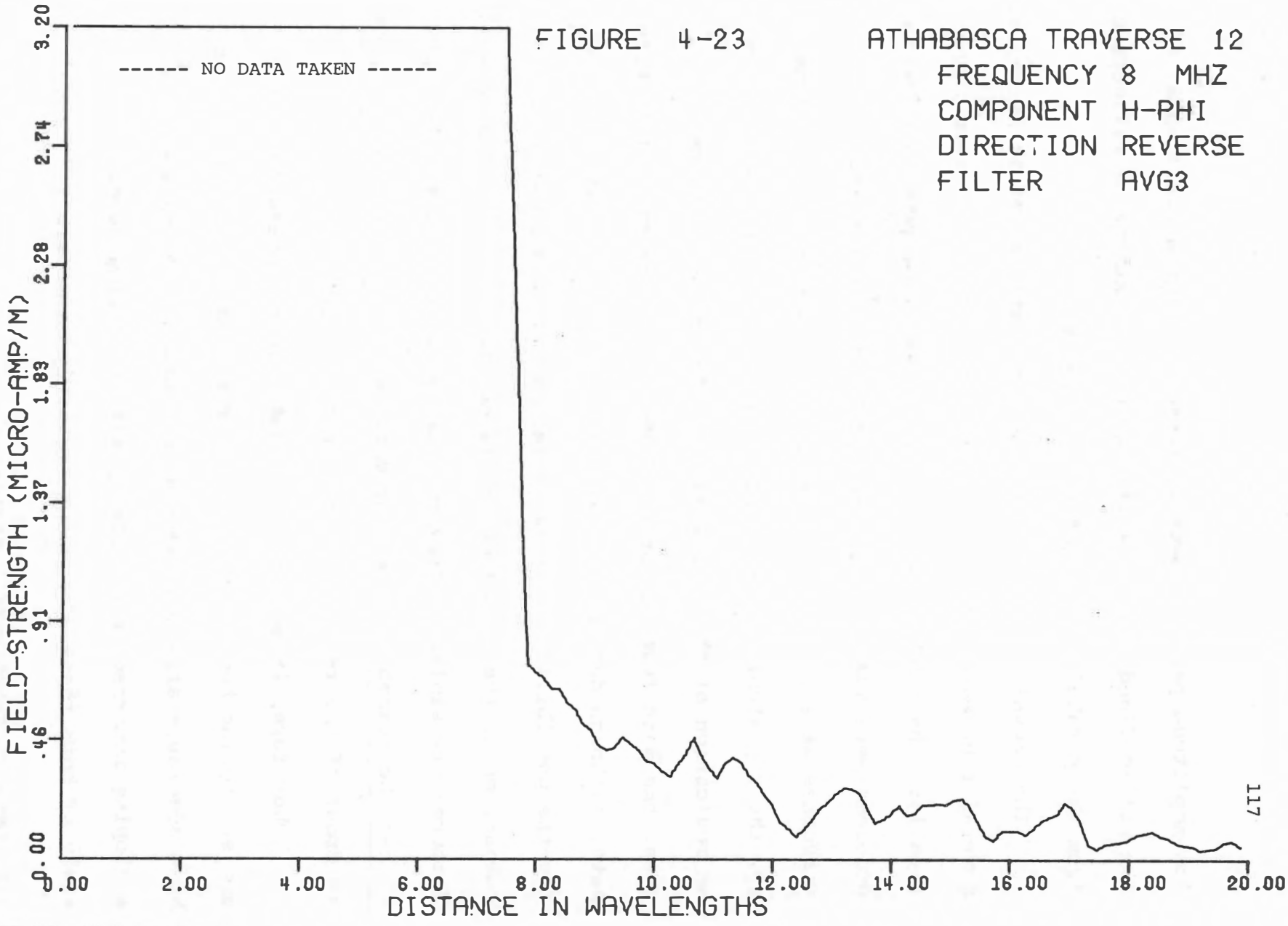

low-amplitude peaks. However, traverse 7 has a clear null and two well-defined peaks. These may be indications of reflections from the parabolic sides of the glacier valley.

The amount of instrumental or systematic error is not clear. Several runs were made over the same traverse, but never identically: the 8 MHz traverses were repeated because instrumental problems were suspected on the first run, and the second 24 MHz traverses were run with the receiver on someone's back. Even so, the repeatability comparisons (Figures 4-24 to 4-27) give an indication of the consistency of the results. As can be seen, the main features of the 8 MHz curves are present in both sets, although degraded somewhat in traverses 13 and 14, supporting the possibility of instrumental error. A good peak-to-peak comparison of the 24 MHz curves is not possible, but the general features are similar. Traverses 18 and 20 compare poorly, but it must be remembered that the data was taken with a body directly in front of the receiving loop during traverse 20.

Therefore, it must be concluded that the presence of random scattering bodies could be important, but does not seem to have adversely affected these data. Lateral reflections from a sloping interface are probably also occurring here. More study of both these effects is certainly in order.

4.4 Rate of Decay with Distance

In order to plan the power requirements of the S.E.P.

FIGURE 4-24: REPEATABILITY OF DATA–ATHABASCA
TRAVERSES 8 (a) and 13(b)
8 MHz H_z FORWARD

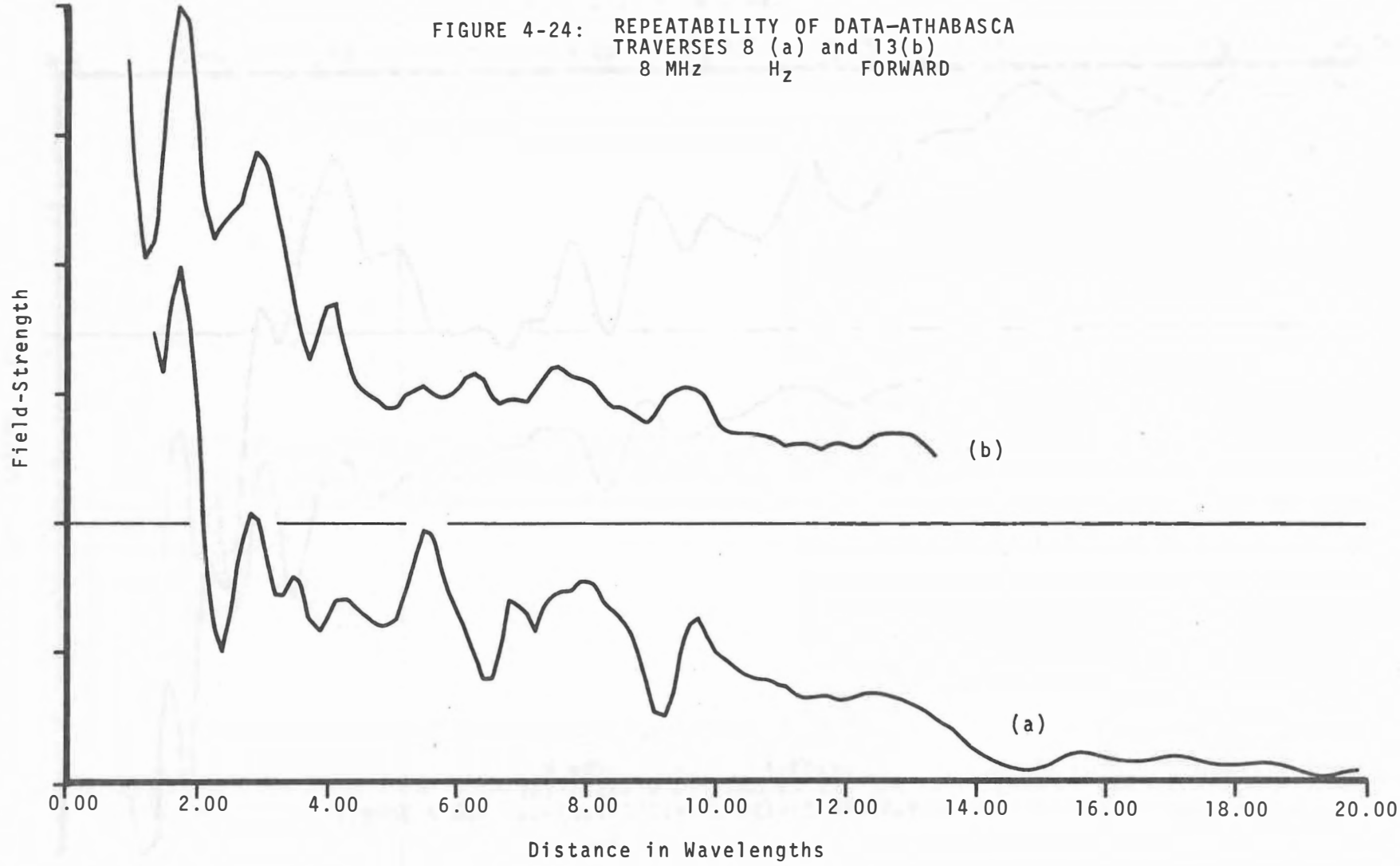

FIGURE 4-25: REPEATABILITY OF DATA-ATHABASCA
TRAVERSES 9 (a) AND 14 (b)
8 MHz H_ρ FORWARD

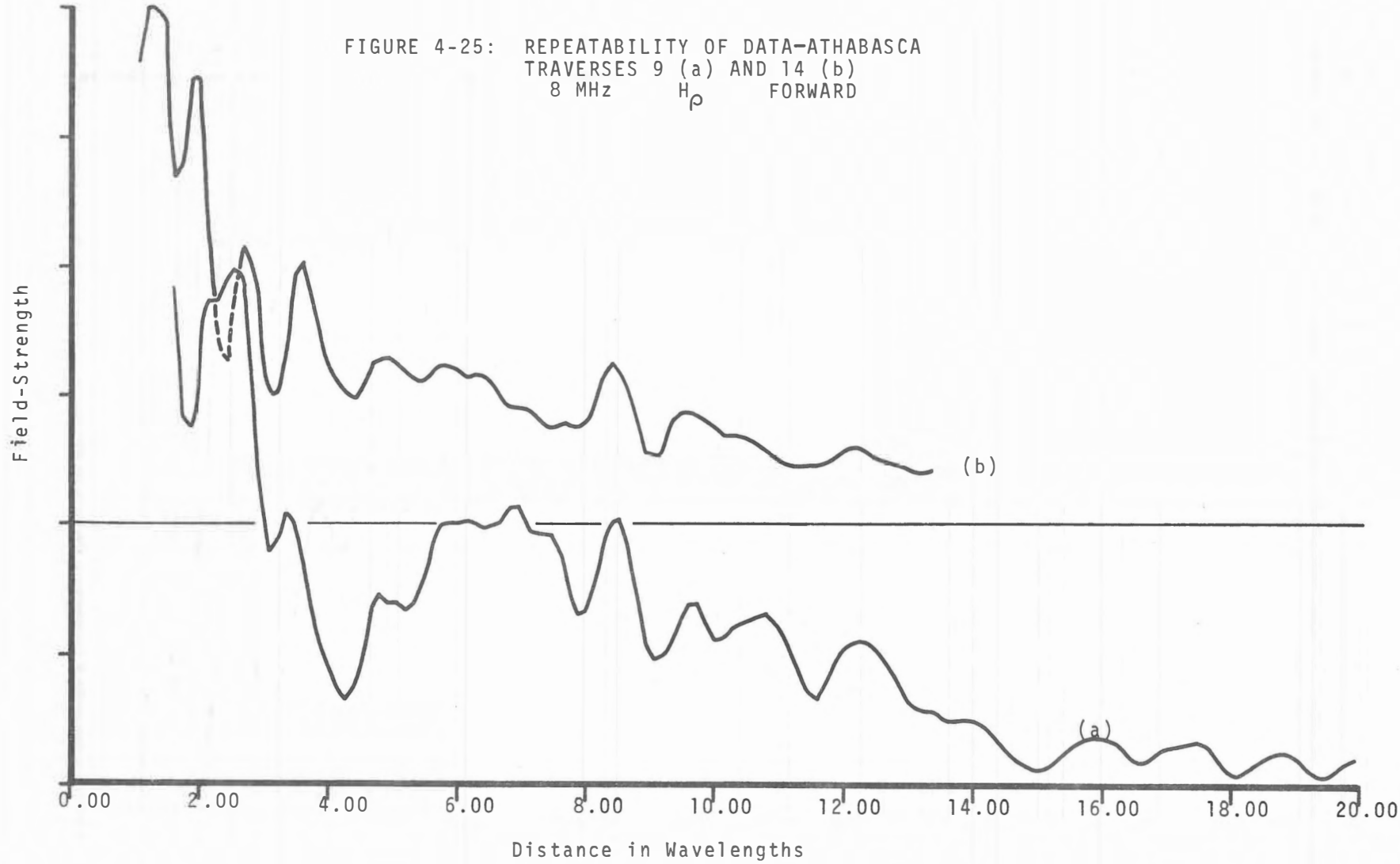

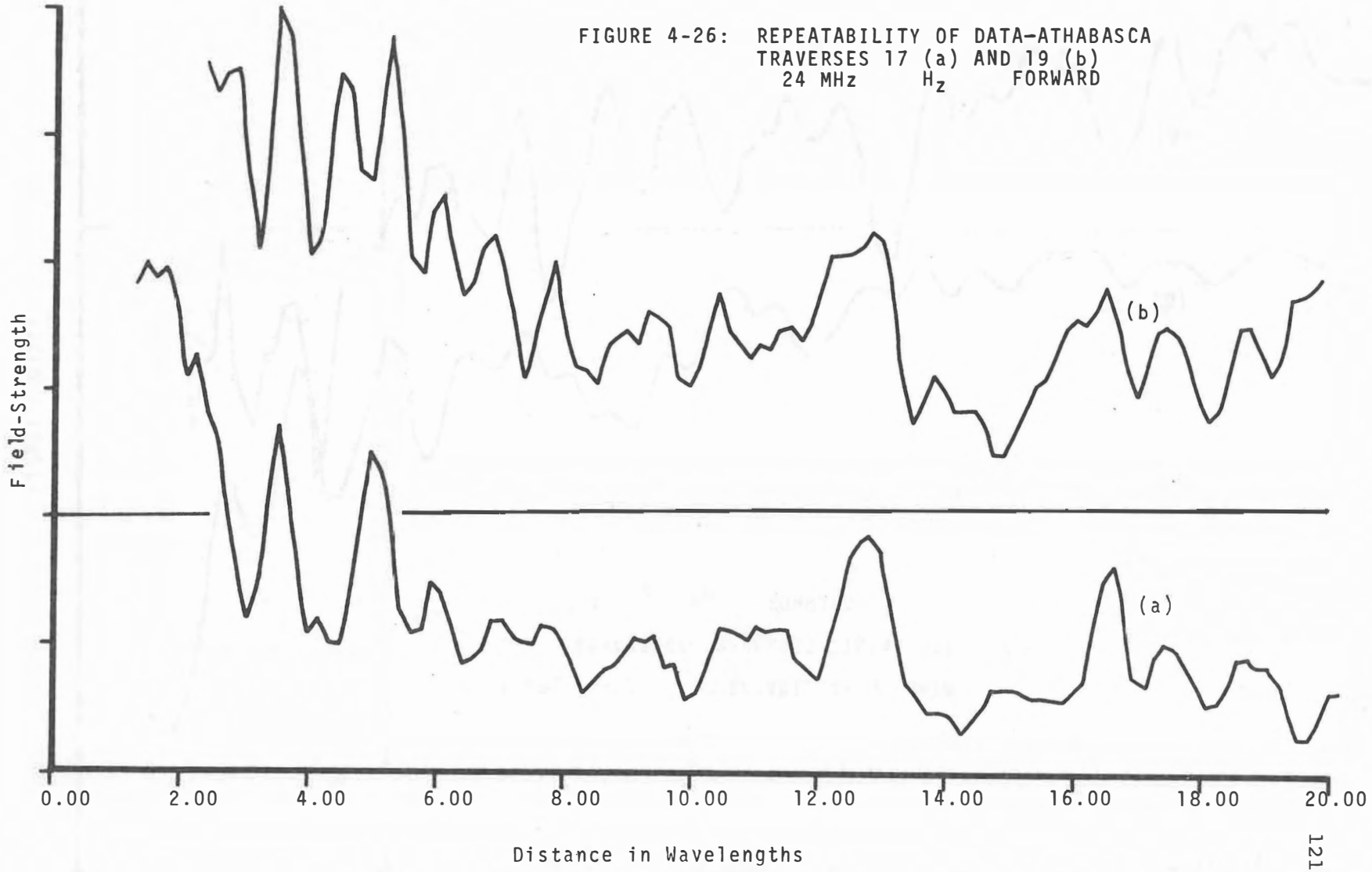

FIGURE 4-26: REPEATABILITY OF DATA-ATHABASCA TRAVERSES 17 (a) AND 19 (b) 24 MHz H_z FORWARD

FIGURE 4-27 REPEATABILITY OF DATA

ATHABASCA TRAVERSES 18(a) AND 20(b)

24 MH_z H_p FORWARD

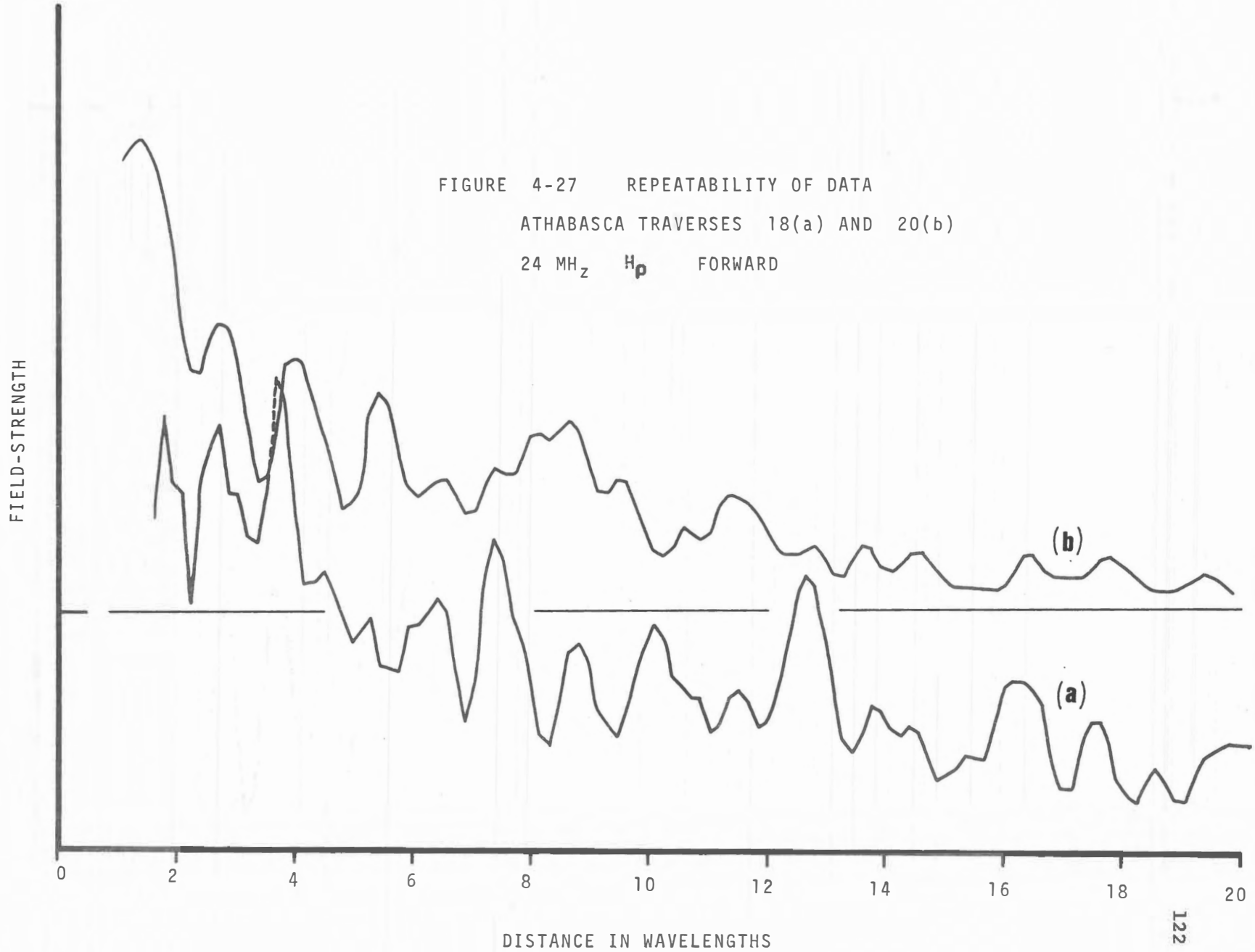

Experiment, it was necessary to know what rate of decay of received signal, with distance, could be expected. It was also hoped that a study of this would yield clues to understanding and interpreting the interference problem. In general the field strength from a point-source falls off as r^{-1}, where r is the distance from the source, due to geometrical spreading. This is also true for dipoles in free space, in the far-field. However, it is not clear a priori what the effect of the dielectric and reflecting boundaries will be. Theoretically it is necessary to find solutions for the fields at various distances, i.e., the solutions of Annan and Sinha. It was of interest to determine whether or not the field data agreed with this, and what dependence there was on the various parameters.

It is reasonable that, to a first approximation, the field strength F has the form

$$F = ar^{-s} \qquad (4\text{-}1)$$

where

a is a constant depending on the output power of the source,

r is the distance from the source, and

s is the rate of decay constant, a small positive number.

Taking logarithms of 4-1:

$$\text{Log}(F) = \log(a) - s \cdot \log(r) \qquad (4.2)$$

Therefore a plot of log(F) vs log(r) will have a slope of -s. Of course, the interference peaks and troughs will be perturbations on this.

At the present time only the theoretical H_z component has been analysed in this way. Table 4-2 lists the values of s for various depths and loss tangents, for both a perfect and a dielectric reflector using theoretical curves. The distance (r) has been taken from 0.6 wavelengths to 20 wavelengths from the source. Unfortunately, the theoretical H_z component does not lend itself to this type of analysis, because of the large effect of the discontinuity, mentioned earlier. Therefore, the changes of s with depth given in Table 4-2 are probably somewhat biased although the changes with loss tangent are probably more significant, since the discontinuity varies with depth.

The rate of decay at the boundary of a half-space, with a value of approximately 2, is greater than that of free space. There is also a slight dependence on loss tangent, which may be partly a function of the particular range over which s is taken. However, as the depth is decreased, the rate of decay decreases to a value ranging from less than 1 to more than 2,

Table 4-2(a): Theoretical rate of decay, H_z, perfectly reflecting bottom, K1 = 3.2

Depth Wavelengths	Loss Tangent 0.008	0.015	0.025	0.050	0.100	0.20
2.0	0.7	1.1	1.5	2.6	2.4	2.1
3.0	0.8	1.1	1.6	2.4	2.2	2.1
4.0	0.5	0.9	1.3	2.2	2.2	2.1
5.0	0.5	0.8	1.2	2.2	2.2	2.1
6.0	0.4	0.7	1.1	2.2	2.1	2.1
7.0	0.4	0.7	1.2	2.2	2.1	2.1
8.0	0.3	0.7	1.3	2.2	2.1	2.1
9.0	0.4	0.8	1.4	2.2	2.1	2.1
10.0	0.5	0.9	1.5	2.2	2.1	2.1
11.0	0.6	1.0	1.7	2.2	2.1	2.1
12.0	0.7	1.2	1.9	2.3	2.1	2.1
15.0	1.1	1.7	2.5	2.3	2.1	2.1
20.0	1.6	2.2	2.4	2.3	2.1	2.1
HALF-SPACE	2.3	2.5	2.4	2.3	2.1	2.1

Table 4-2(b): Theoretical rate of decay, H_z, dielectric bottom, K1 = 3.2

K2 = 10.0 $\tan \delta_2 = 0.10$

Depth Wavelengths	Loss Tangent 0.008	0.015	0.025	0.050	0.100	0.200
2.0	1.3	1.5	1.9	2.5	2.2	2.1
3.0	1.1	1.3	1.7	2.4	2.2	2.1
4.0	0.8	1.1	1.5	2.3	2.2	2.1
5.0	0.7	1.0	1.5	2.3	2.1	2.1
6.0	0.7	1.0	1.5	2.3	2.1	2.1
7.0	0.7	1.1	1.6	2.2	2.1	2.1
8.0	0.8	1.1	1.7	2.2	2.1	2.1
9.0	0.8	1.2	1.8	2.2	2.1	2.1
10.0	0.9	1.4	2.0	2.3	2.1	2.1
11.0	1.1	1.5	2.1	2.3	2.1	2.1
12.0	1.2	1.7	2.2	2.3	2.1	2.1
15.0	1.6	2.2	2.5	2.3	2.1	2.1
20.0	2.1	2.5	2.4	2.3	2.1	2.1

depending largely on the loss tangent. This indicates that the boundary is guiding the wave to a certain extent, giving a loss-dependent rate of decay, which does not seem to change greatly with depth. It is interesting to note that when the boundary is not a perfect reflector the rates of decay are higher (Table 4-2(b)), indicating that losses at a subsurface boundary are important. The rate of decay does not change significantly with small changes of dielectric constant.

These values may now be compared to those of the Athabasca Glacier data, given in Table 4-3. The rates of decay vary from larger values at the low frequencies, to lesser ones at the higher frequencies. This agrees with the inverse dependence of loss tangent on frequency in ice. There also seem to be no systematic differences among the various components. If an average value of the rate of decay for each depth (from Table 4-2) is plotted against log(tan δ), nearly a straight line results, over the loss tangents of interest to interferometry (0.005 to 0.050). If the rates of decay of the field data are plotted in the same way, but plotting -log(frequency) on the abscissa, the same type of line results, as shown in Figure 4-28. By superimposing the lines, and combining log(tan δ) with log(f),

$$\log(\tan \delta \cdot f) = -0.7 \pm .3 \qquad (4\text{-}3)$$

Table 4-3: Rates of Decay of Athabasca Glacier Data

Traverse Number	Frequency (MHz)	Component	Direction	Rate of Decay (s)	Shown in Figure
1	2	H_z	Forward	2.2	4-29
2	2	H_ρ	Forward	1.9	
3	4	H_z	Forward	1.5	4-30
4	4	H_ρ	Forward	1.4	
5	4	H_z	Reverse	1.3	4-31
6	4	H_ρ	Reverse	1.3	
7	4	H_Φ	Reverse	1.0	
8	8	H_z	Forward	1.4	4-32
9	8	H_ρ	Forward	1.3	
10	8	H_z	Reverse	1.2	4-33
11	8	H_ρ	Reverse	1.4	
12	8	H_Φ	Reverse	1.9	
13 (1)	8	H_z	Forward	0.7	
14 (1)	8	H_ρ	Forward	0.8	
15 (1)	16	H_z	Forward	1.2	
16 (1)	16	H_ρ	Forward	0.9	
17	24	H_z	Forward	0.6	4-34
18	24	H_ρ	Forward	0.7	
19	24	H_z	Forward	0.7	
20	24	H_ρ	Forward	1.1	
21	24	E_Φ	Forward	0.6	

(1) Dubious data

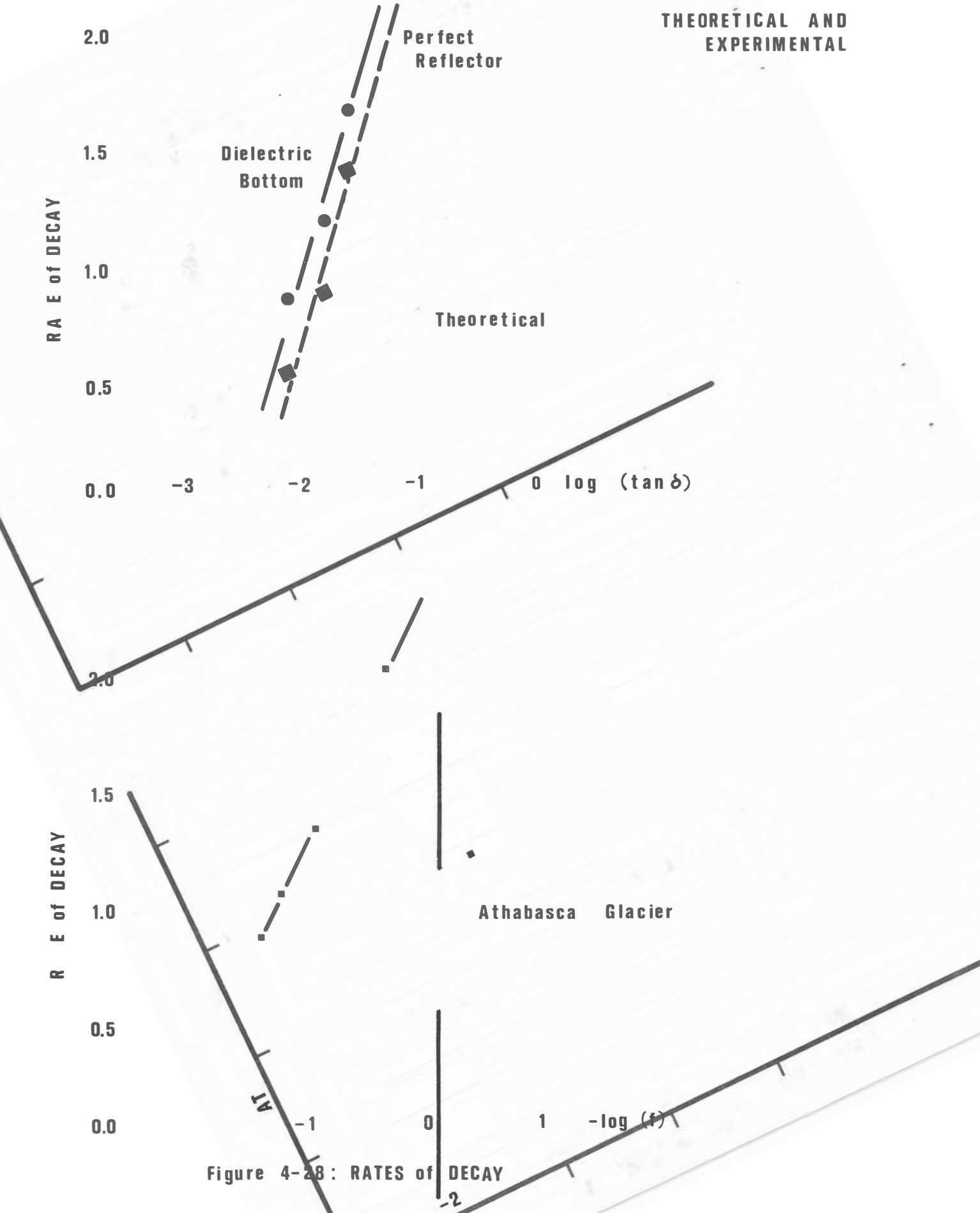

Figure 4-28: RATES of DECAY

This becomes, taking antilogs,

$$\tan \delta = (0.25 \pm .15)/f \qquad (4\text{-}4)$$

which is in good agreement with the published data on the loss tangent of ice.

Log-log plots of the H_z Athabasca traverse data are shown in Figures 4-29 to 4-34. A representative theoretical curve is included with each for comparison. The slope, which gives rate of decay, is shown, and is calculated by a least-squares fit to all the points. Of course there is a fair amount of scatter in the results due to interference peaks and nulls. Although individual comparisons are not in complete agreement, the trend is clear: as the loss tangent increases, the decay ra increases. It is also evident that the slope will depend rather critically on how the points are chosen. The plots almost all show a decreasing tail, for example, and it is possible that several different slopes should be taken over different ranges. However, as a first approximation, the rate of decay has been shown to be a useful parameter.

It appears, then, that the rate of decay of the field strengths using the interference technique varies from 0.5 to 2.5. The measured results agree reasonably well with theory, with few exceptions. Therefore, the received power may fall off as quickly as r^{-5}. This is critical in the design of power requirements and receiver sensitivity of equipment for

FIGURE 4-29: COMPARISON OF RATES OF DECAY
ATHABASCA GLACIER TO THEORETICAL

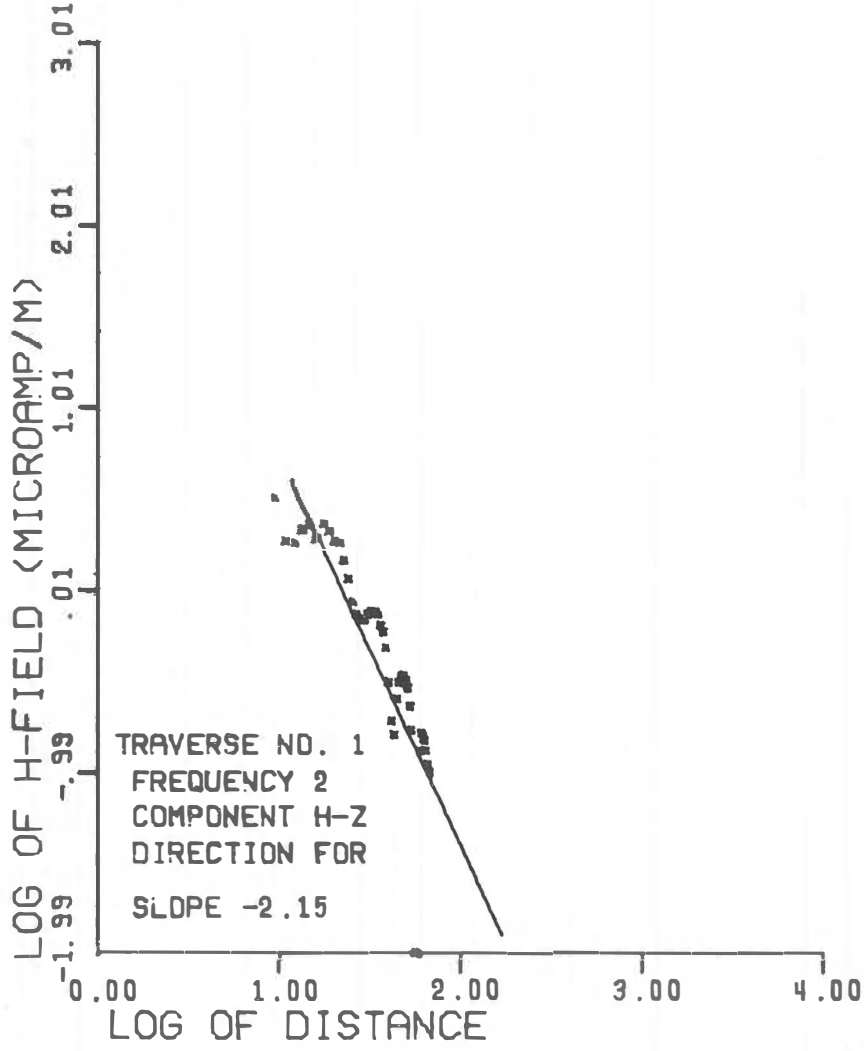

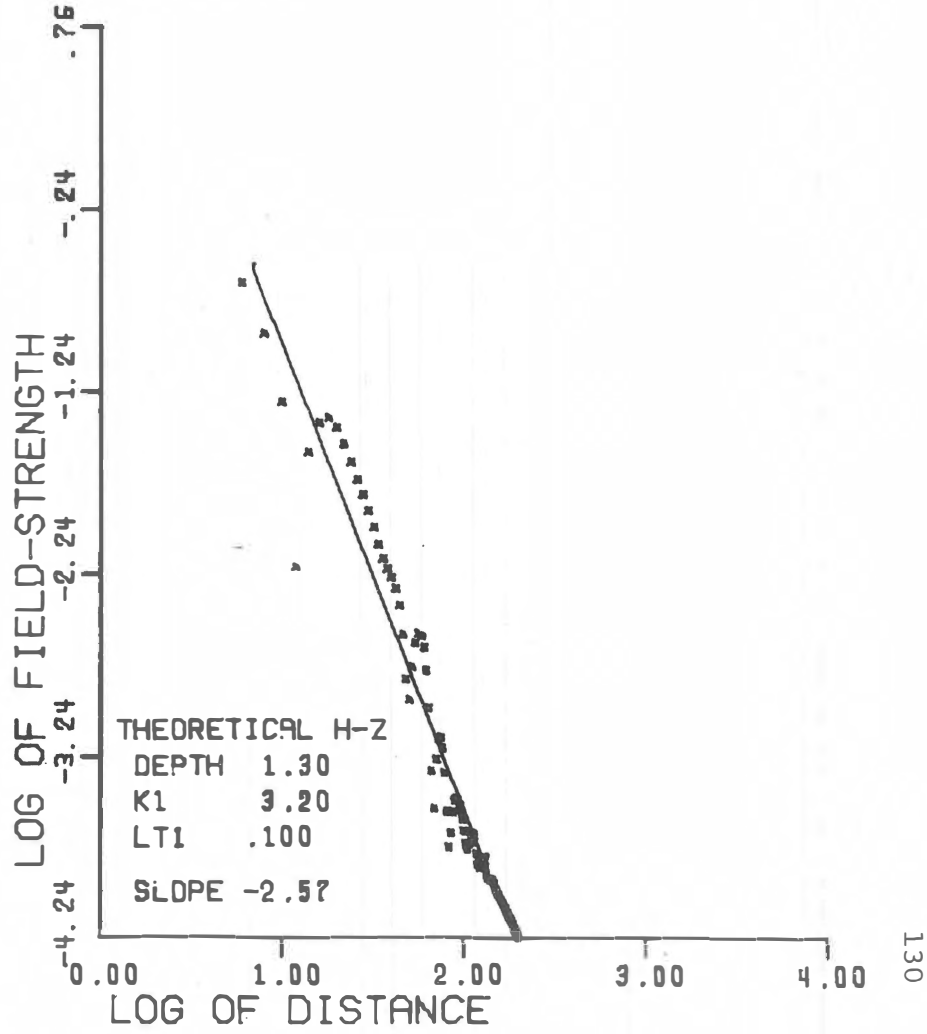

FIGURE 4-30: COMPARISON OF RATES OF DECAY
ATHABASCA GLACIER TO THEORETICAL

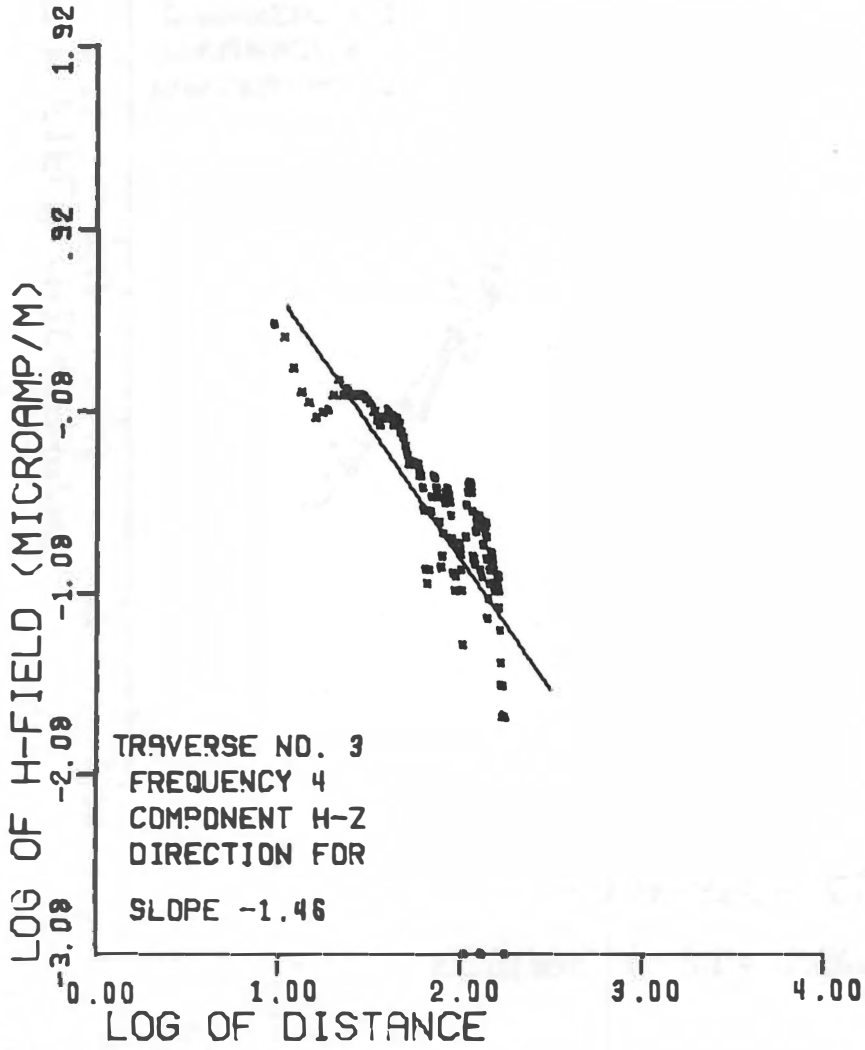

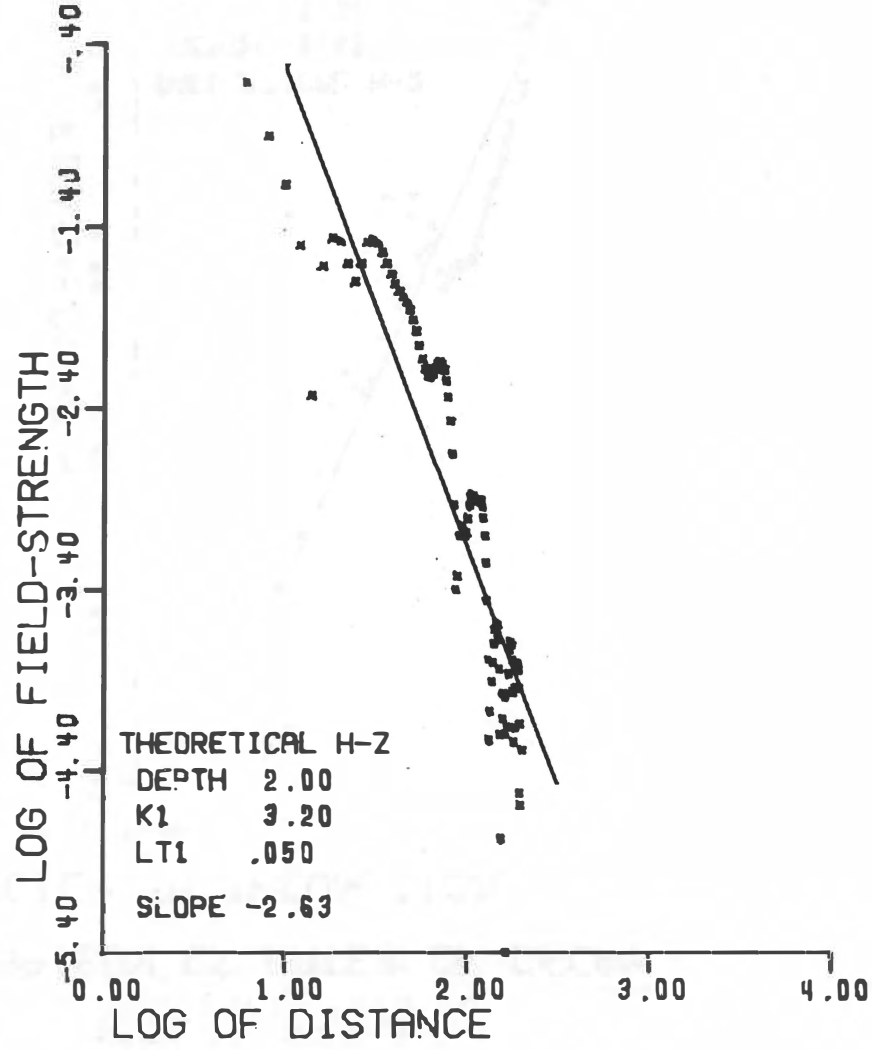

FIGURE 4-31: COMPARISON OF RATES OF DECAY
ATHABASCA GLACIER TO THEORETICAL

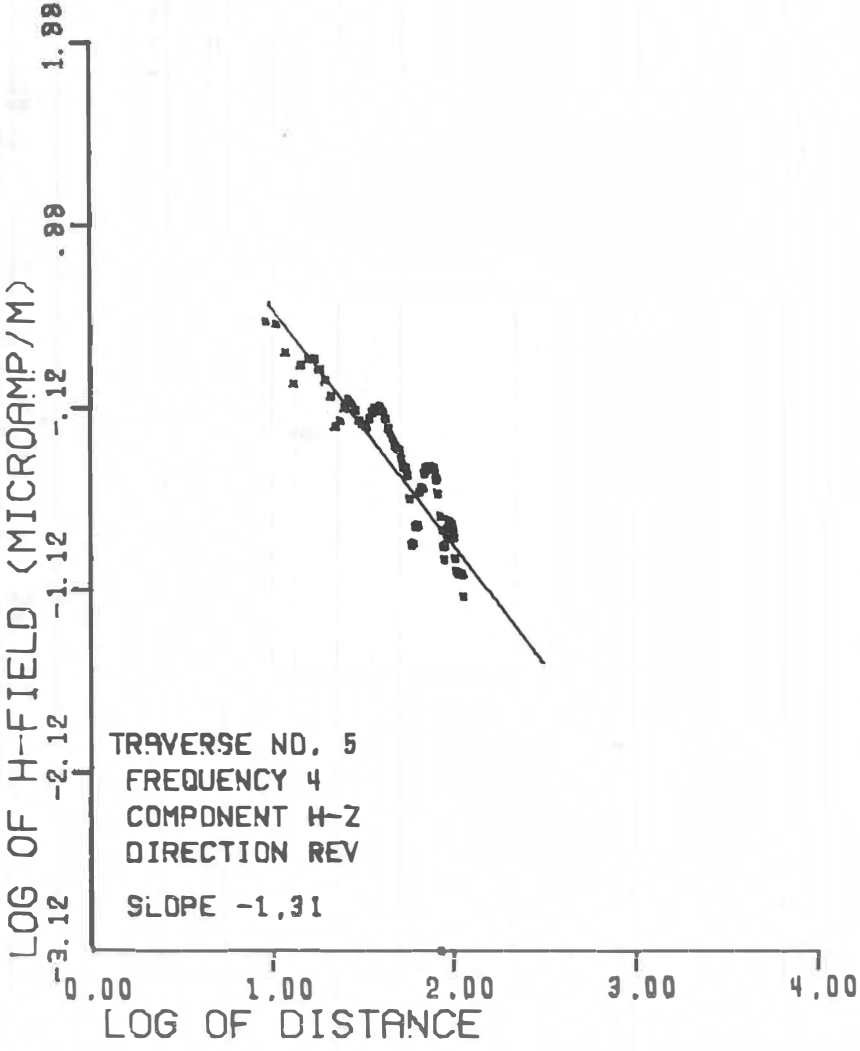

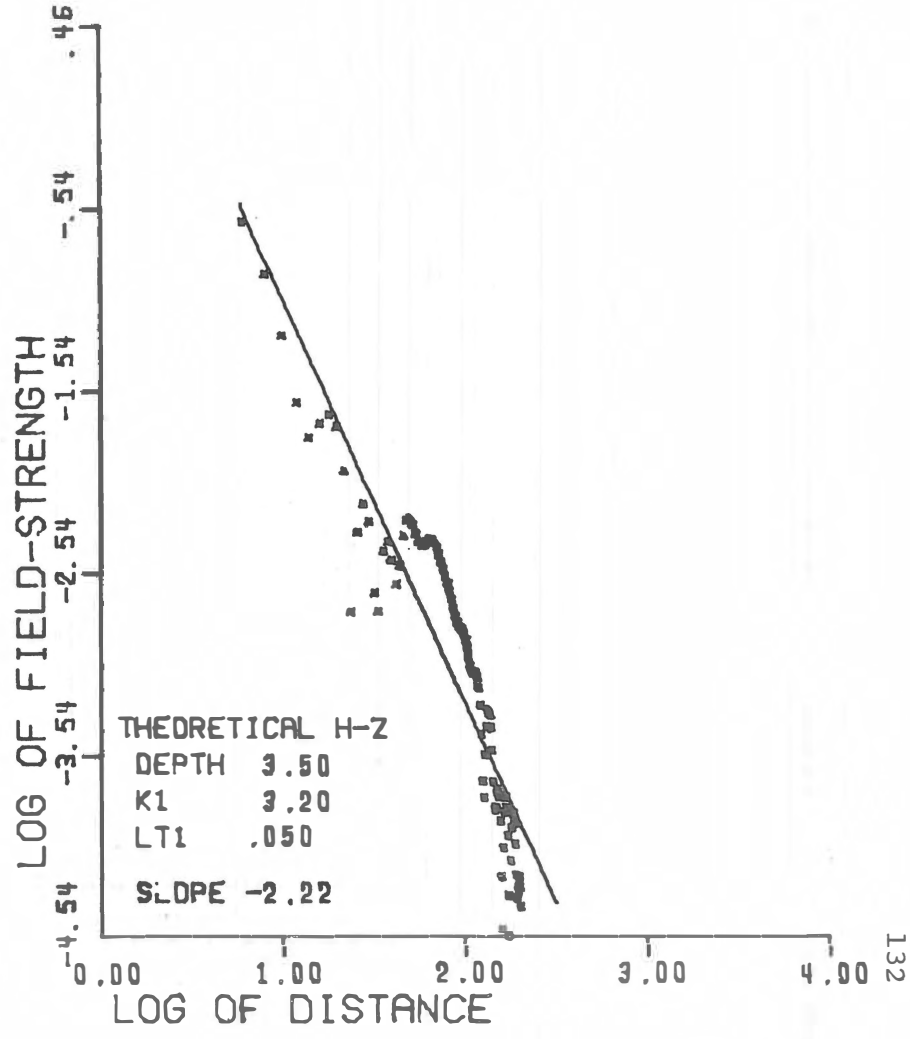

FIGURE 4-32: COMPARISON OF RATES OF DECAY
ATHABASCA GLACIER TO THEORETICAL

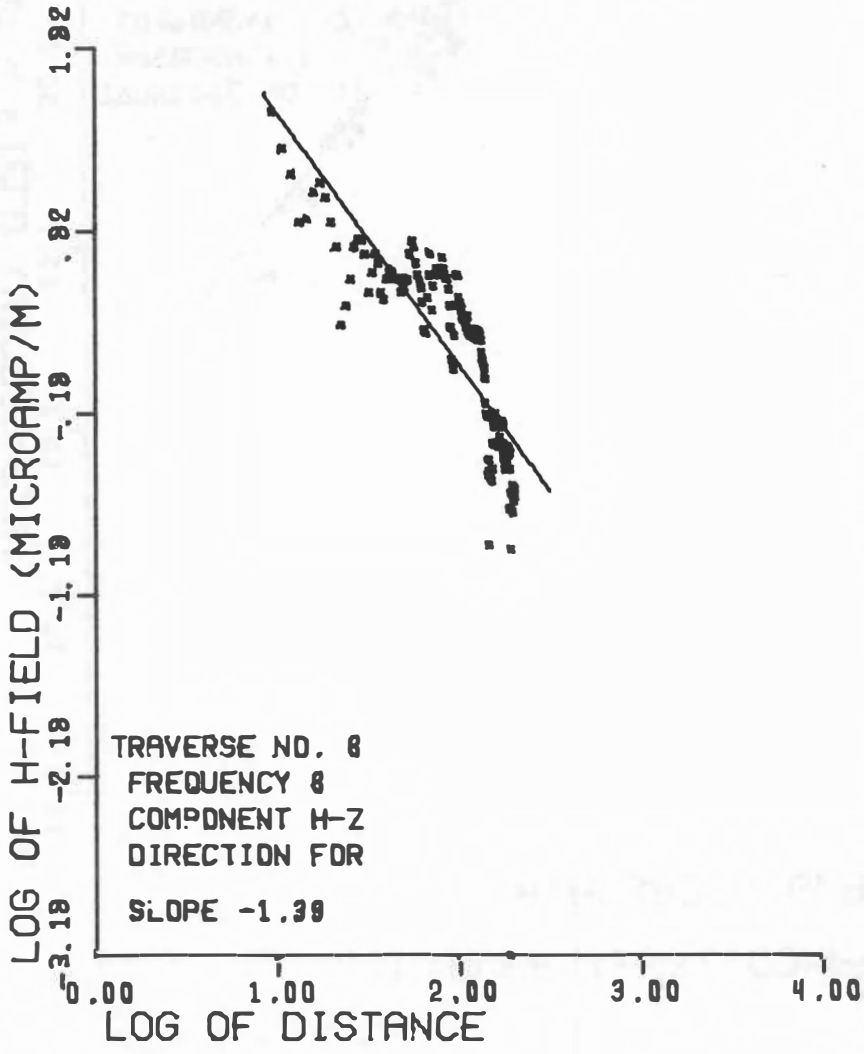

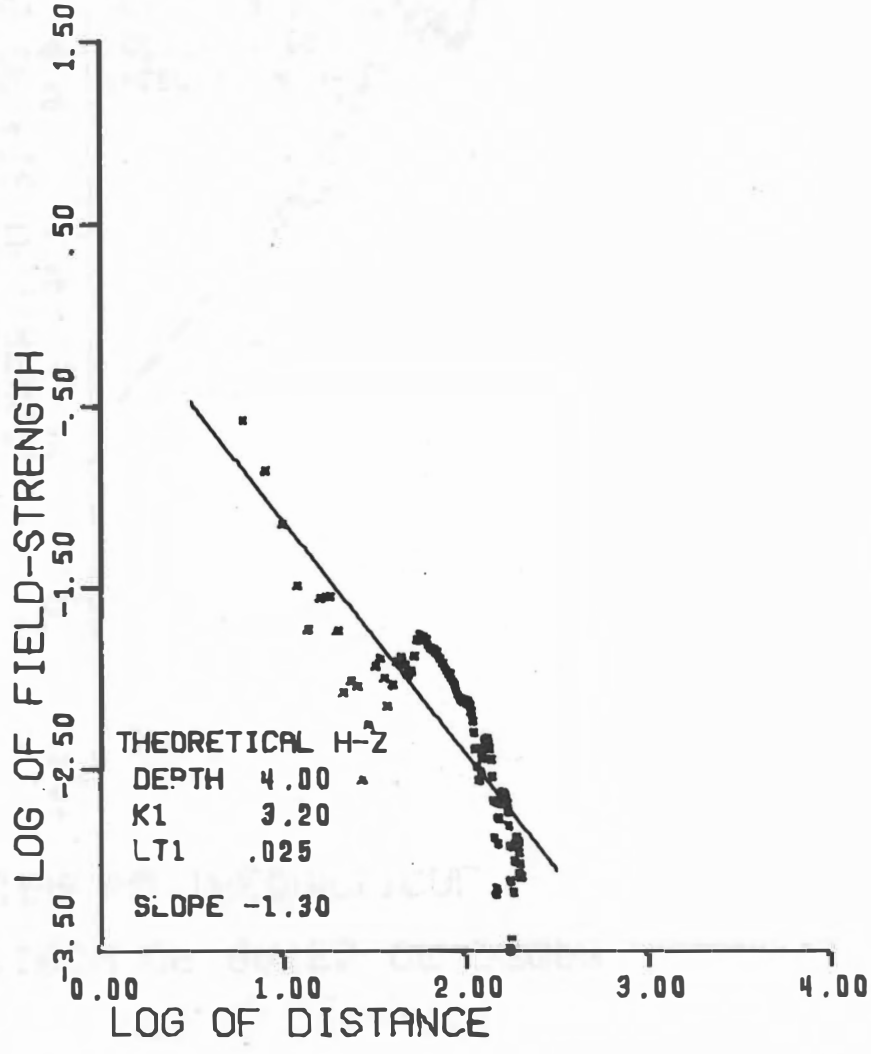

FIGURE 4-33: COMPARISON OF RATES OF DECAY
ATHABASCA GLACIER TO THEORETICAL

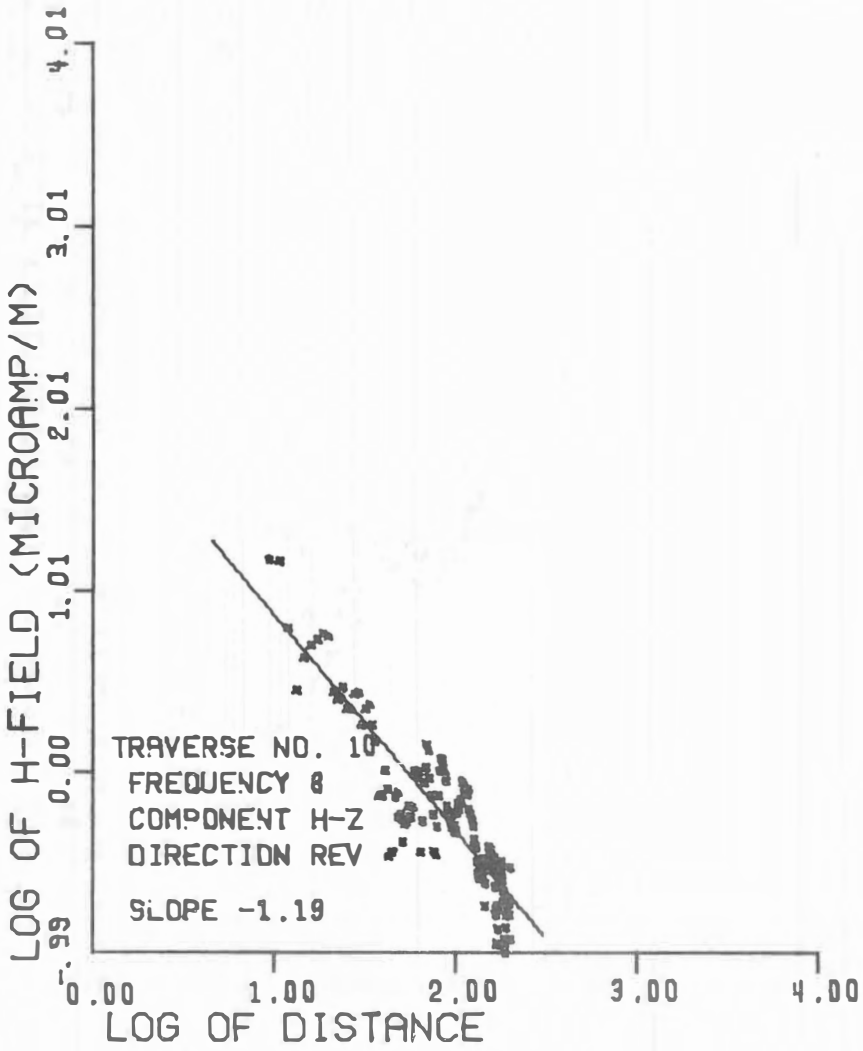

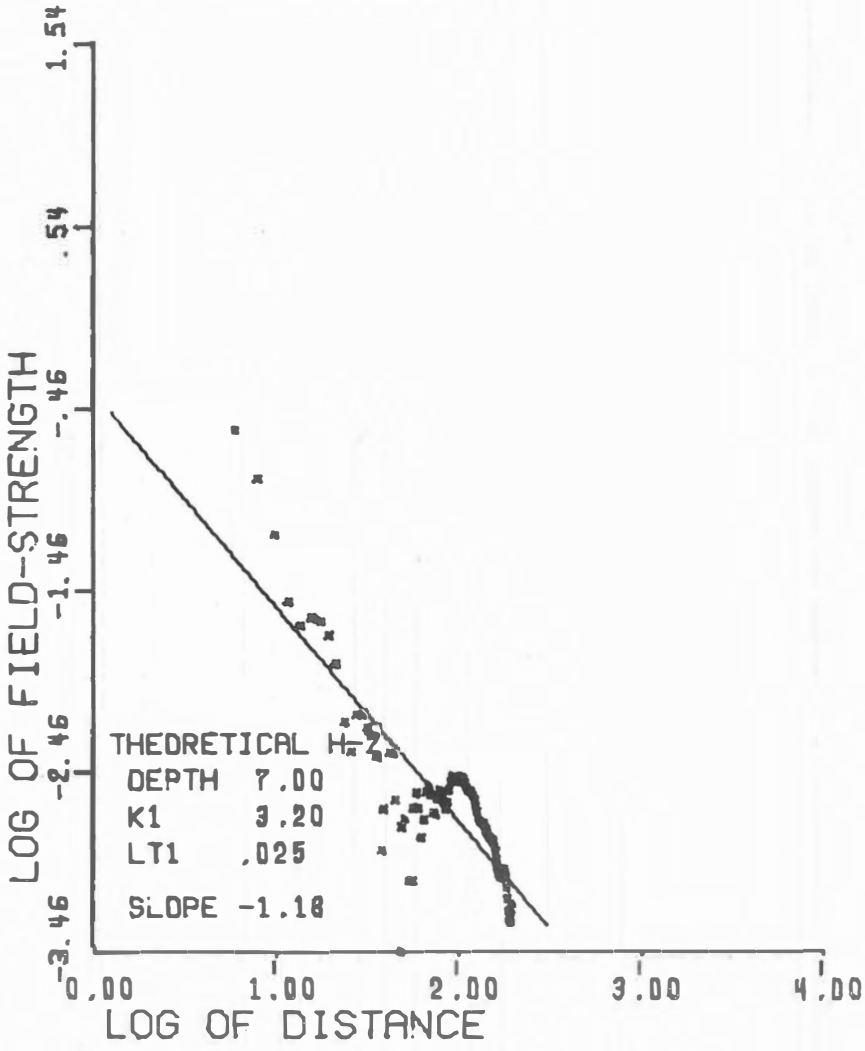

FIGURE 4-34: COMPARISON OF RATES OF DECAY
ATHABASCA GLACIER TO THEORETICAL

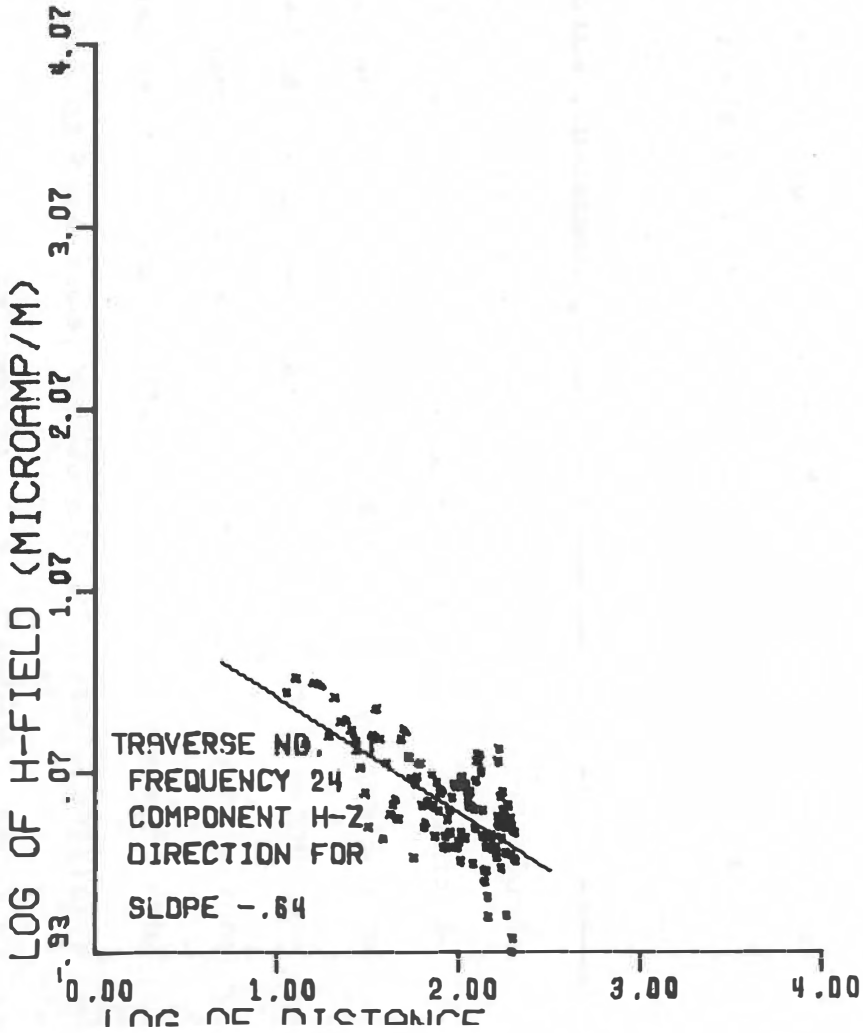

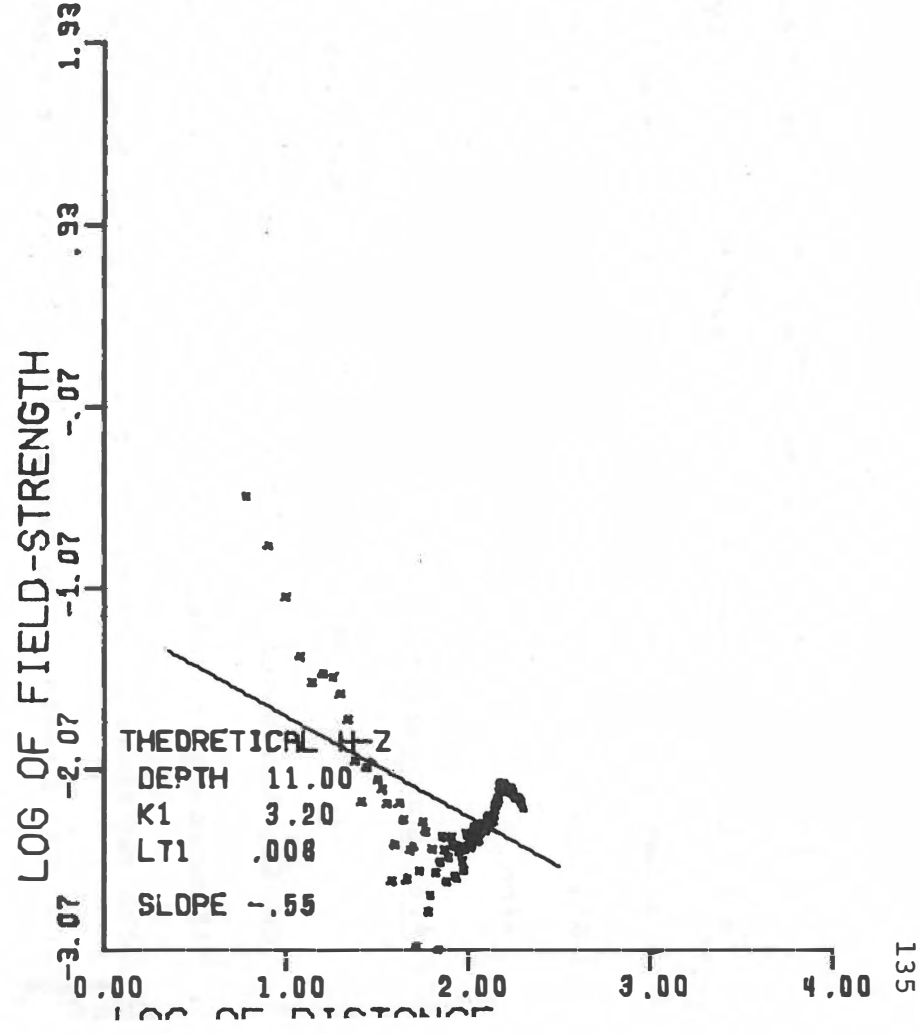

the interference technique. The rate of decay also increases with the loss tangent of the dielectric. This type of analysis is one quantitative way in which interference data may be significantly manipulated in order to extract useful information.

4.5 Conclusions

In this chapter data collected in March and April, 1970, on the Athabasca Glacier have been analysed and compared to theoretical models. Several limitations are important. First, the physical model of the glacier is not identical to the theoretical models. The theory is for smooth, horizontal, boundaries, and a perfectly conducting bottom. The bottom of the glacier is probably rough, and slopes both along the traverse path and laterally. Moreover, the upper surface of the ice has alternate ridges of snow and ice. Either of these differences could account for the presence of the H_ϕ component, which theoretically should be small, but isn't. Secondly, the multiple dipole transmitting antenna may introduce unknown effects, although none were directly attributable to it. Thirdly, the cable from the loop antenna to the receiver was long enough to be a possible source of spurious signals, and, as noted above, almost certainly does on some traverses. Fourthly, the receiver used is not sensitive enough for the output power used to allow traverses to 20 wavelengths at all frequencies.

In spite of these limitations, the data compared favorably to the theory. A systematic method of interpreting field results has not yet been developed, but various possibilities are now open. The reduction of scattering in the data has been accomplished by a simple filter. An understanding of the rate of decay of the signal is now available, and agreement between the theoretical and field results is good. This has not been presented before. It is concluded, therefore, that while improvements to the technique are apparent, the interference method will give interpretable data from a geological environment.

CHAPTER FIVE: CONCLUSIONS AND SUGGESTIONS FOR FURTHER WORK

5.1 Summary and Conclusions

On the basis of the agreement between the theoretical and field data presented in Chapter 4, it has been concluded that the interferometry technique will give interpretable information about the dielectric constant and loss tangent of a dielectric layer, and about the depth to an underlying reflector. Although it is perhaps after the fact, it is interesting to see what problems might be encountered in interpreting the data if the parameters were not known beforehand.

As mentioned earlier, the method of fitting field curves to suites of theoretical curves is not particularly satisfactory. Good peak-to-peak matches were not possible, largely because of the more complex geometry of the natural surrounding. However, several salient features are beginning to emerge.

The general nature of the curves does show a gradation as the depth to the interface changes. The redundancy of using several frequencies over the same traverse allows many ambiguities to be resolved. Probably the depth could have been resolved to within a factor of two without other information, assuming horizontal layering.

The changes of the patterns with dielectric constant are less clear. Although the details of the patterns change

considerably with dielectric constant, the overall changes are not very great. There is also some ambiguity with depth—i.e., a shallow depth with a high dielectric constant is similar to a deeper depth with a lower dielectric constant. This is not unexpected, since the wavelength in a dielectric varies inversely with the square root of the dielectric constant. In the presence of a half-space, however, the interference patterns are very sensitive indications of dielectric constant (see Figure 1-14). Therefore, if a considerably higher frequency were used, this information could be extracted. However, using the 24 MHz data, and taking only the major peaks, an estimate of $K1 = 4 \pm 2$ could have been made for the dielectric constant, using Annan's technique.

The loss tangent is the most easily determined parameter at present. It has been shown earlier that the rate of decay is closely associated with loss tangent, so that a simple calculation may be able to give an 'apparent' loss tangent for the dielectric layer (if the reflector is considerably less than perfect). In the case of ice, the loss tangent appears to be inversely proportional to frequency, and has been estimated to be $(0.25 \pm .15)/f$, as in equation 4-4.

Evidently the most important factor in interpreting the data presented here, is the geometry. It is not feasible to study complex geometries theoretically, but an analogue scale-model could. An understanding of the effects of different

geometries on the various components, especially H_{ϕ}, is important. Also, the radiation pattern of the source is important, and off-orthogonal traverses have not yet been used successfully.

Considerable progress has been made during the duration of this work in the development of the interferometry technique. Before this period the theory had been only partially developed and evaluated. Scale-model results indicated that the system should work, but no field results had indicated that it would work. And there were still doubts about the nature of the lunar surface material.

At the present time, the theoretical solutions have been re-worked and extended. The field results presented here are in general agreement with the theory, and suitable field equipment has been developed and evaluated. A number of independent measurements of the dielectric properties of lunar samples indicate that the surface material is almost certainly highly transparent to radio waves. Therefore, the method promises to be very useful as a method both to probe the subsurface of the moon to a possible depth of a kilometer, and to estimate the electrical properties and depth of ice in situ.

5.2 Suggestions for Further Work

Various continuations of this work are already in progress. These include more extensive field tests, development of a

systematic interpretive procedure of the interference patterns, an analogue scale-model, and examination of other types of theoretical solutions. A brief description of how these might best be utilized in developing the interference technique is given here.

Certainly further testing of full-size equipment and S.E.P. hardware prototypes must be continued. The optimum configuration for both transmitting and receiving antennas is of prime importance, and is still unclear. Ice layers seem to be the logical place to do this, although working conditions are not often ideal. The Athabasca Glacier has several advantages; however, to obtain different geometries, other glaciers must be used. These might include the Tasman or Fox Glaciers in New Zealand, the ice sheet near Thule, Greenland, or the Gorner Glacier, Switzerland, depending on the time of year. Only in the field can the problems of realistic data collection, new types of equipment, scattering effects, and field patterns near a dielectric boundary, be satisfactorily evaluated and solved.

Along with field testing will come the development of a systematic interpretive procedure for evaluating the data and for determining the inverse problem, i.e., interpreting the structure associated with given data-sets. This is the fundamental problem in exploration geophysics, and it rarely has an unambiguous solution. Several techniques, admittedly heuristic,

already are emerging. For example, the application of filtering to the data may help to unveil some of the pertinent features.

Examination of the theoretical curves indicates that the frequency of the interference patterns is related to the various parameters. Therefore, a harmonic analysis of the patterns might provide another useful diagnostic parameter, similar to the rate of decay constant. This type of analysis can be aided by the use of large-scale processors. These allow cross-correlation of a large number of parameters with, for example, many theoretical curves.

Scale-model studies will certainly play a key role in understanding both the theory and the field results. They provide far more complexity than can be hoped for from mathematical solutions, but much more control than is possible in the field. In addition, they might lead to an understanding of the nature of the source at a dielectric boundary, which does not seem to have been well-studied in the past. The present model under development will use a liquid dielectric. This will allow very good comparisons to be made with the present theoretical solutions. It will also provide a flexible system to study the effects of various geometries (such as a dipping reflector and lateral reflections), of random scatterers, and of rough interfaces.

Mathematical models do, however, provide an important independent check of experimental data. New solutions are being sought, perhaps using integral equations rather than differential equations (R. D. Watts, private communication).

Finally, in planning the experiment for the moon, as much information on the expected conditions as possible should be gathered. This includes further dielectric properties measurements on lunar samples, with particular emphasis on eleminating water contamination. Measurements on lunar fines over a wide temperature range will be necessary to understand the dielectric mechanisms. It may also be possible to get a rough in situ measure of the loss tangent of lunar material by studying the automatic gain control of the communications bands (around 250 MHz) as the astronauts go behind a crater during moonwalks. The seismic results may also give information very pertinent to the S.E.P. Experiment. The indication of high scattering, for example, has already made that problem of prime importance in scale-model work for this experiment. Future analyses of the active seismic experiments on Apollo 14, should be particularly interesting.

The specific immediate problems in the development of the interference technique are briefly:

(1) what are the optimum configurations for both the source and the receiver?

(2) what are the effects of random scattering, and can they be measured or removed?

(3) what are the effects of lateral inhomogeneities?

(4) are there any common features in the data that are characteristic of the parameters involved, especially off the orthogonal of the dipole?

The method has been shown to work as expected theoretically; now it must be established as a practical geophysical tool.

APPENDIX ONE: THE SURFACE ELECTRICAL PROPERTIES EXPERIMENT

A brief summary of the concept of the Surface Electrical Properties Experiment at the time of writing, as planned for Apollo 17 (currently scheduled for December, 1972), is given here. Since the details are still in a state of flux, there will certainly be changes in the final design. However, the main points are fixed. The following has been updated from C.S.R. Report, CSR TR 70-7 (1970).

A schematic diagram of the experiment is shown in Figure A1-1. The source is an array of two sets of orthogonal centre-fed dipoles laid on the surface of the moon, near the Lunar Module. Each set of the array will be powered in turn by a small transmitter producing continuous waves at discrete frequencies of 1, 2, 4, 8, 16, and 32 MHz successively, and about 3 watts power. This sequence will be repeated about once per second.

The receiving antenna will consist of three orthogonal loops or dipoles, about 1/3 meter in diameter or length, mounted on the Lunar Roving Vehicle. These will detect the three orthogonal components of the field strength at each successive frequency during the Rover traverse. The data will be recorded on a small analogue tape recorder, and returned to earth for analysis and interpretation.

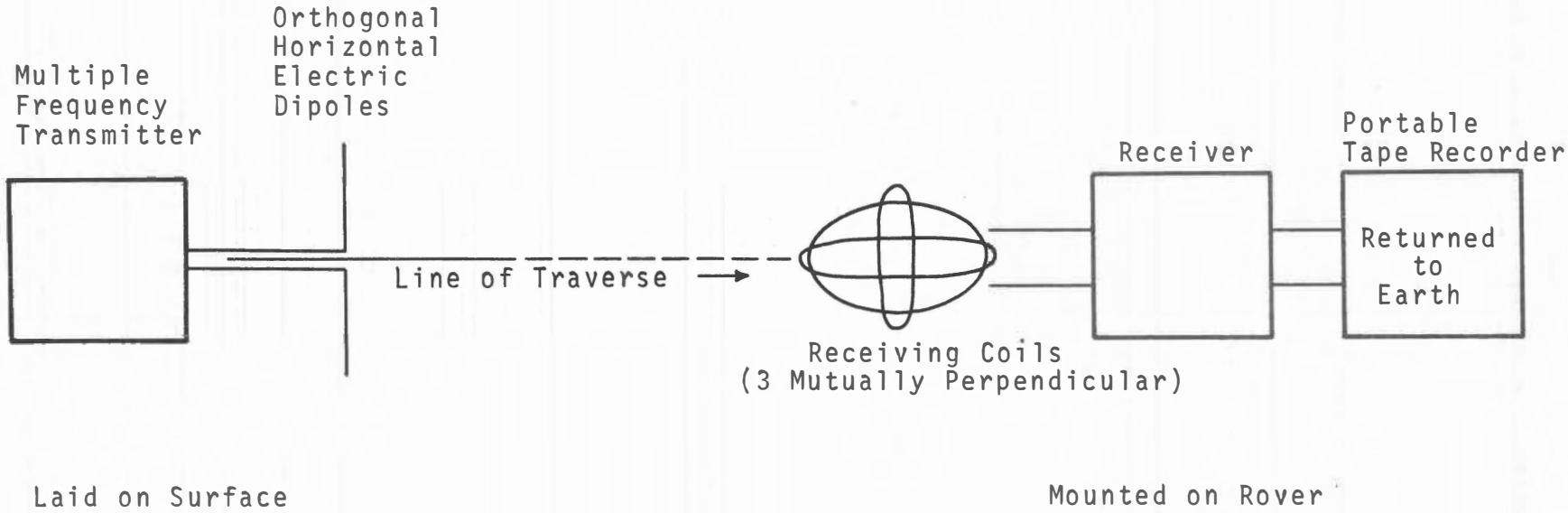

FIGURE A1-1: LAYOUT OF BASIC EXPERIMENT (AFTER CSR TR 70-7)

Position information will be reconstructed from the Rover's odometer and navigation system, photographs, television coverage, and voice comments by the astronauts. A short, well documented traverse may be made while near the transmitting antennas, in order to obtain more accurate position information for the higher frequencies.

REFERENCES

Aarons, Jules, editor "Solar System Radio Astronomy," Plenum Press, New York, 1965.

Annan, A. P., "Radio Interferometry Depth Sounding," M.Sc. Thesis, Dept. of Physics, U. of Toronto, 1970 (reprinted as NASA Report, Grant #NGL 22-009-257, 1970).

Cameron, Eugene N., "Opaque Minerals in Certain Lunar Rocks from Apollo 11," Proceedings of the Apollo 11 Lunar Science Conference, editor A. A. Levinson, Pergamon Press, New York, v. 1, pp. 221-245. 1970.

Campbell, M. J., & Ulrichs, J., "Electrical Properties of Rocks and their Significance for Lunar Radar Observations," J. Geophys. Res., v. 74, pp. 5867-5881, 1969.

Chung, D. H., Westphal, W. B., and Simmons, Gene, "Dielectric Properties of Apollo 11 Lunar Samples and their Comparison with Earth Materials," J. Geophys. Res., v. 75, pp. 6524-6531, 1970.

Chung, D. H., Westphal, W. B., and Simmons, G., "Dielectric Behavior of Lunar Samples: Electromagnetic Probing of the Lunar Interior," submitted to Second Lunar Science Conference, Houston, Texas, January, 1971.

Collett, L. S., and Katsube, T. J., "Electrical Properties of Apollo 11 and Apollo 12 Lunar Samples," submitted to Second Lunar Science Conference, Houston, Texas, January, 1971.

Dekker, A. J., "Solid State Physics," Prentice-Hall, 1957.

El-Said, M.A.H., "Geophysical Prospection of Underground Water in the Desert by Means of Electromagnetic Interference Fringes," Proc. I.R.E., v. 44, pp. 24-30 and 940, 1956.

England, A. W., Simmons, Gene, and Strangway, D., "Electrical Conductivity of the Moon," J. Geophys. Res., v. 73, pp. 3219-3226, 1968.

Evans, S., "Radio Techniques for the Measurement of Ice Thickness," Polar Record, v. 11, pp. 406-410 and 795, 1963.

Evans, S., "Dielectric Properties of Ice and Snow — A Review," J. Glaciol, v. 5, pp. 773-792, 1965.

Gold, T., "Processes on the Lunar Surface," in The Moon, editors Z. Kopal and Z. K. Mikhailov, Academic Press, London, pp. 433-439, 1962.

Gold, T., Campbell, M. J., and O'Leary, B. T., "Optical and High-frequency Electrical Properties of the Lunar Sample," Science, v. 167, pp. 707-709, 1970 (reprinted in Proceedings of the Apollo 11 Lunar Science Conference, 1970).

Gold, T., O'Leary, B. T., and Campbell, M. J., "Physical Properties of the Apollo 12 Lunar Fines" (with supplement), submitted to Second Lunar Science Conference, Houston, Texas, January, 1971.

Grant, F. S., and West, G. F., "Interpretation Theory in Applied Geophysics," McGraw-Hill, New York, 1965.

Hagfors, T., "Review of Radar Observations of the Moon," in The Nature of the Lunar Surface, editors, Hess, W. N., Menzel, D. H., and O'Keefe, J. A., Johns Hopkins Press, Baltimore, pp. 229-239, 1966.

Harrison, C. H., "Reconstruction of Subglacial Relief from Radio Echo Sounding Records," Geophysics, v. 35, pp. 1099-1115, 1970.

Hess, W. N., Menzel, D. H., O'Keefe, J. A., editors, "The Nature of the Lunar Surface," Johns Hopkins Press, Baltimore, 1966.

Jiracek, G. R., "Radio Sounding of Antarctic Ice," Research Report Number 67-1, Geophysical and Polar Research Center, U. of Wisconsin, 1967.

Johnston, E. A., LaTorraca, G. A., Rossiter, J. R., and Strangway, D. W., "Preliminary Report on the Athabasca Glacier Field Expedition, April, 1970," NASA Report, Grant #NGL 22-009-257, 1970.

Kanasewich, E. R., "Gravity Measurements of the Athabaska Glacier, Alberta, Canada," J. Glaciol, v. 4, pp. 617-631, 1963.

Keller, G. V., and Frischknecht, F. C., "Electrical Resistivity Studies on the Athabasca Glacier, Alberta, Canada," J. Res. U. S. Nat. Bur. Stan., v. 64D, pp. 439-448, 1960.

Keller, G. V., and Frischknecht, F. C., "Induction and Galvanic Resistivity Studies on the Athabasca Glacier, Alberta,

Canada," Geology of the Arctic (International Symposium), editor G. O. Raasch, v. 2, pp. 809-832, U. of Toronto Press, 1961.

Kittel, Charles, "Introduction to Solid State Physics," Third Edition, John Wiley and Sons, New York, 1968.

Kopal, Z., and Mikhailov, Z. K., editors, "The Moon," Academic Press, London, 1962.

Kraus, John D., "Antennas," McGraw-Hill, New York, 1950.

Oberbeck, V. R., and Quaide, W. L., "Estimated Thickness of a Fragmental Surface Layer of Oceanus Procellarum," J. Geophys. Res., v. 72, pp. 4697-4704, 1967.

Ogilvy, A. A., "Geophysical Studies in Permafrost Regions in the U.S.S.R.", in Mining and Groundwater Geophysics/1967, editor L. W. Morley, Geological Survey of Canada Economic Geology Report No. 26, Ottawa, pp. 641-650, 1970.

Olhoeft, Gary R., "Pulse Measurement of Magnetic Properties," Research Report submitted to Dept. of Electrical Engineering, M.I.T., 1970.

Parkhomenko, E. I., "Electrical Properties of Rocks," Plenum Press, New York, 1967.

Paterson, W. S. B., and Savage, J. C., "Geometry and Movement of the Athabasca Glacier," J. Geophys. Res., v. 68, pp. 4513-4520, 1963.

Pettengill, G., "Lunar Radar Reflections," in Solar System Radio Astronomy, editor J. Aarons, Plenum Press, New York, pp.

355-369, 1965.

Rossiter, James R., "Supplement to Interferometry Depth Sounding on the Athabasca Glacier," NASA Report, Grant #NGL 22-009-257, 1971.

Röthlisberger, Hans, "Electrical Resistivity Measurements and Soundings on Glaciers: Introductory Remarks," J. Glaciol., v. 6, pp. 599-606, 1967.

Röthlisberger, Hans and Vögtli, Kurt, "Recent D. C. Resistivity Soundings on Swiss Glaciers," J. Glaciol., v. 47, pp. 607-621, 1967.

Saint-Amant, Marcel, "Frequency and Temperature Dependence of Dielectric Properties of Some Common Rocks," M.Sc. Thesis, Dept. of Geology and Geophysics, M.I.T., 1968, (reprinted as NASA Report, Grant #NGR 22-009-257, 1968).

Saint-Amant, M., and Strangway, David W., "Dielectric Properties of Dry, Geologic Materials," Geophysics, v. 35, pp. 624-645, 1970.

Schubert, Gerald, Lingenfelter, Richard E., and Peale, Stanton J., "The Morphology, Distribution, and Origin of Lunar Sinuous Rilles," Rev. Geophys. Space Phys., v. 8, pp. 199-224, 1970.

Shoemaker, E. M., Hait, M. H., Swann, G. A., Schleicher, D. L., Dahlem, D. H., Schaber, G. G., and Sutton, R. L., "Lunar Regolith at Tranquillity Base," Science, v. 117, pp. 452-455, 1970a.

Shoemaker, E. M., Hait, M. H., Swann, G. A. Schleicher, D. L., Schaber, G. G., Sutton, R. L., Dahlem, D. H., Goddard, E. N., and Waters, A. C., "Origin of the Lunar Regolith at Tranquillity Base," Proceedings of the Apollo 11 Lunar Science Conference, editor A. A. Levinson, v. 3, pp. 2399-2412, Pergamon Press, 1970b.

Sinha, A. K., "Theoretical Studies on the Radiofrequency Interferometry Method of Sounding," NASA Report, Grant #NGL 22-009-257, 1971.

Strangway, David W., "Possible Electrical and Magnetic Properties of Near-Surface Lunar Materials," NASA Report, Grant #NGR 22-009-257, 1968.

Strangway, D. W., "Moon: Electrical Properties of the Uppermost Layers," Science, v. 165, pp. 1012-1013, 1969.

Strangway, D. W., Larson, E. E., and Pearce, G. W., "Magnetic Properties of Lunar Samples," Science, v. 167, pp. 691-693, 1970a.

Strangway, D. W., Larson, E. E., and Pearce, G. W., "Magnetic Studies of Lunar Samples - Breccia and Fines," Proceedings of the Apollo 11 Lunar Science Conference, editor A. A. Levinson, Pergamon Press, New York, v. 3, pp. 2435-2451, 1970b.

Strangway, D. W., Pearce, G. W., Olhoeft, G., and Larson, E. E., "Magnetic Properties of Lunar Samples," Abstract only, EOS, v. 51, p. 586, 1970c (presented at Annual Meeting, American

Geophysical Union, April 1970, Washington, D. C.).

Tyler, G. L., "Oblique-Scattering Radar Reflectivity of the Lunar Surface: Preliminary Results from Explorer 35," J. Geophys. Res., v. 73, pp. 7609-7620, 1968.

von Hippel, Arthur R., "Dielectrics and Waves," M.I.T. Press, 1954a.

von Hippel, Arthur R., editor "Dielectric Materials and Applications," M.I.T. Press, 1954b.

Ward, Stanley H., "Gross Estimates of the Conductivity, Dielectric Constant, and Magnetic Permeability Distributions in the Moon," Radio Science, v. 4, pp. 117-137, 1969.

Walford, M. E. R., "Field Measurements of Dielectric Absorption in Artic Ice and Snow at very High Frequencies," J. Glaciol., v. 7, pp. 89-94, 1968.

Watt, A. D., and Maxwell, E. L., "Measured Electrical Properties of Snow and Glacial Ice," J. Res. U. S. Nat. Bur. Stan., v. 64D, pp. 357-363, 1960.

Weaver, Harold, "The Interpretation of Thermal Emissivity from the Moon," in Solar System Radio Astronomy, editor J. Aarons, Plenum Press, New York, pp. 295-354, 1965.

Zohdy, Adel A. R., and Jackson, Dallas B., "Application of Deep Electrical Soundings for Groundwater Exploration in Hawaii," Geophysics, v. 34, pp. 584-600, 1969.